August 2013

Continuum Deformation Model for Drug-Eluting Stent (DES) Medical Devices Using Finite Element Analysis (FEA)

Solki Lee
University of Wisconsin-Milwaukee

CONTINUUM DEFORMATION MODEL FOR DRUG-ELUTING STENT (DES) MEDICAL DEVICES USING FINITE ELEMENT ANALYSIS (FEA)

by

Solki Lee

A Thesis Submitted in

Partial Fulfillment of the

Requirements for the Degree of

Master of Science

in Engineering

at

The University of Wisconsin-Milwaukee

August 2013

ABSTRACT
CONTINUUM DEFORMATION MODEL FOR DRUG-ELUTING STENT (DES)
MEDICAL DEVICES USING FINITE ELEMENT ANALYSIS (FEA)

by

Solki Lee

The University of Wisconsin-Milwaukee, 2013
Under the Supervision of Professor Chang-Soo Kim

The development of coronary stent medical devices was originally considered as a major advance in the treatment of obstructive cardiovascular disease. The implantation of stent, however, involves clinical adverse effects such as re-narrowing of arterial wall after stenting. Drug-eluting stents (DES) have been developed to prevent such adverse effects by slowly delivering anti-proliferative and/or anti-inflammatory drugs from coating composites of drug-containing polymers. One of the major issues in DES implantation is, however, that the coatings comprised of drug and polymer composite phases are often fractured or delaminated during the deployment of stent, which can lead to more serious clinical complications. In this study, we developed a computational model employing the finite element analysis (FEA) technique to predict the stress distributions of various components in DES medical devices including coating composites. This work is considered as one of the first attempts to address the stress concentrations of DES medical devices upon implantation using 2D/3D computational approaches. The ABAQUS commercial package (Hibbit Karlsson & Sorences Inc., Pawtucket, RI, USA) was used to perform computational analyses for systems with large elastic/plastic deformations. Designs of three commercial products (SYNERGY, TAXUS Express, and

FLEX stents) available in the market have been modeled in this thesis. The displacement control method has been adopted in developing our model for the deployment of DES. Throughout the present thesis, the impacts of geometry and material variables such as stent strut/coating thicknesses and material contents in composites on the mechanical performance of the DES were quantitatively examined. Moreover, to predict the rate of in-stent restenosis (ISR), we developed a model to include the physiological environments, i.e., arterial wall and atherosclerotic plaque, in the system. From the results, it has been monitored that the strut thickness and coating thickness of DES are one of the major factors determining the amount of stress concentration on the inner surfaces of arterial wall and atherosclerotic plaque. The higher von-Mises stress accumulation was observed with thicker strut and coating. The findings indicate that the optimizing geometry of stent and coating is a critical variable to manipulate its mechanical performance and the rate of ISR. The computation results also demonstrate that the stress concentrations in the SYNERGY and FLEX DES are much lower than those observed in the TAXUS Express stents.

This thesis is dedicated to God Almighty who has been my eternal rock and source of refuge, and for His word in Job 23:10 that kept me all through the journey of completing this work. I also dedicate this work to my wife, Mrs. Hyelim Song and my family, Faith and Glory for being great pillars of support.

TABLE OF CONTENTS

LIST OF FIGURES

LIST OF TABLES

LIST OF ABBREVIATIONS

BMS – Bare metal stent
CABG – Coronary artery bypass grafting
CAD – Coronary artery disease
Co-Cr – Cobalt-chromium
DES – Drug-eluting stent
FEA – Finite element analysis
ISR – In-stent restenosis
PBMA – Poly-n-butyl methacrylate
PCL – poly(caprolactone)
PDO – Poly(pdioxanone)
PEVA – Polyethylene-co-vinyl acetate
PGA – Polyglycolides
PLA – Polylactic acid
PLGA – Copolymer, polylactic-co-glycolic acid
POE – Polyorthoesters
PTCA – Percutanueous transluminal coronary angioplasty
Pt-Cr – Platinum-chromium
PVDF-HFP – Co-polymer poly(vinylidene fluoride-co-hexafluropropylene)
SIBS – Tri-block co- polymer poly(styrene-b-isobutylene-b-styrene)

ACKNOWLEDGMENTS

I would like to express my gratitude to my supervisor Professor Chang-soo Kim, for the useful comments, remarks and engagement through the learning process of this master thesis. Furthermore I would like to thank my wife, Hyelim Song for standing beside me whenever she breathes. Also, I would like to thank Pastor Han, Mrs. Han and my friends from church who supported me during my life in UWM. I will be grateful forever for your love.

Lastly, I truly thank my loving family and God who have supported me during this process.

Chapter 1. Introduction

In this chapter, a brief overview, motivations, and the objective of current research is given. In the overview section, we provide an introductory information about drug-eluting stents (DES) medical devices and finite-element analysis (FEA).

1. Overview

1.1 Drug-Eluting Stent (DES)

Drug-eluting stent (DES) is considered as a pivotal biomedical device to treat coronary artery disease (CAD) resulted from the plague accumulated in arteries that may deteriorate into atherosclerosis. With growing rate of increase in CAD, many medical interventions have been developed and applied for those who undergoing CAD. Coronary Artery Bypass Grafting (CABG) has been commonly applied to surgical intervention for CAD since 1970s to enhance blood flow to the heart by grafting arteries narrowed by blockages called plague with healthy arteries that can freely pump in and out blood [1,2], however, this intervention has been proven as high-risk clinical protocol for CAD. To avoid such high-risk procedure, Percutaneous Transluminal Coronary Angioplasty (PTCA) was introduced and initially performed as supplementary intervention during the CABG procedure [1]. Balloon angioplasty is a well-known type of PTCA, which was considered as a minimally invasive surgical intervention by inserting a balloon tipped catheter into and expanding clogged arteries. However, it had a major risk of sudden closure and restenosis caused by intimal hyperplasia, which essentially led the

development bare metal stent (BMS) [1]. BMS is a small, tubular, wire-mesh devise that is pre-loaded in a collapsed form onto a catheter balloon, threaded to the narrowed section of the artery and expanded within the vessel. It is considered that BMS generally result in extremely favorable initial clinical results, however re-narrowing of the treated artery due to in-stent restenosis (ISR) is commonly observed [3].

ISR occurs when the treated vessel is narrowed again after implementing a stent in the vessel. Initially, new tissues consist of healthy cells from the lining of arterial wall grows inside the stent, which allows blood to flow well over the treated area without clotting. When ISR occurs, scar tissues forming underneath the new lining obstruct the blood flow and produce a blockage inside the stent [4]. To deal with this ISR, localized drug delivery to the targeted vessel wall was introduced, which is widely known as drug-eluting stents (DES). DES has in principle the very similar structure of BMS comprised of tubular, a wire-mesh device, but DES is coated with anti-proliferative/anti-inflammatory drugs onto coronary stents to prevent ISR on the operated arteries. There have been studies that the use of DES appeared to be significantly less risky than BMS with regards to the mortality rates, safety, and efficacy [5,6]. There have been many initiatives and developments in applying the type of the anti-proliferative drug agents, the design of DES stent platform, and the materials used for DES to reduce complications after implantation and increase efficacy. In the early stage of DES, silolimus-eluting (Cypher, Johnson & Johnson, 2003) and paclitaxel-eluting (Taxus, Boston Scientific, 2004) stents contributed to reducing the risk of ISR. However, it has been discovered that those stents are likely to result in higher chance of occurring late clinical adverse effects such as stent thrombosis [3]. Following that, more advanced DES to improve long-term

safely and anti-restenotic efficacy have been suggested such as zotarolimus eluting (Endeavor, Medtronic, 2009) and everolimus eluting (Xience V, Abbott, 2008) stents [3]. Details of commercialized DES products will be address in Chapter 2.

1.2 Finite element analysis (FEA)

Finite element analysis (FEA) is one of the widely used computational tools to predict the mechanical behaviors of continuum objects/systems. Typical FEA is performed based on a complicated domain that is subdivided into a finite number of smaller regions, called 'elements', and differential equations are calculated inside the element called 'integration points'. The calculated value is extrapolated to the vertices of each element, called 'nodes', which is the intersections of elements. After the equations are calculated, the smaller sub-regions are assembled, which formulates the overall behavior of the entire domain. FEA can use a complex system of nodes which generate a grid called a mesh element. This mesh is programmed to contain the material and structural properties that define how the structure will react to certain loading conditions. Nodes are assigned at a certain density throughout the material depending on the anticipated stress levels of a particular area. Regions which will receive large amounts of stress usually have a higher node density than those which experience little or no stress. The mesh looks like a spider web in which each node is expanded to the adjacent nodes by a mesh element. This web of vectors is what carries the material properties to the object, creating many elements [7].

There are generally two types of analysis that are used in industry with respect to the dimensional analysis; 2D and 3D modeling. While 2D modeling takes the advantage

of simplicity and does not require huge computational resources, it tends to yield less accurate results. It is known that 3D modeling, however, generally produces more accurate results though it requires more computational resources and time. FEA has been served as a reliable tool to estimate a solution to the task of predicting failure due to external stresses [7]. A variety of specializations under the umbrella of the mechanical engineering discipline (such as aeronautical, biomechanical, and automotive industries) commonly use integrated FEA in designing and developing their products. Several modern FEA packages include specific components such as thermal, electromagnetic, fluid, and structural working environments. In a structural simulation, FEA can guide to produce stiffness and strength visualizations and also to minimize weight, materials, and costs. FEA allows detailed visualization of where structures bend or twist, and it can indicate the distribution of stresses and displacements. FEA software provides a wide range of simulation options for controlling the complexity of both modeling and analysis of a system. Similarly, the desired level of accuracy required and associated computational time requirements can be managed simultaneously to address most engineering applications. FEA allows entire designs to be constructed, refined, and optimized before the design is manufactured.

This powerful design tool has significantly improved both the standard of engineering designs and the methodology of the design process in many industrial applications. The introduction of FEA has substantially decreased the time to take products from concept to the production line. It is primarily through improved initial prototype designs using FEA that testing and development have been accelerated [8]. Benefits of FEA include increased accuracy, enhanced design and better insight into

critical design parameters, virtual prototyping, fewer hardware prototypes, a faster and less expensive design cycle, increased productivity, and increased revenue. Considering such advantages, throughout the current thesis, advanced FEA computational approach has been primarily applied in understanding the mechanical behaviors of DES medical devices.

2. Motivations

As stated in the previous section, in predicting the performance of medical stents, FEA has a great potential. When we consider the fact that even a small-scale clinical trial using stents on human body can give rise to fatality, the more precise computer simulation on designing stents would be preferred to reduce practical errors, which can be derived from utilizing FEA on mechanically modeling stents.

Even though utilizing DES clearly decreases the possibility of ISR occurrence, it still accompanies several critical drawbacks. One of the major issues in DES implantation is that the coatings comprised of drug and polymer phases are often fractured or delaminated during the deployment of stent. Upon expansion, localized regions of high plastic strain, such as hinge or intersection of stent struts, experience complicated mechanical deformation that leads to the fracture of the coating (see Fig. 1.1). It is important that the coating maintain its mechanical integration and adhesion to the stent platform because the fracture of coating could affect the delivery of the drug and it can cause a more serious problem such as stroke. Further, stent coating failure after implantation could lead to various clinical problems, such as restenosis and thrombosis. The amount of drug dosage, in addition, could possibly change or the delivery misguided

by such coating delamination and/or fragmentation. Even toxic or irritant ions from the metallic stent strut can be released if there is a breakdown of the coating barrier, precipitating the inflammatory response [9]. There is a very large plastic deformation during the stent expansion, and the coated polymer layer could be delaminated from the metal platform. If the polymer layer is separated from the stent strut, the debris or particle could drift along blood which can reach anywhere in humans' body. This could cause serious problem such as stroke. Though it is known that the coating delamination/fragmentation is an important issue in DES implantation, not many computational modeling work has been reported. C. G. Hopkins et al [10] have developed a FEA model of coating delamination of DES in 2010. In this study, a cohesive zone model of the stent-coating interface is implemented to investigate coating de-bonding during stent deployment. This study provided insight into the critical factors governing coating delamination and offers a predictive framework that can be used to improve the design of coated stents. However, there is a limitation that this work has only 2D perspective and the consideration of the presence of artery and plaque was not taken into account. Fig. 1.2 shows the FEA of coating delamination phenomena.

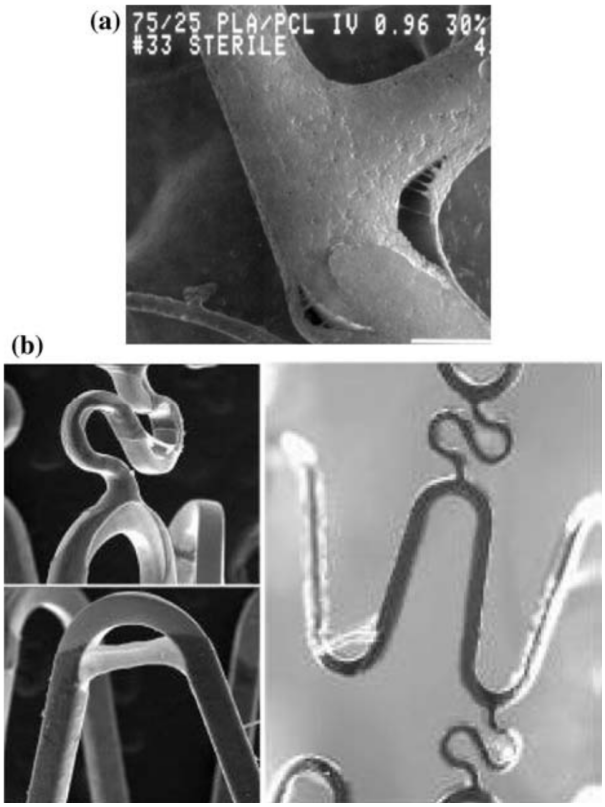

Fig. 1.1 Delamination of stents coatings after stent deployment (a) stent hinge region (b) Cypher stent (Adopted from C. G. Hopkins et al [10]).

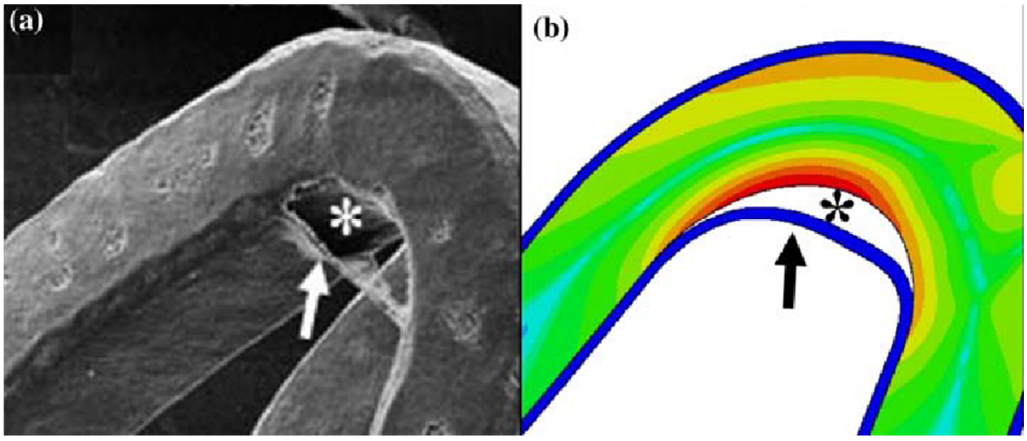

Fig. 1.2 (a) Real stent coating delamination. (b) FEA model of coating delamination [10].

3. Objectives of Research

In this study, a computational model is developed to predict the stress distributions of various components in DES medical devices. Especially, our objective of this thesis is that:

- *FEA computational model development including the coating components in the system to understand the mechanical responses in the drug-polymer coating upon DES deployment.*

Though our focus is on the coating fracture of DES, in the present work, we developed our model to include comprehensive components of the DES + arterial wall system including stent platform, coating, plaque, and arterial walls, to investigate other phenomena such as recoiling and stress distributions in the arterial walls. In developing the model, the necessary elastic and plastic physical properties of constituent materials such as metallic platform, polymer, atherosclerotic plaque, and arterial wall are incorporated. In the following chapters (Chapters 2, 3, and 4), the detailed background, previous modeling efforts, and our model development are addressed, respectively. In the result chapter (Chapter 5), the impacts of geometry and material variables such as coating thickness and material contents in composites on the mechanical performance of the medical device will be discussed.

References

1. B. L. Hoeven, N. M. Pires, H. M. Warda, Drug-eluting stents: results, promises and problems, International Journal of Cardiology 99 (2005) 9-17.

2. T. Parker, V. Dave, R. Falotico, Polymers for Drug Eluting Stents, Current pharmaceutical 16 (2010) 3978-3988.

3. S. Garg, MB, ChB, W. Patrick, Coronary Stents: Current status, Journal of American College of Cardiology 56 (2010).

4. Dangas, G. & Kuepper, F. (2002). Restenosis: Repeat narrowing of a coronary artery. Circulation, 105, 2586-2587.

5. Mauri, L., Silbaugh, T. S., Garg, P., et al. (2008). Drug-eluting or bare-metal stents for acute myocardial infarction.*The New England Journal of Medicine*, 359(13), 1330-1342.

6. Kirtane, A.J., Gupta, A., Iyengar , S., et al. (2009). Safety and efficacy of drug-eluting and bare metal stents: Comprehensive meta-analysis of randomized trials and observational studies. *Circulation*, 119 (25), 3198–3206.

7. Widas, P. (1997). Introduction to Finite Element Analysis.Virginia Tech Material Science and Engineering. Retrieved from

8. Allison C., David C., Julian Gunn. (2004). The influence of physical stent parameters upon restenosis. *PathologieBiologie*, 52, 196-205.

9. Levy, Y., D. Mandler, J. Weinberger, and A. J. Domb. Evaluation of 'drug-eluting stents' coating durability clinical and regulatory implications. *J. Biomed. Mater. Res. B: Appl. Biomater*. 2009 (in press).

10. C. G. Hopkins, P. E. McHugh, J. P. McGarry, Computational investigation of the delamination of polymer coatings during stent deployment, annals of Bio Eng 38 (2010) 2263-2273.

Chapter 2. Drug-Eluting Stents (DES)

Cardiovascular stenting has made a remarkable improvement in the field of coronary disease management during the last several decades. Bare-metal stents (BMSs) were introduced in 1994, but the long-term results have been shattered by the adverse problems including in-stent restenosis (ISR) and stent thrombosis associated with BMSs. Although stent thrombosis became much less frequent after the introduction of antiplatelet therapy, the occurrence of ISR, however, remained as a significant problem. The intense work on stent development has successfully led to the introduction of drug-eluting stents (DES) in 2002, as an effort to address this ISR problem. In this chapter, we provide the basic information of DES and its drug components. In addition, the general development trends of DES will be covered at the later part of this chapter.

1. Components of Drug-eluting Stents (DES)

DES is composed of three main components; stent platform, polymer, and drug. The platform functions as a scaffold to keep a diseased artery open, and the polymer carries the drug while the drug is directly delivered into the injured site. The polymers and drugs typically form a thin composite coating on the platform surface.

1.1 Platform

Available platforms in DES applications are generally made of stainless steel, cobalt-chromium, or platinum-chromium alloys. The platforms made with a thinner strut

may result in less arterial injury and reduce the risk of restenosis, with lower thrombogenicity. Platinum-chromium alloys are used in an effort to improve radial strength and conformability of DES [1].

1.1.1 Platform Geometry (Design)

The type of stents is in general categorized into two groups, self-expanding and balloon-expandable stents. In self-expanding design, stents can be constructed from coil, mesh, or zig-zag configuration, of which an outer sheath forces the stents to elastically spring open into a predetermined size. The balloon-expandable stents are supplied in the crimped form, pre-mounted on a balloon, inflation of which plastically deforms the stent to the size of the inflated balloon [2]. In addition, the balloon-expandable stents may be divided into coil and tube designs. The coils may be fashioned from a continuously wound wire or a series of flat sheet coils. The tube stents are cut from a steel tube or, occasionally, from a flat sheet of metal, which is then rolled into a tube and welded. For the coil stents, the strut width is generally greater than that of the tubular stents, but so are the gaps between the struts, and there are fewer or no connections between the struts [3]. Due to these geometrical characteristics, the coil stents exhibits more flexibility, but they have a poor radial strength and they allow tissue prolapse between the widely-spaced wire elements. The differences between these coil and tube stents are schematically described in Fig. 2.1.

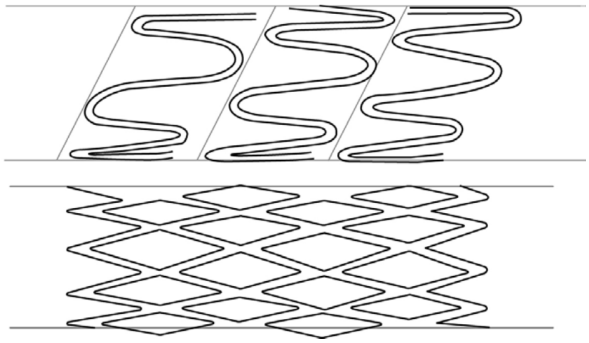

Fig. 2.1 Example of coil (top) vs tube (bottom) designs of stents. (Adopted from A. C. Morton et al. 2004 [4])

Moreover, the tubular balloon-expandable stents may be divided into 'slotted tube' and 'modular tube' designs. Both are laser-cut from a tube of metal, although some modular designs are composed of rings of wires that are welded together. The distinction between 'slotted tube' and 'modular tube' is less clear in modern stent designs because the tubes can be cut with few links and 'open cell' designs to produce a quasi-modular structure. The slotted tube stents with 'closed cell' designs, such as the NIR (Medinol/Boston Scientific) and Bx Velocity (Cordis/Johnson and Johnson) are close to the original concept of a slotted tube. On the other hand, the 'open cell' designs, such as the Multilink Penta (Guidant), are more like a modular stent. Fig. 2.2 illustrates examples of closed- and open-cell designs of stents. The slotted tubes, in particular, with a closed cell design, are inherently less flexible than a modular design, but much ingenuity has been exercised in designing articulations for the slotted stents with either closed- or open cell design to provide reasonable flexibility. It seems that both stents have retained their popularity in the latest generation of stents [5]. Recently, the number of curves on a ring for DES has been increased as it could increase the stent radial force and the potential surface area for DES and it may decrease neointimal proliferation. In the meantime, a

thickness of strut is decreasing as it can decrease the inside injury of vessel after implementing. However, reducing the thickness of a strut has certainly limitations due to the strut fatigue and variation with the types of metal used.

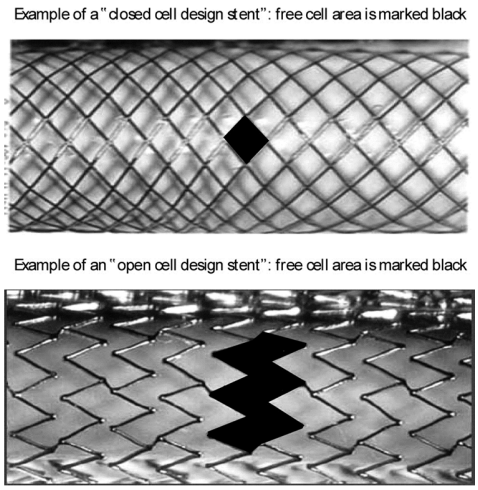

Fig. 2.2 Examples of a closed-cell design stent (top) and an open-cell design stent (bottom). The black shaded areas represent free cell area of stents.

1.1.2 Platform Material

There are many required properties for relevant materials used in stent platform. It is critical to obtain not only the biocompatibility or biostability for the platform material, but also the balance between radial strength and deformability for the thicknesses required for stent manufacture, without a tendency to corrode. For the last 15 years, the standard material applied to balloon-expandable stents was 316L stainless steel that meets the criteria mentioned above. However, visualizing the small stainless steel devices under X-ray fluoroscopy was a challenge. It this early stage, flexibility was listed as one of the principal requirements of a stent, so as to easily track through the guide catheter and through the tortuous anatomy of the coronary arteries. Improved flexibility may be

achieved by reducing stent strut thickness when the strength of the material allows for such reductions. Thinner struts result in even less X-ray attenuation, further reducing device visibility during deployment. These conflicting requirements of reducing strut thickness, while maintaining or improving device radiopacity, were initially addressed by the addition of highly radiopaque materials such as tantalum, platinum, or gold, in manufacturing coatings or marker bands.

Coatings on a stent strut appeared to offer the ideal solution, allowing radiopacity to be tuned in proportion to coating thickness. Gold (Au), one of the most inert metals, has been studied as a potentially neutral stent coating. However, surprisingly, it has been reported that Au is associated with increased rates of ISR and thrombosis [6]. Likewise, the properties of stainless steel stents interfaced with other metals can be influenced by the surface metals in terms of the possibility of ISR and/or thrombosis. As the main constituent of stents, the supremacy of stainless steel (i.e., 316L) is now being challenged by the advanced alloys of cobalt, chromium and platinum. These metals with a thinner strut can provide a similar mechanical property to stainless steel. The ISAR-STEREO trial demonstrated the advantage of thinner struts for patient outcomes, that is, thinner struts resulted in lower restenosis rates compared to thicker struts [7]. It was hypothesized that thinner struts resulted in lower vascular injury and therefore less subsequent neointimal growth. With the thinner struts now being linked to both improved procedural and clinical outcomes, the development of the stent material became focused on higher strength alloy as it was becoming evident that the moderate yield strength of 316L stainless steel would become a limiting factor. Specifically, it would not be possible to maintain stent compression strength in 316L devices with thinner flexible struts. In

addition, thin-walled 316L devices will lead to undesirably low radiopacity. The effort to find the alloys with a higher strength with improved X-ray attenuation compared to 316L, initially resulted in the selection of the commercially available cobalt-chromium based alloys such as L605 (Co-20Cr-15W-10Ni) and MP35N® (Co-20Cr-35Ni-10Mo). Sketch et al. [8] reported on the first clinical usage of a L605 stent in 2003, demonstrating the benefits of the reduced strut thickness achievable with this material. It was subsequently followed by a study comparing devices made from MP35N® against these L605 stents, which showed the comparable long-term performance of both devices [9]. The introduction of these higher strength materials had facilitated the development a new generation of stents with the thinner strut thicknesses in the range of 80-90 μm, compared to the strut thicknesses of 130-140 μm for the earlier 316L devices. While these Co-Cr materials possess higher radiopacity than 316L, the diminution of the strut thickness from 316L to Co-Cr materials was relatively moderate. It can be proven by the comparison of the density values; 9.1 g/cm^3 and 8.4 g/cm^3 for L605 and MP35N®, respectively, and 8.0 g/cm^3 for 316L [10]. In searching for further improvements in radiopacity with a high strength, a new alloy was tailored specifically, for stent applications in mind. These alloys are typically based on stainless steel, but in many cases, platinum is substantially added to enhance both the mechanical (i.e., tensile) properties and radiopacity [11].

Other than metallic materials, polymeric materials also have been applied to the stent platform. The first generation of polymer stents, using materials such as polyester (PE), revealed some promises on its mechanical properties [12]. Unfortunately, however, most of these polymers elicited a marked local inflammatory response with excessive neointimal formation [13]. There has been a recent revival of the interest in

biodegradable polymer stents. A study of the physical properties of a poly-L-lactic acid (PLA) stent showed some favorable results in inclusion of a collapse pressure of >2 atm; a value similar to that of a metal Multilink Tetra stent (Guidant; slotted tube) [14]. If the stent platform material is made of non-radiopaque such as biodegradable polymer, it needs to have radiopaque markers at the proximal and distal ends of the stent. The corrosion phenomenon is, in addition, another important factor, and therefore, it is considered as essential to select a material that would develop a passive oxide layer to avoid the corrosion.

1.2 Polymer Coatings: Drug Delivery Vehicle

In general, it is known that percutaneous transluminal coronary angioplasty (PTCA) cannot be operated without damaging blood vessels and eliciting restenosis. Drug elution at the target site is a clear solution to this problem. As a result, most of currently approved DES consist of a metallic scaffold surrounded by polymer matrix containing drug. Polymer coatings are required for most drugs because they do not easily adhere to the metallic stent surface. The polymer coating also modifies and controls drug elution kinetics, which can be varied by using multiple polymer layers to achieve optimal drug release over time. These polymers bind the drug to the stent and modulate the elution of the drug to the arterial tissue. Polymer has advantageous characteristics as drug delivery vehicle for DES such as biocompatibility, metabolization in the body, minimal drug release into the circulation, no alteration of incorporated drug activity and structural and operational stent characteristics, competitive adhesion to the stent material of choice, and surface finish, and etc.

The aforementioned characteristics of polymer may be closely aligned with the required features of drug delivery vehicle for DES applications. Taking advantage of these beneficial properties, the polymeric materials have been widely used as drug delivery vehicles in DES. There are two types of drug delivery vehicles; *i)* non-absorbable biostable polymer coating and *ii)* biodegradable polymer coating. The non-absorbable biostable polymer coating is a technically simpler design, which leads to easier handling and applying onto the struts. However, in the non-absorbable biostable polymer coating, the coated drug is passively diffused to the treated vessel, which can lead to the necessity of manipulating the diffusion rate of the drug by controlling the polymer architecture and/or porosity of the top coat. The biodegradable polymer coating method, on the other hand, improves dosing consistency and is able to support a customized diffusion pattern of the drug. Also, the multi-drugs can be coated and delivered simultaneously and sequentially. With the biodegradable polymer coating, the coated drug is diffused via the surface and/or bulk erosion, and the composition of the polymer is intentionally controlled to manipulate the delivery rate of the drug.

In recent years, the biodegradable polymer coating has received much more attention as drug delivery vehicle to improve the performance of DES. It comes from the characteristic that biodegradable polymers can be hydrolyzed with ease into metabolized molecular weight degradation products in a body. This characteristic also, leads to the fact that a biodegradable delivery system does not have to be removed after completion of drug release. In vitro studies showed that biodegradable polymers were highly biocompatible in a porcine coronary artery model and the histopathological evaluation showed only a mild inflammatory response. The extent of ISR in a single polymer

coating stent was comparable with that of bare metal stents. More seriously, the clinical adverse effects including ISR and thrombosis are often observed from the patients implanted with non-degradable polymer DESs. However, unfortunately, some adverse reactions may be caused by both of these polymers. It has been reported that, in an early stage of the polymeric DES implantation, both biodegradable and non-biodegradable polymers could cause a deteriorated inflammatory reaction and neo-intimal proliferation [14]. In this next sub-sections, the general requirements, types, and the current trend of using polymers as a drug carrier in DES system will be discussed.

1.2.1 Requirements for a polymer used in a DES

For the successful commercial DES products, the materials chosen to deliver the drug from the stent must meet several key requirements, including physical properties, stability (processing, aging, and sterilization), non-reactivity with the incorporated drug, process compatibility, biocompatibility with vascular tissue, and the ability to control the elution of drug from the stent. In Fig. 2.3, the illustration is presented to address the important factors for the polymers used in DES applications.

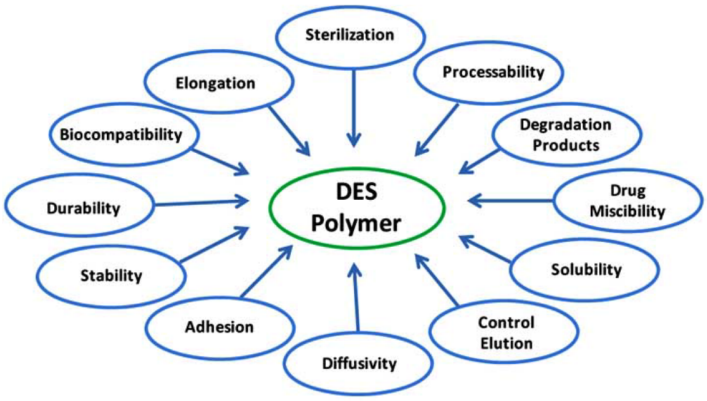

Fig. 2.3 Required polymer properties in DES medical device applications (schematics adopted from T. Parker et al. 2010 [14])

1.2.1.1 Physical properties

First of all, the polymer must not adhere to the deployed balloon at storage and processing temperatures. In the meantime, the polymer must accommodate stent deformation during deployment without cracking or peeling, and must adhere strongly to the stent surface, generally stainless steel or Pt-Cr alloy, or to a primer layer such as poly(butyl methacrylate) (PBMA).

1.2.1.2 Stability

The polymer coating must remain stable during processing, storage and use (coating, crimping, sterilization, packaging, shelf storage and stent deployment). Stability infers no change in chemical composition (e.g., oxidation), physical integrity of the coating, or distribution of drug in the coating. For most DES, solvents are used to apply the polymer-drug mixture to the stent. For the chemical stability with the polymer and stent, the type of solvents must be carefully considered. Since DESs are sterilized in the later stage of manufacturing, the polymer matrix must be stable to ethylene oxide, electron beam, or gamma irradiation [14]. Often the choice of polymer will be dictated by the desired mode of sterilization and the potential for polymer reactivity or degradation.

1.2.1.3 Compatibility with the drug

The polymer needs to remain physically and chemically compatible with the incorporated drug. Physical compatibility requires the invariability of the drug-polymer morphology after manufacturing in any way that may adversely affect the drug release profile. Chemical compatibility requires a lack of chemical reactivity between polymer

and drug during processing or shelf storage. Generally, this is not a problem for hydrocarbon- or fluorocarbon-based matrices due to the stability of C-H and C-F bonds, but polymers may contain the functional groups (such as esters, amides, anhydrides, etc.) that could react with the drug [14]. Consequently, the drugs that contain a reactive functional group need to be evaluated for the long-term chemical stability to ensure that no polymer-drug adducts are formed.

1.2.1.4 Biocompatibility with vascular tissue

When DESs are implanted in arteries, the polymers are in direct contact with the vessel wall. Therefore, it is critical to maintain good biocompatibility in a long-term period. Vascular compatibility of the polymer must be extensively evaluated using in vitro and in vivo test methods. Animal safety testing will determine the potential of the polymer coating to inhibit re-endothelialization, induce inflammation and produce vessel injury or necrosis over a period of one to six months or longer. The extrapolation of animal data to human safety must be carefully conducted because certain species may be more prone to inflammation after the implantation of foreign materials than other species. The demonstration of long-term safety in humans may require years to ascertain.

While a biostable polymer has its limitation on the permanent fixity onto the implanted DES, a bioabsorbable polymer arouses the necessity of considering the degradation products and degradation time. In evaluating the biocompatibility of bioabsorbable polymer systems, it is important to test the final drug/polymer formulation in preclinical models for the entire resorption period of the polymer.

1.2.1.5 Control of drug elution

Drug release is controlled by the physiochemical properties of the specific drug and the polymer, particularly the morphology of the drug-polymer mixture. To be effective, the polymer matrix must control the elution of the drug and provide the desired concentration and release profile to produce the maximal therapeutic benefit. Generally, it has been determined through clinical experiences that a rapid burst release of a drug from a DES is far less effective when compared to sustained release. For instance, it has been found that, for paclitaxel used to treat restenosis, a sustained release of at least 30 days can safely and effectively attenuate neointimal hyperplasia and minimize restenosis [14].

1.2.2 Types of polymers

1.2.2.1 Non-biodegradable polymers

In the area of non-absorbable, biostable, permanent polymers, a variety of chemical classes have been used as a drug carrier for a local delivery [15, 16]. Although a particular polymer may be tolerated in another location of the body, for DES application, the polymer material must be hemocompatible, non-thrombogenic, and non-inflammatory. A limited number of biocompatible polymers are commercially used in DES products (available in the US) as shown in Table 2.1.

Stent	Company	Polymer Matrix Composition	Year
Cypher	Cordis	PEVA[a]+ PBMA[b]	2003
Taxus® / Taxus Liberte®	Boston Scientific	SIBS[c]	2004
Xience V	Abbot Vascular	PVDF-HFP[d]	2008
Promus	Boston Scientific	PVDF-HFP	2009
Endeavor	Medtronic	Methacrylated phosphorylcholine-based (PC (cross-linked))	2009

Table 2.1 Permanent polymers used as the drug delivery matrix for DES products approved in the US [12]. In the Table, the symbols represent as, a: Poly(ethylene-co-vinyl acetate); b: Poly(n-butyl methacrylate); c: Poly(styrene-block-isobutylene-block-styrene); d: Poly (vinylidene fluoride-co-hexafluoropropylene)

1.2.2.2 Biodegradable polymers

One of the potential advantages of biodegradable polymers comes from the fact that they provide a matrix to release a drug, and then, fully degrade over time. It can, therefore, eliminate the concerns about vascular biocompatibility in a long term period. The selection of a biodegradable polymer for a drug-eluting device is based on the degradation mechanism, degradation time, time-dependent physical properties, and processing conditions (drug-polymer interaction and stability). There is a myriad of the factors that will affect the degradation of the polymers including chemical composition, distribution of repeat units, presence of ionic groups, presence of chain defects, molecular weight and molecular weight distribution, morphology (amorphous/semi-crystalline; microstructure, etc), presence of low molecular weight compounds, processing conditions, annealing, shape and surface area, sterilization process, storage history, implantation site, and mechanism of hydrolysis [17].

Biodegradable polymers can fall into bulk-erodible and/or surface-erodible materials in terms of degradation mechanism [18]. Theoretical models have been developed to predict the erosion mechanism of water insoluble bioabsorbable materials [19,20]. Surface erosion polymers are typically hydrophobic with water labile linkages. Hydrolysis tends to occur quickly on the surface of surface erodible polymers with no water penetration in bulk. A summary of the different polymer systems for a controlled drug release has been provided in the review article [21]. The typical examples of surface-erodible polymers include polyanhydrides [22-24] such as poly(carboxyphenoxy hexane-sebacic acid), poly(fumaric acidsebacic acid), poly(carboxyphenoxy hexane-sebacic acid), poly (imide-sebacic acid), and poly(imide-carboxyphenoxy hexane), and polyorthoesters (POE) [25]. Bulk-erodible polymers, on the other hand, are typically hydrophilic with water labile linkages. Hydrolysis of bulk-erodible polymers tends to occur more uniformly across the polymer matrix of the device. The examples of bulk-erodible polymers include poly(α-hydroxy esters) such as poly(lactic acid) (PLA), poly(glycolic acid) (PGA), and poly(lactic acid-co-glycolic acid) (PLGA), and also poly(caprolactone) (PCL), poly(pdioxanone) (PDO), poly(trimethylene carbonate) (PTMC), poly(oxaesters), poly(oxaamides), and their co-polymers and blends [26]. The most widely used bioabsorbable polymers for drug eluting stents are from the poly(α-hydroxy ester) family of materials that include poly(lactic acid) (L-PLA and DL-PLA) and their copolymers (PLGA).

Stent	Company	Polymer/Drug Matrix Composition
Biomatrix™	Biosensors	DL-PLA/Biolimus A9
Epitome™	Elixir	Polyester/Myolimus
Genous™	OrbusNeich	SynBiosys™/Sirolimus/anti-CD-34
Infinnium™	Sahajanand	DL-PLA/Paclitaxel
JACTAX™	Labcoat	DL-PLA/Paclitaxel
NEVO™	Cordis	DL-PLGA/Sirolimus
Nobori™	Terumo	DL-PLA/Biolimus A9
Sparrow™	CardioMind	SynBiosys™/Sirolimus
Supralimus™	Sahajanand	DL-PLGA/Sirolimus

Table 2.2 Biodegradable Polymer Coatings for DES [27].

Recently, a number of drug eluting stents has been developed using bioabsorbable polymers [28,29], which is summarized in Table 2.2. PLGA is a widely investigated biodegradable polymer that has been used in a variety of the approved biomedical applications, including absorbable sutures, orthopedic devices and controlled drug delivery implants [30-33]. PLGA consists of a broad family of the polymers with varying ratios of lactide and glycolide monomer and a range of molecular weights. The ratio of lactide of glycolide co-monomer units determines the rate of PLGA hydrolysis and degradation, as well as the drug elution profile. It has been found that bioresorption time is fastest for the 50/50 mole ratio copolymer, and slows as the proportion of lactide is increased [34,35]. Additionally, the drug type can affect the degradation rate of PLGA matrices [36], as can irradiative sterilization [37]. In vivo, PLGA is degraded by random hydrolytic scission of the ester linkages to oligomers of successively lower molecular weight. The ultimate fate of PLGA in the body is the degradation to lactic acid and glycolic acid residues that are subsequently fully metabolized via the Krebs cycle to carbon dioxide and water [38,39].

1.3 Drugs

In DESs, the drug melded in the polymer is a biologically active agent to inhibit arterial neointimal hyperplasia by suppressing platelet activation, inflammatory response, smooth muscle cell migration, and proliferation in an artery. Ideally, the drug should have an outstanding overall safety profile and a broad therapeutic window. Besides the biological effects, the drug has its own chemical properties that influence achieving optimal tissue concentrations and the possibilities for loading on a stent. Some drugs can be loaded directly onto the metallic surface of the stent, but most drugs need a polymer coating, which forms a reservoir for them.

Local delivery of a drug using a DES provides both biological and mechanical solution and has emerged as a very promising approach effective in management of ISR. For the local drug delivery to be successful, the challenges to be addressed include the *(i)* decision on the most appropriate agent to be use, *(ii)* determination of the proportion of the systemic dose needed locally, and *(iii)* identification of a biocompatible vehicle that can deliver drug for the required therapeutic window [40,41]. Four classes of the drugs (anti-inflammatory, anti-thrombogenic, anti-proliferative, and immunosuppressive) are generally considered as a candidate to be used in DES. These drugs inhibit one or more biochemical pathways leading to restenosis. Some studies have been also, conducted using antibodies blocking specific receptors as active compounds [42]. Several reports have been published evaluating these drugs regarding their release kinetics, effective dosage, safety in clinical practice, and benefits [42-44]. In the next sub-sections, some information about the commonly used drugs in DES applications will be provided.

1.3.1 Paclitaxel

Paclitaxel, a lipophilic molecule derived from the Pacific yew tree *Taxus brevifolia*, is a very common component of chemotherapy for cancer treatment. The vascular compatibility and efficacy of paclitaxel in reducing neointimal hyperplasia after balloon and stent mediated injury have been shown both in vitro and in vivo [43]. The mode of action is the polymerization of the α- and β- units of tubulin, thereby stabilizing microtubules that are needed for G2 transition into M-phase. Paclitaxel is also able to inhibit the proliferation and the migration of smooth muscle cells because of the structural changes in the cytoskeleton, one of the major steps in the development of atherosclerosis and restenosis [44,45].

1.3.2 Sirolimus/rapamycin

Till date, the six drugs of the limus family have been studied including sirolimus, zotarolimus, everolimus, biolimus A9, tacrolimus, and pimecrolimus [46]. Sirolimus, also called rapamycin, is a macrocyclic antibiotic with the potent immunosuppressive properties. It acts as a pro-drug that binds to specific cytosolic proteins (FK-506 binding protein-12), which blocks the cell proliferation. Rapamycin also inhibits several phases of the restenosis cascade, such as inflammation, neointimal hyperplasia formation, total protein and collagen synthesis, and migration of smooth muscle cells. Sirolimus is also a strong inhibitor of inflammation without cellular toxicity in a low dose [44,45,47].

1.3.3 Zotarolimus and everolimus

Zotarolimus and everolimus are analogues of rapamycin. Both have a similar action mechanism for the prevention of restenosis. They bind to cytosolic FK-506 binding protein-12 and inhibit the proliferation of smooth muscle cells and T-cells. The compound with them has also higher noctanol/water partition coefficients than rapamycin that favors a slow release from the stents. Despite the structural changes, the biological activity of rapamycin was retained. The slow rate of release and subsequent diffusion of the molecule facilitates the maintenance of the therapeutic drug level from the stent. In addition, its lipophilic character favors crossing cell membranes to inhibit neointimal proliferation of the targeted tissue [1,22,40].

2. Current Commercial DES Products

2.1 General trend of DES development

The development of DES in the industry can be categorized into three stages in a time order; first, second, and third generation of DES. The potential of the first generation stents to cause thrombosis due to a permanent polymer has led to extensive researches in developing the new polymers. These efforts have led to the second generation of DESs that have more biocompatible non-erodible polymers, which have been shown in the animal studies to have a greater degrees of re-endothelialization compared to the first generation stents [48]. The researches afterward have also led to the design of the third generation DESs that have a biodegradable polymer or novel coating, or are completely polymer-free. Table 2.3 shows the summary of the specific names of the products and types of the drugs that have been applied, and Fig. 2.4 shows the images

of the various commercial DESs. The general trend nowadays, prefers a thinner strut than the thicker since it reduces the induced stress on an artery wall and plaque so that the rate of restenosis and thrombosis could be decreased. In general, the mechanical properties of a stent material are weakened if the thickness of the strut becomes thinner. Therefore, the alternative materials, such as Pt-Cr alloy, are developed so as to replace the conventional metals such as 316L stainless steel. As mentioned above, the tensile properties and density of this Pt-enhanced alloy compare favorably, with stainless steel and Co-Cr alloys. It enables the stent designs to have both thinner strut and higher radiopacity. The design used for the stent platform also changed from the slotted tube-like to the crown-shaped to obtain more blood flow.

	First generation	**Second generation**	**Third generation**
Drug used	Sirolimus, Paclitaxel	Zotarolimus, Everolimus	Biolimus, Everolimus
Material/design used for platform	Stainless steel/ slotted Tube design	Co-Cr/ thin struts stents	Pt-Cr, Ni-Ti, etc
Polymers used	Durable	Persistent	Biodegradable polymer coated DES, Polymer free & Biodegradable DES
Commercial products	Cypher, TAXUS	Endeavor, Xience V	SYNERGY, Biomatrix Flex

Table 2.3 The generations of DES [revised from Khan (2012, pp.704)] [27]

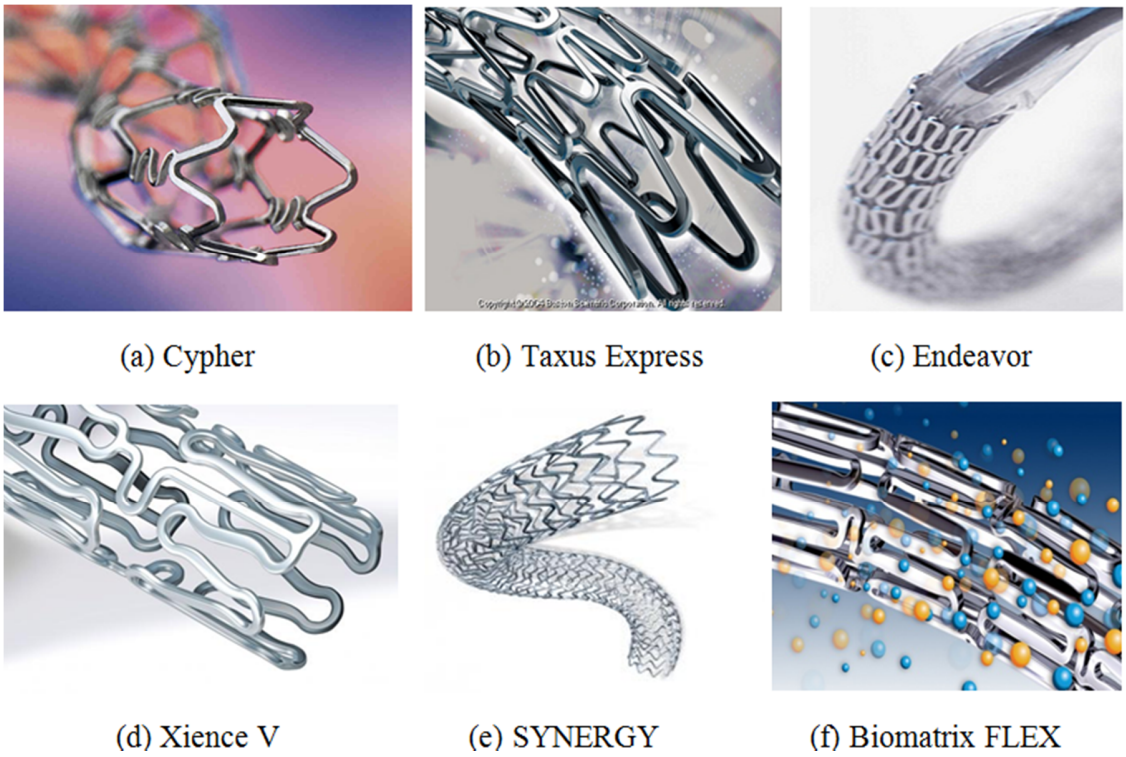

Fig. 2.4 Several types of commercial DES [49].

2.2 Future stents

Although the first-generation DESs achieved higher efficacy in reducing the occurrence rate of ISR, the long-term safety issue has arisen, learning these devices stand in a delicate balance of the occasionally conflicting key properties of deliverability, efficacy and, safety. As part of an effort to resolve these issues, there are various trends leading to various improved DES platforms; e.g., DESs with more biocompatible stent coatings, new metallic platforms, new drug combinations, biodegradable polymers, and polymer-free and/or fully-biodegradable DESs. Most of these devices are under investigation in clinical trials, and recently, some of them have become commercially available for the clinical use. Although the best DES has yet to be identified, it will

probably, incorporate many of the modern materials and delivery systems described earlier to enhance the safety, efficacy and cost-effectiveness. The ideal DESs should be composed of the backbone that provides adequate radial strength, deliverability, and radiopacity with a minimal vessel wall injury. The drug vehicle should have an ideal drug release that does not result in inflammatory response, and the drug or the drug combination should inhibit smooth muscle cell proliferation and inflammation effectively without delaying re-endothelialization or causing endothelial dysfunction. By combining the new drug carriers and structural design improvements with a modern mechanical and manufacturing approach, the development of an ideal DES appears to proceed in an iterative fashion; with slow but continuous improvements for this revolutionary class of the medical device.

References

1. The New England journal of medicine, Drug-Eluting Coronary-Artery stents, Giulio G. Stefanini, M.D., and David holmes, Jr., M.D. 368;3 2013

2. A.E. Alahmar, A.D. Grayson, M. Andron, M. Egred, E.D. Roberts, B. Patel, R.K. Moore, K. Albouaini, M. Jackson, R.A. Perry, Reduction in mortality and target-lesion revascularization at 2 years: a comparison between drug-eluting stents and conventional bare-metal stents in the "real world", Int. J. Cardiol. 132 (3) (2009) 398–404.

3. Mosseri M, Rozenman Y, Mereuta A, et al. New indicator for stent covering area. Cathet Cardiovasc Diagn 1998;44:188–92.

4. A. C. Morton, D. Crossman, J. Gunn, The influence of physical stent parameters upon restenosis, Pathologie Biologie (52) (2004) 196-205.

5. Kandzari DE, Tcheng JE, Zidar JP. Coronary artery stents: evaluating new designs for contemporary percutaneous intervention. Cathet Cardiovasc Interv 2002;56:56276.

6. Kastrati A, Schomig A, Dirschinger J, et al. Increased risk of restenosis after placement of gold-coated stents. Circulation 2000;101:2478–83.

7. Kastrati A, Mehilli J, Dirschinger J, Dotzer F, Schuehlen H, Neumann FJ, et al. Intracoronary stenting and angiographic results: strut thickness effect on restenosis outcome (ISAR–STEREO) trial. Circulation 2001;103:2816–21.

8. Sketch MH, Ball M, Rutherford B, Pompa JJ, Russell C, Kereiakes DJ. Evaluation of the medtronic (driver) cobalt–chromium alloy coronary stent system. Am J Cardiol 2005;95:8–12.

9. Craig CH, Radisch HR, Trozera TA, Turner PC, Govier RD, Vesely EJ, et al. Development of a platinum-enhanced radiopaque stainless steel. (Stainless steels for medical and surgical applications, ASTM STP 1438. West Conshohocken, PA: ASTM; 2003. pp. 28–38.

10. B. J. O'Brien, J. S. Stinson, S. R. Larsen, M. J. Eppihimer,, W. M. Carroll, A platinum-chromium steel for cardiovascular stents, Biomaterials 31 (2010) 3755-3761

11. B. J. O'Brian, J. Stinson, S. R. Larsen, M. J. Eppihimer, W. M. Carroll, Biomaterials, A platinum-chromium steel for cardiovascular stents (31) (2010) 3755-3761

12. Van der Giessen WJ, Slager CJ, Gussenhoven EJ, et al. Mechanical features and in vivo imaging of a polymer stent. Int J Card Imaging 1993;9:219–26.

13. Van der Giessen WJ, Lincoff AM, Schwartz RS, et al. Marked inflammatory sequelae to implantation of biodegradable and non-biodegradable polymers in porcine coronary arteries. Circulation 1996;94:1690–7.

14. T. Parker, V. Dave, R. Falotico, Polymers for Drug Eluting Stents, Current Pharmaceutical Design (16) (2010) 3978-3988

15. Kuehler M, De Scheerder I. Drug delivery coatings. USA: Taylor & Francis 2003.

16. Shen WX. Controlled drug delivery systems. Lancaster, Pennsylvania: Technomic Publishing Co. 1996.

17. Brannon-Peppas L. Polymers in controlled drug delivery. Medical Device and Diagnostic Industry 1997.

18. Langer R. Biomaterials and biomedical engineering. Chem Eng Sci 1995; 50(24): 4109-21.

19. Gopferich A. Mechanisms of polymer degradation and erosion. Biomaterials 1996; 17(2): 103-14.

20. von Burkersroda F, Schedl L, Gopferich A. Why degradable polymers undergo surface erosion or bulk erosion. Biomaterials 2002; 23(21): 4221-31.

21. Uhrich KE, Cannizzaro SM, Langer RS, Shakesheff KM. Polymeric systems for controlled drug release. Chem Rev 1999; 99(11): 3181-98.

22. Tamada J, Langer R. The development of polyanhydrides for drug delivery applications. J Biomater Sci Polym Ed 1992; 3(4): 315-53.

23. Staubli A, Mathiowitz E, Lucarelli M, Langer R. Characterization of hydrolytically degradable amino acid containing poly(anhydrideco- imides). Macromolecules 1991; 24: 2283-90.

24. Anastasiou T, Uhrich K. Novel polyanhydrides with enhanced thermal and solubility properties. Macromolecules 2000; 33: 6217- 21.

25. Schwach-Abdekkaoui K, Heller J, Gurny R. Hydrolysis and erosion studies of autocatalyzed poly(orthoesters) containing lactoyllactyl acid dimers. Macromolecules 1999; 32: 301-7.

26. Middleton JC, Tipton AJ. Synthetic biodegradable polymers as medical devices. Med Plastics Biomater 1998.

27. W. Khan, S Farah, A. J. Domb, Drug eluting stents: Developments and current status, J Bontrolled Release (161) (2012) 703-712.

28. Daemen J, Serruys PW. Drug-eluting stent update 2007: part I. A survey of current and future generation drug-eluting stents: meaningful advances or more of the same? Circulation 2007; 116(3): 316-28.

29. O'Brien B, Carroll W. The evolution of cardiovascular stent materials and surfaces in response to clinical drivers: a review. Acta Biomater 2009; 5(4): 945-58.

30. Middleton JC, Tipton AJ. Synthetic biodegradable polymers as orthopedic devices. Biomaterials 2000; 21(23): 2335-2346.

31. Jeong B, Bae YH, Lee DS, Kim SW. Biodegradable block copolymers as injectable drug-delivery systems. Nature 1997; 388(6645): 860-2.

32. Berges R, Bello U. Effect of a new leuprorelin formulation on testosterone levels in patients with advanced prostate cancer. Curr Med Res Opin 2006; 22(4): 649-55.

33. Southard GL, Dunn RL, Garrett S. The drug delivery and biomaterial attributes of the ATRIGEL technology in the treatment of periodontal disease. Expert Opin Investig Drugs 1998; 7(9): 1483- 91.

34. Li S. Hydrolytic degradation characteristics of aliphatic polyesters derived from lactic and glycolic acids. J Biomed Mater Res 1999; 48(3): 342-53.

35. Lu L, Garcia CA, Mikos AG. In vitro degradation of thin poly(DLlactic-co-glycolic acid) films. J Biomed Mater Res 1999; 46(2): 236-44.

36. Siegel SJ, Kahn JB, Metzger K, Winey KI, Werner K, Dan N. Effect of drug type on the degradation rate of PLGA matrices. Eur J Pharm Biopharm 2006; 64(3): 287-93.

37. Loo JS, Ooi CP, Boey FY. Degradation of poly(lactide-coglycolide) (PLGA) and poly(L-lactide) (PLLA) by electron beam radiation. Biomaterials 2005; 26(12): 1359-67.

38. Shive MS, Anderson JM. Biodegradation and biocompatibility of PLA and PLGA microspheres. Adv Drug Deliv Rev 1997; 28(1): 5-24.

39. Jain RA. The manufacturing techniques of various drug loaded biodegradable poly(lactide-co-glycolide) (PLGA) devices. Biomaterials 2000; 21(23): 2475-90.

40. D. Teomim, I. Fishbien, G. Golomb, L. Orloff, M. Mayberg, A.J. Domb, Perivascular delivery of heparin for the reduction of smooth muscle cell proliferation after endothelial injury, J. Control. Release 60 (1) (1999) 129–142.

41. C.A. Kavanagh, Y.A. Rochev, W.M. Gallagher, K.A. Dawson, A.K. Keenan, Local drug delivery in restenosis injury: thermo responsive co-polymers as potential drug delivery systems, Pharmacol. Ther. 102 (1) (2004) 1–15.

42. E. Grube, U. Gerckens, R. Muller, L. Bullesfeld, Drug eluting stents: initial experiences, Z. Kardiol. 91 (Suppl. 3) (2002) 44–48.

43. G.W. Stone, S.G. Ellis, D.A. Cox, J. Hermiller, C. O'Shaughnessy, J.T. Mann, M. Turco, R. Caputo, P. Bergin, J. Greenberg, J.J. Popma, M.E. Russell, A polymerbased,paclitaxel-eluting stent in patients with coronary artery disease, N. Engl. J. Med. 350 (3) (2004) 221–231.

44. E. Deconinck, J. Sohier, I. De Scheerder, G. Van den Mooter, Pharmaceutical aspects of drug eluting stents, J. Pharm. Sci. 97 (12) (2008) 5047–5060.

45. B.L. van der Hoeven, N.M. Pires, H.M. Warda, P.V. Oemrawsingh, B.J. van Vlijmen, P.H. Quax, M.J. Schalij, E.E. van der Wall, J.W. Jukema, Drug-eluting stents: results, promises and problems, Int. J. Cardiol. 99 (1) (2005) 9–17.

46. C. Tamburino, D. Capodanno, Evolution of stents: past, present and future, Expert. Rev. Cardiovasc. Ther. 7 (5) (2009) 443–446.

47. L.K. Pendyala, X. Yin, J. Li, J.P. Chen, N. Chronos, D. Hou, The first-generation drug-eluting stents and coronary endothelial dysfunction, JACC Cardiovasc. Interv. 2 (12) (2009) 1169–1177.

48. Joner M, Nakazawa G, Finn AV, et al. Endothelial cell recovery between comparator polymer-based drug-eluting stents. J Am Coll Cardiol 2008;52:333– 42.

49. (a) http://www.startribune.com/business/123908064.html?refer=y, (b) http://www.scoopweb.com/Drug-eluting_stent, (c) http://www.bloomberg.com/news/2012-01-17/fda-misses-deadline-in-clash-with-device-makers-over-review-cost.html (d) http://www.dicardiology.com/article/rising-cost-inpatient-care-linked-medical-devices-not-imaging (e) http://www.multivu.com/mnr/43510-boston-scientific-fda-promus-element-plus-platinum-chromium-stent-system (f) http://market.peto.co.uk/Clinical/Medical_Surgical_Equipment/Cardiology_Vascular_imaging_interventional_cardiac_catheterization_lab/Drug-Eluting_Stents/AA548BMX-2224.html?tab=substitute

Chapter 3. Previous Models

This chapter contains a review of previous FEA models for DES applications. Numerous models and theories using FEA have been proposed to address various aspects (i.e., mechanical and pharmaceutical) of DES implantation. Here in our review, only some important previous studies are introduced. For convenience, we have categorized the previous models into two groups; models without and with arterial wall systems. At the end of the Chapter, a brief summary on the prior FEA modeling efforts is also provided.

1. Models without Arterial Wall System

FEA models that do not include arterial wall system are relatively simpler than the models with cardiovascular environment systems. Due to the limitation of computational resources, the maximum number of elements in the system must be considered during the analysis. In this sense, the models without arterial wall system have an advantage in evaluating the performance of stent platform itself since much more number of elements can be applied to it.

1.1 C. Dumoulin and B. Cochelin, 2000 [1]

Dumoulin and Cochelin [1] have opened the area of study of FEA application for stent in 2000. The objective of their study was to evaluate the long-term performance and the deployment characteristics of a Palmaz-Schatz stent (Johnson & Johnson, New Brunswick, NJ, USA) during free expansion. The simplest of the numerical models

considered in this study was based on the repeating unit cell of the Palmaz-Schatz stent and applied internal pressure load on its inner surface so as to achieve expansion. This stent product appears like a little slotted metallic tube with diamond-shaped cells after expansion (Fig. 3.1). The decision to consider only the repeating unit cell of the stent was justified after the investigators examined the in vitro expansion of a Palmaz-Schatz stent, concluding that it was almost uniformly expanded and evenly dilated, except at its distal ends. They calculated and compared the results of radial and longitudinal recoil rates with the manufacturer's data. Additional numerical models were then proposed to evaluate the buckling and fatigue life of the Palmaz-Schatz stent.

- This study is meaningful because it is considered as the first attempt to apply FEA for stent medical devices to predict their mechanical performance. The comparison of radial and longitudinal recoil rates between computation and manufacturer's experimental data was successfully conducted. However, the developed model in this study only has the stent strut without the existences of artery, plaque, and coating components. In addition, the evaluation of stresses on stent strut is not included as well. Still, the numerical results reported in this study are widely cited in many literatures to demonstrate that stent-free expansion may be accurately simulated using FEA.

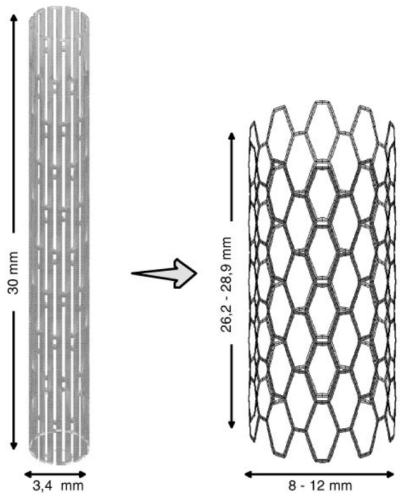

Fig. 3.1 Initial and expanded configuration of the stent with expanded range size; with expansion, the staggered slots in the wall assume a diamond shape (Figure adopted from C. Dumoulin et al., 2000 [1]).

1.2 Migliavacca et al., 2002 [2]

The model presented by Migliavacca et al. [2] has an investigation of the effect of geometrical parameters such as metal-to-artery ratio, strut thickness and cell length on the deployment characteristics of a Palmaz-Schatz stent. In addition, this study has a comparison with the performance of Palmaz-Schatz stent and two other next generation stents: the Carbostent (Sorin Biomedica, Saluggia, Italy) and Multi-Link Tetra (Guidant, Indianapolis, IN, USA) stents. All of the stent models are expanded by pressure control, which is carried out by applying pressure load on the inner surface of stent strut. The stent has a length L of 16m, an outer diameter D of 1.2mm, a thickness s of 0.1mm, five slots in the longitudinal direction and 12 lots in the circumferential direction with length l of 2.88mm, and a metal/artery index of 0.3 (Fig. 3.2). The results showed that geometrical parameters have a remarkable influence on the mechanical characteristics of Palmaz-Schatz stent during free expansion. It was shown that a lower metal-to-artery

surface ratio, in particular, contributes to higher rates of radial and longitudinal recoil and lower rates of dog-boning effect. The model with metal-to-artery ratio of 0.3 shows 2.9% of recoil, 6.69% of foreshortening and 27.87% of dog-boning, whereas the model with 1.46 shows 1.74% of recoil, 11.97% of foreshortening and 66.33% of dog-boning. Furthermore, the impacts of geometries of two stents (Carbostent and Multi-Link Tetra) on their mechanical performances were compared and Fig. 3.3 shows the geometries of two stents.

- This study has revealed the potential of FEA in evaluating stent performance and conducting an optimization for stent geometry, which is considered as the first attempt to have simulated the future generation stents. However, the results are focused on only strut itself as a perspective view of recoil, foreshortening, and dog-boning. Even though the recoil, foreshortening, and dog-boning phenomena have significant contributions to the rate of ISR, the direct stress evaluation on the artery and plaque should be more important.

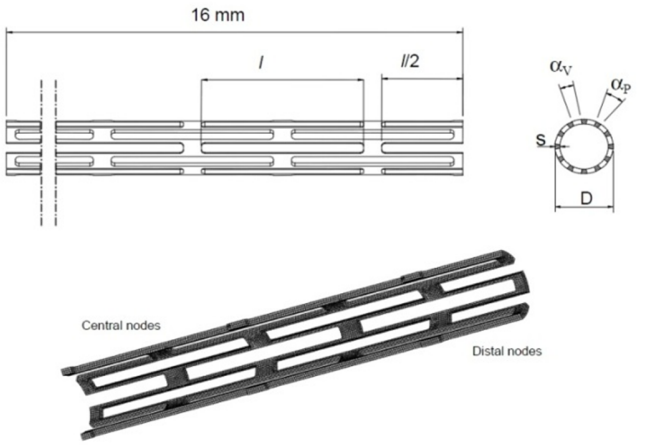

Fig. 3.2 Geometry of the unexpanded stent strut; l: length of the slot, s: thickness, αp: angle described by the metallic surface, αv: angle described by the slot and D: outer

diameter; finite element mesh for a quarter of stent model (Figure adopted from Miglia Migliavacca et al., 2002 [2]).

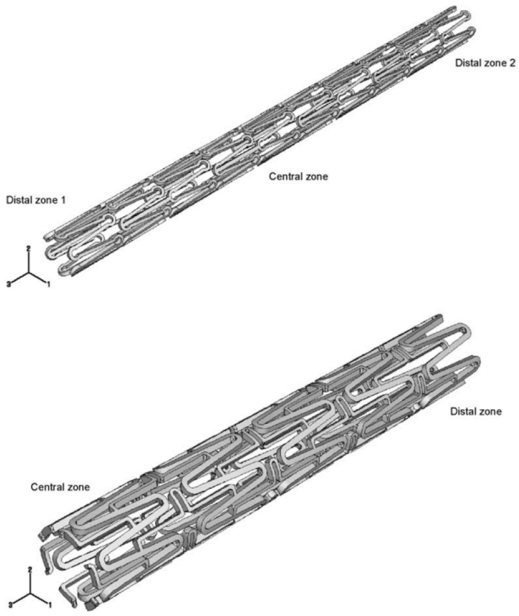

Fig. 3.3 Two models of commercial stents. The former is Multi-Link Tetra, and latter is Carbostent [2].

1.3 Chua et al., 2004 [3]

Chua et al. [3] introduced the results from a similar study that had conducted to evaluate the effect of geometrical parameters including the number, width, and length of individual stent cells on deployment characteristics of Palmaz-Schatz stents during free expansion. In this study, however, they applied pressure load to inner surface of cylindrical balloon, not to the stent platform itself. Fig. 3.4 shows the finite element models of one-eighth of the slotted tubes for the five designs after meshing. In their results, it has been shown that the width and length of the stent cell are not strongly related to the diameter and foreshortening of the stent but they contribute to the rate of

elastic recoil that diminishes as the number of cells increases and the uniformity of cell distribution increases. The maximum deployment pressure for 4 designs varied from 7.08 mm to 7.886 mm, whereas the elastic recoil varied from 12.23% to 19.70%.

- This study is important because it is thought as one of the first simulation models to incorporate a balloon component within the model system. However, the transient behavior of stent was not observed and analyzed even though the balloon inflation was driven by pressure control. Furthermore, the geometry variation of balloon was not carried out, and the effect of balloon geometry was not included in the analysis.

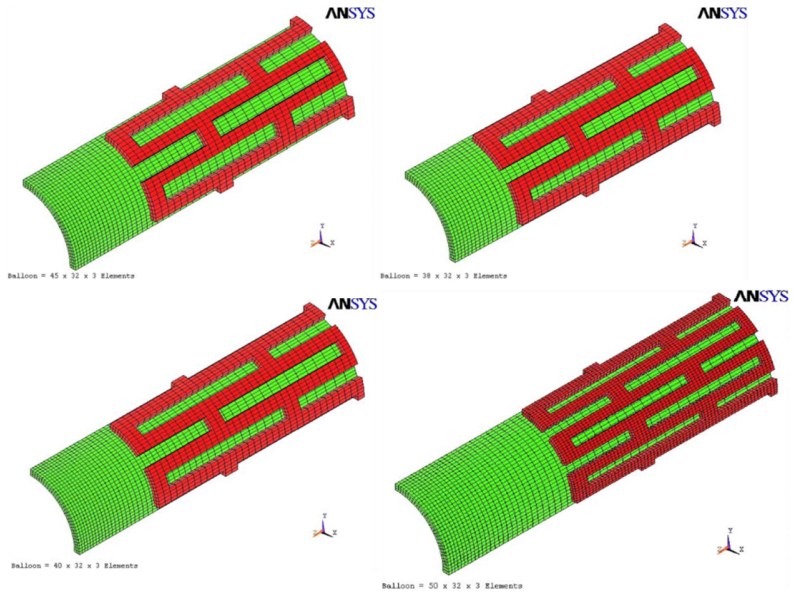

Fig. 3.4 Four FEA models of stents with different geometries [3].

1.4 Lim et al., (2008) [4]

Lim et al. (2008) [4] presented results from a study of the deployment characteristics of several different stents during free expansion. The objective of the study was to identify potential stent design parameters capable of reducing the possibility of ISR driven by foreshortening and dog-boning. The study simulated 3D numerical models of seven commercial stents with tri-folded catheter balloon. The interesting point on the methods used was that the catheter balloon was discretized by a number of shells and fluid elements. Then, the expansion of each stent was achieved through a volume control process. Validation of this approach was accomplished by comparing predicted pressure–diameter relationships to experimental data reported in the literature (Dumoulin and Cochelin 2000 [1]; Migliavacca et al. 2005 [5]; Wang et al. 2006 [6]). Similar expansion profiles were observed for each stent, and predicted rates of foreshortening and dog-boning were measured. The study noted that the stents with closed unit cells connected by straight-line links elements had generally higher rates in foreshortening and dog-boning than those with open unit cells connected by bend-shaped link structures.

- This study provides a first look at the realistic transient non-uniform balloon-stent expansion by investigating the mechanical properties, behaviors, and design parameters capable of reducing the possibility of restenosis risk induced by the foreshortening or the dog-boning. The authors adopted the pressure control with explicit method to observe the transient behavior of stent and show the results of foreshortening and dog-boning rate. However, the relationship between the rate of foreshortening and ISR is unclear. Moreover, not only artery and plaque

components are excluded, but also the consideration of coating polymer is omitted in their model.

1.5 Hopkins et al., (2010) [7]

Hopkins et al. (2010) [7] introduced the novel approach to express the coating delamination behavior by adopting cohesive zone model. In this paper, the cohesive zone model of the stent-coating interface is implemented to investigate coating de-bonding during stent deployment. Simulations reveal that coatings de-bond from the stent surface in tensile regions of the plastic hinge during deployment. The critical parameters governing the initiation of delamination include the coating thickness and stiffness, the interface strength between the coating and stent surface, and the curvature of the plastic hinge. The coating is also computed to de-bond from the stent surface in compressive regions of the plastic hinge by a buckling mechanism. The results showed that the computed patterns of coating delamination correlate very closely with experimental images.

- This study is regarded as the first attempt to include the coating component into the FEA model and address the point of focus on the coating component. The authors successfully demonstrated the coating delamination phenomena using the cohesive zone model. However, this study also has several limitations. The model was developed based only on the single hinge area with the 2D analysis perspective and very simplified boundary conditions.

2. Models with Arterial Wall System

Experimental evidence indicates the mechanical interaction between the stent and the artery as a significant cause for the activation of ISR. According to these considerations, the aim of this sub-section is to review the biomechanical interaction between a balloon-expandable stent and a stenotic artery, highlighting considerations able to improve the general understanding of the problem. To date, several studies have been carried out to investigate how geometrical properties, material properties, and deployment methods affect the expansion characteristics and biomechanical impact of stents when deployed within both normal and occluded coronary arteries.

2.1 Auricchio et al., (2000) [8]

Auricchio et al. [8] examined the deployment characteristics of a Palmaz–Schatz stents when they are expanded within an idealized stenotic artery. The stenotic artery was modeled as a cylindrical vessel with a parabola-shaped plaque. Fig. 3.9 shows the final configuration of the stent and the artery after the balloon deflation. Both the artery and the plaque were simplified as isotropic, homogeneous, incompressible materials, and their mechanical behaviors were approximated using the hyper-elastic constitutive models based on the data reported in the literature (Hayashi and Imai 1997) [9]. The expansion of the stent was achieved through the application of a pressure load on its inner surface, and a number of stent deployment characteristics such as elastic recoil, foreshortening and metal-to-artery ratio were calculated. As a result, the numerical outcomes were validated against experimental data in the literature proving that the deployment of a stent within a vessel may be accurately simulated using the FEA.

- This study is regarded as one of the first attempts to utilize FEA in analyzing the expansion of stent within a stenotic artery environment. Furthermore, it has an important meaning that the artery and plaque components were expressed as adopting hyper-elastic constitutive models which are continuously utilized in further studies. However, this study also has a critical limitation that the stress analysis on artery and plaque wall has not been conducted. The developed model only takes the mechanical behaviors of stent itself into account.

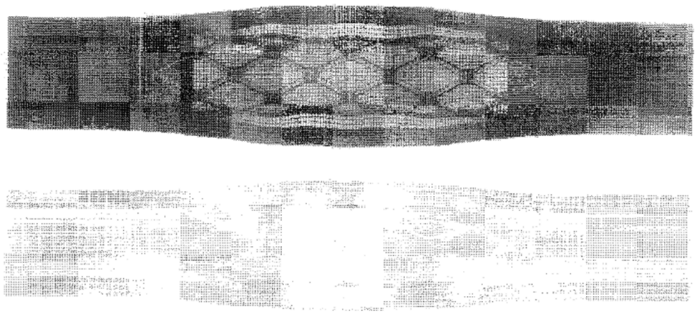

Fig. 3.5 The finite element stent model including a stenotic artery component [8].

2.2 Chua et al., (2004) [10]

Chua et al. [10] developed a model to evaluate the deployment characteristics of a Palmaz–Schatz stent under an idealized stenotic artery and to assess the degree of stent-induced arterial stresses accumulated in the vessel. The stenotic artery was modeled as a cylindrical vessel with a parabola-shaped plaque. Artery and the plaque were simplified as homogenous, isotropic and incompressible materials, and their mechanical behavior was predicted using linear elastic material models based on data reported in the literature (Veress et al. 2000) [11]. Fig. 3.10 shows the entire assembly of the model for the balloon

catheter, slotted tube stent, plaque and arterial wall. The expansion of the stent was achieved through the application of a pressure load on the inner surface of an idealized cylindrical balloon. It was observed that the regions which were subject to the highest stresses in the stenotic artery coincided with places where the most plaque ruptures have been reported. Also, the study confirmed that the maximum diameter achieved when the stent was expanded within the stenotic artery was significantly smaller than that during free expansion. Although the behavior of the stenotic artery was idealized using linear elastic material models, the results clearly identify the possible regions of high stresses that may be induced during stent deployment within a stenotic artery.

- This study is considered as the first attempt to assess the degree of stent-induced arterial stresses incurred in the vessel and to contain the balloon component in the model. The von-Mises stresses on the artery and plaque wall have been analyzed and the mechanical performances of stent, such as recoil and foreshortening, were also investigated. However, the geometrical parameterization analysis was excluded and the model was developed with only one-fourth of its model using symmetrical boundary condition. With the consideration of BMS (not DES), this study has developed the cornerstone of FEA model for further studies with artery and plaque components.

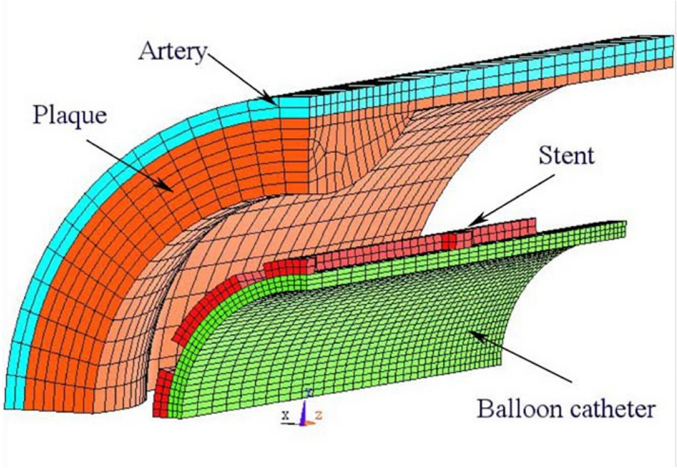

Fig. 3.6 Finite element model of the assembly with balloon component [10].

2.3 Holzapfel et al., 2005 [12]

Holzapfel, Stadler, and Gasser (2005) [12] simulated three different stents expanded in a patient-specific model of stenotic artery and investigated the effects of various geometrical parameters such as stent cell dimensions and strut thickness on the biomechanical impacts of the stents. Three stent designs based on respectively, Multi-Link, NIR, and In Flow Gold stents, were considered in the study. Fig. 3.12 shows the geometrical parameters of 3 different stents. A realistic model of a stenotic artery was generated using magnetic resonance images of an actual iliac artery. The properties of several sections of the stenotic artery were defined using a number of hyper-elastic constitutive material models based on experimental data (Holzapfel et al. 2000) [13]. The pressure load on the inner surfaces of the stents was the driving force behind the expansion within the vessel. The results of this study were used to investigate the influences of mismatch (see Fig. 3.13), strut thickness, and cell geometry on intimal pressure concentrations and the degree of stent-induced arterial stresses. Based on the

investigated stenosis and the performed parameter studies it reveals that the best results for all three indicators can be achieved with stent S1 whereas the worst results were achieved with stent S3.

- The major strength of this study could be considered as the incorporation of patient customized artery model. In addition, this study is regarded as the first attempt to conduct the stent geometry parameterization analysis in inclusion of artery and plaque components. Adopting three different commercial stent models for result comparison is similar to the approach in the current thesis. However, the consideration of recoil and coating component is excluded, which could be a limitation of this study.

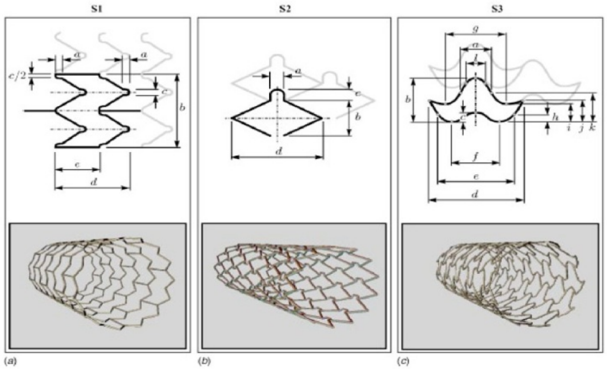

Fig. 3.7 Three different stent geometries described by a number of parameters, denoted by lowercase letters. (a) Multi-Link TetraTM stent (Guidant): S1, (b) NIROYALTM-Elite stent (Boston-Scientific): S2, (c) InFlow-Gold-FlexTM stent (InFlow Dynamics): S3 [12].

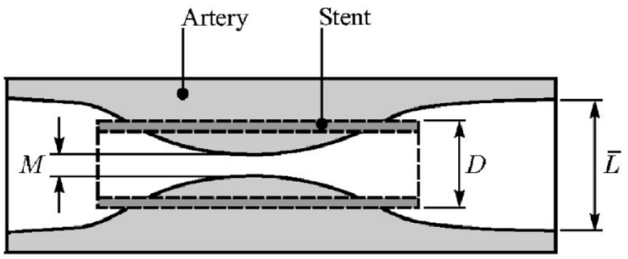

Fig. 3.8 Mismatch ΔM=D-M between the smallest lumen diameter M in the stenosis and the diameter D of the expanded stent. The lumen diameter of the healthy arterial region is characterized by L [12].

3. FEA for Stent Modeling

3.1 Computational methods

3.1.1 Numbers and types of meshes

Determining the number of meshes (or elements) in FEA model is a critical step due to the cost issue for computation. At the early stage of previous FEA studies, the total number of meshes is relatively small compared to the current stage of work since they tend to focus on single curve or unit cell instead of a full complete model of stent. They generated meshes from dozens to hundreds and the maximum number of the meshes was up to thousands. Over time, the aggregate number of meshes has been increased with the remarkable development of computational resources. Nowadays, nearly millions of meshes can be created, which leads the range of researcher's focus to expand to the full model of stent. However, even with current technologies and computational resources, the total number of meshes could easily overshoot a couple of millions when we apply a multiple components such as arterial wall, plaque and/or polymer coating. Therefore, an optimizing the number of meshes still remains as an important step for conducting an FEA computation.

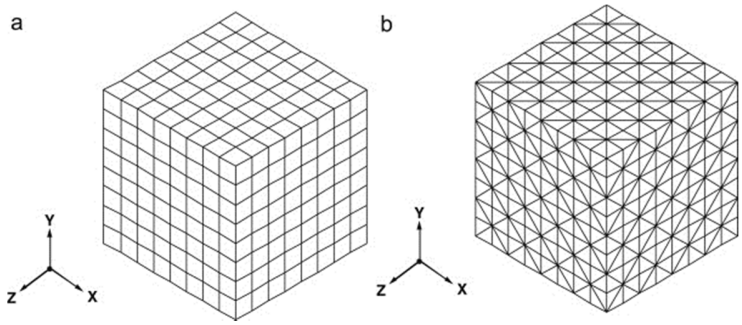

Fig. 3.9 Types of mesh. (a) Hexahedral and (b) Tetrahedral

On the contrary, the types of mesh seem not to have a tendency over time. There are two dominant types among the mesh, hexahedral and tetrahedral mesh (see Fig. 3.18). In general, the hexahedral mesh is preferred for any given analysis since the total number of elements, in the same density, is much less than that of tetrahedral. However, tetrahedral mesh has an advantage in terms of its usability and convenience of creating good quality of mesh. In the area of FEA for stent, even though the majority of studies adapted hexahedral meshes, the simulations of FEA using tetrahedral mesh show relatively accurate results which indicates the result seems irrelevance with selecting a type of mesh.

3.1.2 Element types

A number of types of elements can be used in FEA, but in modeling stents with FEA, three element types are generally used; 3D solid element, 2D shell element, and 2D membrane element. For most of the components in stent systems except for the coating and/or balloon components, a 3D solid element is employed. In general, 2D shell element and 2D membrane element are used for the coating component and balloon component,

respectively. However, there are some studies that have adopted 3D solid elements for the balloon component [4,12]. The 3D solid element has an advantage on evaluating the stress along the cross-section direction although it requires a high level of computational resources due to a massive amount of nodes for the same mesh size. There was a study using 1D or 2D elements instead of the 3D to reduce the problem size [6]. Although the results of them are not exactly same, it turned out that those elements in three different dimensions showed the similar results.

With the recent development of computational technologies and resources, the maximum number of the elements to be calculated has been enormously increased. In addition, reduced integration point method, one of the options for computing the elements in FEA, can save the computational costs.

3.1.3 Boundary conditions

To reduce the computational costs, a symmetric boundary condition is often applied in FEA. In imposing the symmetric boundary condition, the nodes belong to a symmetric plane are required to have zero displacement in the direction normal to the symmetric plane. To prevent rigid-body motions, a set of nodes at the distal end of an artery or stent platform are constrained to move to the longitudinal direction so as to ensure free expansion in the radial direction. In the loading conditions with displacement control, any constraints for the nodes are not necessarily required to prevent rigid-body motions whereas the pressure control does.

3.1.4 Displacement and pressure control methods

Stent expansion is generally operated through the displacement control or pressure control. The displacement control method is to apply the displacement boundary condition onto the inner surface of stent strut along the radial direction using cylindrical coordinate system while the pressure control method is to apply an internal pressure onto the inner surface of a stent or balloon. When a study focuses on evaluating the stress distribution on every component regarding the convenience of reaching convergence, adopting the displacement control is likely to be preferred.

In the meantime, the pressure control method is often combined with the explicit method to choose, which enables the observation of transient behaviors of a stent during the expansions, such as dog-boning and foreshortening phenomena. However, this method normally requires much longer computational time since smaller increments, compared to the displacement control method, are needed to stabilize the dynamic behaviors and interactions between the components.

3.2 Material properties and geometrical parameters

The dominant aim of previous studies was to evaluate the influences of geometrical parameters and material properties of stents on their mechanical behavior during deployment. The followings provide the summaries of stent/balloon geometry effectiveness of various models.

- In comparison of tubular stent and coil stent, the result from FEA showed that tubular stent is very rigid and coil stent is significantly more flexible, and the stresses are locally concentrated at the link nodes.

- Lower metal-to-artery surface ratio contributes to higher rates of radial as well as longitudinal recoil and lower rates of dog-boning effect.
- The width and length of the stent cell are not strongly related to the diameter and foreshortening of the stent, but they contribute to the rate of elastic recoil that diminishes as the number of cells increases and the uniformity of cell distribution increases.
- The stents with closed unit cells connected by straight-line links elements had generally higher rates in foreshortening and dog-boning than those with open unit cells connected by bend-shaped link structures.
- Both proximal/distal stent strut geometry and balloon length have a significant effect on the degree of dog-boning exhibited during stent deployment.
- Large stent strut-spacing, radius of strut curvature, and axial ring amplitude are associated with lower levels of stent-induced arterial stress.
- The material properties of a plaque have a significant influence on the underlying arterial stresses induced during stent deployment with stiffer plaques playing a protective role during stent deployment.

3.3 Limitations of previous works

As described in the previous sections, a number of studies for stent modeling with FEA have been conducted so far. Many researchers have been trying to optimize the geometry of stent and loading methods of balloon catheters. At the early stage, it is true to say that majority of their work were concentrated on the mechanical performance of

stent such as foreshortening and/or dog-boning. Over time, few studies started to focus on the stress on the artery and plaque which could quantitatively describe the rate of ISR, indirectly. Unfortunately, the targets of those works are mostly focused on BMS in spite of the fact the majority of stent medical devices tend to move to next generation of DES. In other words, most of prior research has focused on the mechanical performance of BMS and models including 3D coating components have not yet been developed.

The research in this thesis improves on existing models by:

- Incorporation of 2D and 3D drug-polymer coating components to develop integrated DES model which enables the evaluation and investigation of von-Mises stresses on artery, plaque, coating and stent strut.
- Full 3D DES model without symmetric boundary condition.
- Comparison of three different commercial DES including the most recently released products.
- Provision of novel methods to analyze and predict the accurate location of stress concentrated area within 3 commercial DES.
- Various stress components analysis on drug-polymer coating element.
- Suggestions of quantitative values of bonding strength between stent strut and coating components.

References

1. C. Dumoulan, B. Cochelin, Mechanical behavior modeling of balloon-expandable stents, Journal of Biomechanics 33 (2000) 1461-1470.

2. F. Migliavacca, L. Petrini, M. Colombo, F. Auricchio, R. Pietrabissa, Mechanical behavior of coronary stents investigated through the finite element method, Journal of Biomechanics 35 (2002) 803-811.

3. S. N. David Chua, B. J. MacDonald, M. S. Hashmi, Effects of varying slotted tube (stent) geometry on its expansion behavior using finite element method, Journal of Materials processing technology 155-156 (2004) 1764-1771.

4. D. Lim, S. Cho, W. Park, A. Kristensson, J. Ko, S. T. S. Al-Hassani, H. Kim, Suggestion of potential stent design parameters to reduce restenosis risk driven by foreshortening or dog-boning due to non-uniform balloon-stent expansion, Annals of biomedical engineering 36 (2008) 1118-1129.

5. F. Migliavacca, L. Petrini, V. Montanari, I. Quagliana, F. Auricchio, G. Dubini, A predictive study of the mechanical behavior of coronary stents by computer modeling, Medical engineering & physics 27 (2005) 13-18.

6. W. Wang, D. Liang, D. Yang, M. Qi, Analysis of the transient expansion behavior and design optimization of coronary stents by finite element method, Journal of biomechanics 39 (2006) 21-32.

7. C. G. Hopkins, P. E. McHugh, J. P. McGarry, Computational investigation of the delamination of polymer coatings during stent deployment, Annals of Biomedical Engineering 38 (2010) 2263-2273.

8. F. Auricchio, M. D. Loreto, E. Sacco, Finite-element analysis of a stenotic artery revascularization through a stent insertion, Computer methods in biomechanics and biomedical engineering 4 (2000) 249-263.

9. K. Hayashi, Y. Imai, Tensile property of atheromatous plaque and analysis of stress in atherosclerotic wall, Journal of biomechanics 30 (1997) 573-579.

10. S. N. Chua, B. J. MacDonald, M. S. Hashmi, Finite element simulation of slotted tube (stent) with the presence of plaque and artery by balloon expansion, Journal of material processing technology 155-156 (2004) 1772-1779.

11. A. I. Veress, D. G. Vince, P. M. Anderson, Vascular mechanics of the coronary artery, ASAJO 89 (2000) 92-100.

12. G. A. Holzapfel, M. Stadler, T. C. Gasser, Changes in the mechanical environment of stenotic arteries during interaction with stents: computational assessment of parametric stent designs, Journal of Biomechanical engineering 127 (2005) 166-180.

13. G. A. Holzapfel, Schulze-Bauer, C. A. J, Mechanics of Angioplasty: Wall, Balloon and Stent, The Americal Society of Mechanical Engineers (ASME), 242 (2000) 141-156.

Chapter 4. FEA Computations

A typical FEA of stent deployment involves a number of the important pre-processing stages. The first step is to generate the geometries of the components and to create the meshes that are incorporated into the FEA. These FE meshes are routinely obtained directly from the computer-generated solid models using the mesh generation or discretization algorithms. The material properties for each individual component must be defined and the appropriate boundary and loading conditions must be applied to them. Finally, a suitable solution methodology must be chosen. In this chapter, these FEA computation steps are articulated and discussed.

1. Model Stent

In the FEA computations, the first stage is to generate a suitable solid model for each individual constituent component. In an FEA of stent deployment, the solid model for a stent platform, catheter balloon, and stenotic artery may be required. Once generated, these solid models must be discretized into acceptable FE meshes. Since most stents have complicated geometrical designs, and strict patent claims keep the information about commercial stents from being distributed, the generation of the solid model for a stent is not an accommodating task.

One strategy that has been utilized to develop FEA meshes for a number of stent designs involves cutting an actual stent along its longitudinal axis and measuring the important geometrical properties such as strut width, thickness, and length using a microscope. Using these measurements, the model of the planar stent geometry can be

reasonably defined within a FEA package. This model can be discretized into a suitable amount of meshes and rotated into its cylindrical configuration by the coordinate transformation as shown in Fig. 4.1 [1]. Another strategy that has been adopted in recent years is using X-ray tomography to generate a detailed 3D model of the stent of interest. For a complex stent design, with using this approach, highly accurate FE meshes can be generated.

In general, the stent model can be simulated into two different element types, 3D solid and 2D shell element. The 2D shell element can save much computation costs since they allow modeling a thin feature with a relatively less amount of elements than the solid element. They are also easier to mesh and less prone to negative Jacobian errors that might occur when used for extremely thin solid features such as balloon. Stent solid models are generally discretized using solid elements. In practice, a stent is crimped and loaded upon a balloon that is both tapered and folded onto a catheter. In the studies in which the expansion of the stent has been simulated through balloon dilation, the catheter balloon was generally modeled as an idealized cylindrical surface and discretized using the shell elements [1]. In this study, since the existence of balloon component is neglected, all of the components (except the coating) in the model are constructed with full 3D solid elements. Generally, in the studies that have evaluated the expansion of a stent within a normal and stenotic artery, including this thesis, the artery and plaque were modeled as an idealized cylinder and discretized using the solid elements [1].

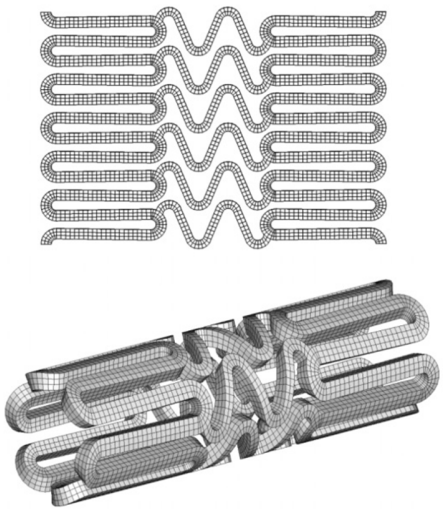

Fig. 4.1 'Wrapping' of planar stent geometry (top) into its cylindrical configuration (bottom) (figures adopted from [1]).

2. Material Properties

Before conducting any FEA computation, the material properties of each component in the system must be adequately defined. As discussed in the previous chapter, coronary stents platforms are generally manufactured using a biologically inert metallic material such as medical grade 316L stainless steel. In this thesis, model B (TAXUS Express2 stent) and model C (Biomatrix FLEX) have adopted 316L stainless steel as the material for stent strut, whereas model A (SYNERGY stent) is consisted with Pt-Cr alloy. The behavior of these materials is elastic–plastic in nature and their response to uniaxial loading could be highly non-linear. In the majority of the previous FEA studies, in this study as well, the stent materials were simplified as homogeneous and isotropic, and their behaviors were typically defined using bilinear and multi-linear plasticity models with isotropic hardening [1]. These plasticity models are incorporated in most commercial FE packages, and they can be generally, defined using the data obtained from an experimental test. The incorporation of the relevant mechanical behaviors of an

arterial tissue has been a difficult task due to the non-linear, anisotropic, stress-stiffening nature of the biological material. In the majority of the previous studies as well as this thesis, the arterial tissue was approximated as a homogeneous, isotropic, and incompressible material, and its behavior was defined using a hyper-elastic constitutive model [1]. The hyper-elastic model assumes an ideal elastic material for which the stress–strain relationship is derived from a strain energy function. The strain-energy function is the measure of the energy stored in a material as a result of its deformation, and it is generally fitted to the data obtained from experimental testing of the arterial tissue. Fig. 4.2 shows the example of stress-strain curve of the hyper-elastic model for an arterial wall [2]. Most commercial FEA packages include a number of hyper-elastic constitutive material models with suitable curve-fitting applications that are capable of capturing the mechanical behaviors of a biological material.

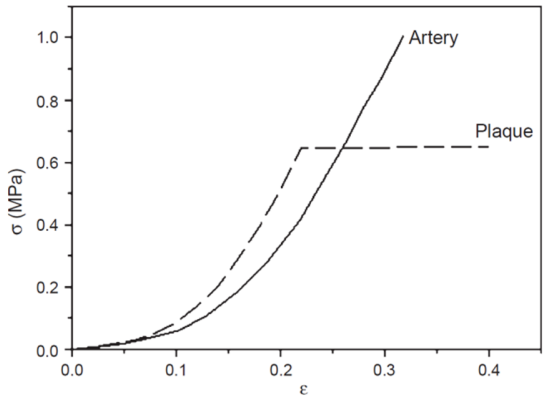

Fig. 4.2 An example of stress-strain curves for the hyper-elastic models. (Adopted from [2])

3. Boundary and Loading Conditions

To predict the reliable results, the boundary and loading conditions of a FEA mesh should be realistic to closely akin to the actual conditions in question. In analyzing

stent deployment, the stent should be free to expand and contract in the radial and longitudinal directions except for the fixed position to prevent rigid-body motions. Generally, a set of nodes located in distal end of each discretized component are constrained from the displacement in a longitudinal direction to avoid any rotational or translational movement. However, in case of our study, additional boundary conditions to prevent rigid body motion are excluded because we applied the displacement control as the loading method. In case of the model with the symmetric boundary condition, it is required that the nodes belonged to a symmetric plane have zero displacement in the direction normal to the symmetry plane. Such symmetric conditions were not implemented in our computation because we used the full 3D models of DES system.

For the loading condition, stent expansion is typically achieved using two methods, displacement control and pressure control. The studies in which the stent expansion was achieved through the displacement control have involved the expansion of an analytical surface within the stent while the studies in which the stent expansion was achieved through the pressure control have involved the application of a pressure load on the inner surface of the stent [1]. Both displacement control and pressure control loading methods have their own characteristics, and depending on the aim of a study, one of two methods is typically selected. The displacement control has a strong advantage with the easiness of computational convergence, and it could be coupled with either implicit or explicit methods. This loading method is generally used when the aim of a study is to evaluate the stress distribution along the stent strut, coating and arterial wall. However, this method has the limitation that the final displacement of stent deformation must be pre-determined with given information and the transient status of the stent expansion

could not be observed. The pressure control can be also operated with both of implicit and explicit methods, and has an ability to obtain stress distribution results for any components. However, unlike displacement control, applying pressure control with implicit method is often computationally unstable and needs further stabilizing factors for convergence of the solutions. Hence, normally, pressure control is performed with explicit method. The pressure control is preferred when the aim of study is focused on the transient phenomena such as dog-boning and foreshortening of stent platform. Fig. 4.3 shows examples of FEA computations from the current thesis using displacement and pressure control methods. Note that we did not apply the pressure control in our computations; the image shown in Fig. 4.3(b) is only for the visualization purpose. The arrows represent the position and direction of displacement imposed in the simulation. Note that the arrows in pressure control are located in the inner side of stent platform.

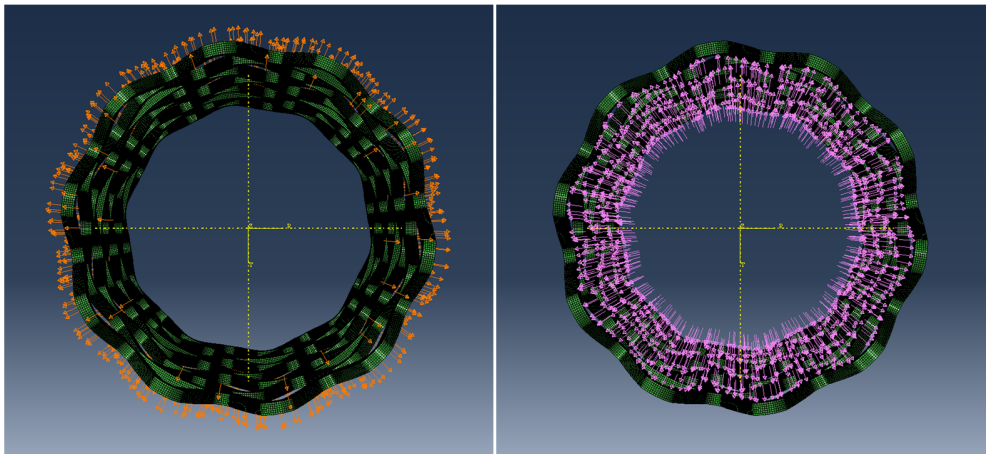

(a) Displacement control (b) Pressure control

Fig. 4.3 Cross-sections of stents to show two different loading methods, (a) displacement control and (b) pressure control.

4. Solver Method

The final step in the pre-processing stage of a structural FEA is the selection of a solution methodology that calculates the nodal displacements, stresses, and strains. This procedure is very last and critical step in pre-processing stage. Typically, stent deployment has typically used either implicit or explicit solution method. The comparison of these two methodologies must be clearly understood. A non-linear implicit structural analysis does not consider dynamic effects; however, due to the presence of large deformations in the analysis, a solution is generally obtained over a series of sub-steps to ensure numerical stability. During each sub-step, a fraction of the loading conditions is applied and the final solution is obtained in a piecewise fashion. Most commercially available FEA packages incorporate a Newton–Raphson iterative solver for solving non-linear static structural problems which is adopted in this thesis as well [3].

In an explicit analysis, the loading conditions are applied over a number of time steps and a solution is obtained through a time-integration procedure. During explicit time integration, the solver will increment a time step and determine if the loads applied to the structure are in equilibrium with the internal forces. Nodal accelerations are calculated directly from Newton's second law and a solution is obtained on an element-by-element basis [3]. As mentioned in the previous section, the analysis using pressure control with explicit method relatively provides a good convergence of calculation since the governing equation of explicit method has an acceleration term that is one of the most differentiated properties from the implicit method. If the model contains complicated interaction constraints, such as contact or collision, the calculation with implicit static method easily becomes unstable. In summary, it is generally thought that the implicit

method is preferred when the model is established to obtain the result of stresses distributions on every component without transient behavior consideration, whereas the explicit method is used to observe the transient phenomena such as dog-boning and foreshortening effect.

5. Issues in Computational Model Development

Other than the computational convergence issues that were previously addressed, it is considered that the multi-scale and material property issues are one of the most challenging roadblocks to overcome in developing more advanced FEA models.

5.1 Multi-scale issue

In general, creation of a good mesh with high quality is critical in the FEA computation since it's directly highly related to the accuracy of results. There are several criteria to measure the quality of mesh such as Jacobian and skew, and the most important factor is the aspect ratio in the shape of FE mesh. Keeping an aspect ratio below 6.00 is highly recommended to obtain reliable results.

For this reason, if the geometry of a component is like a thin-film, a massive amount of elements should be generated. Unlike previous studies, the present study includes the coating component with full 3D solid elements (as well as 2D shell elements). The typical thickness ratio of drug-polymer coating to stent platform strut is small (e.g., < 0.1), hence very large amount of elements must be created to maintain the proper aspect ratio. Fig. 4.4 shows an example of the FE meshes created in this study to incorporate such multi-scales. In the figure, the cross-section of stent platform strut is

displayed, showing coarse platform and fine coating meshes. Another problem resulted from this multi-scale issue is the contact interaction between outer surface of coating component and inner surface of plaque component. In a technical point of view, the mesh density ratio of master surface to slave surface should be in the range of 2 to 1. Here, the slave surface is defined as the surface that are moving toward a different surface, called as the master surface. With this constraint, generation of large number of elements for plaque must be involved as well. To resolve these problems, applying 2D shell elements to the coating component could be one of the solutions. The total number of nodes and degree of freedom (DOF) significantly decreases even with same density of elements so that the computational costs will be decreased.

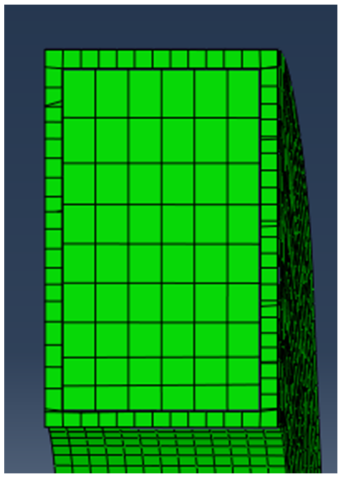

Fig. 4.4 Cross-section of stent strut to show the dual-scale mesh issue. Coarse and fine mesh sizes are required for stent platform and coating materials, respectively.

5.2 Inaccurate/unidentified material properties

Needless to say, applying proper material properties to individual components in the FEA system is most likely to be an essential step of FEA. In the FE package, elastic modulus, Poisson's ratio, density (explicit only), and stress-strain curve data are required

to simulate the model properly. Especially, the stress-strain curve is a key requirement property to realize the elastic and plastic behavior of model. In the case of well-known materials, such as stainless steels (i.e., 316L), it is not difficult to find the appropriate material properties. On the contrary, it is very challenging to obtain stress-strain curves of the materials that have been recently invented or are used in a small part for a specialized purpose. For this reason, in the current thesis, a bi-linear stress-strain behavior has been assumed for the values of elastic modulus, yield stress, tensile strength, and elongation of Pt-Cr alloys [4]. In addition, the drug-polymer coating was approximated as a pure polymer material. Proper friction coefficient between coating material and plaque is also unknown, thus, frictionless surfaces have been considered in our model.

6. Current model and methods

Some general aspects of FEA computational model development have been described up to this point. In the following sub-sections, we detail our FEA model development including geometry generation, material properties, boundary and loading conditions, and simulation conditions. Note that all of computations were conducted using commercial ABAQUS FEA package.

6.1 Stent Model

A 3D FEM model of a typical tubular-shaped intravascular stent (SYNERGY, Boston Scientific, Intervention Cardiology, MA, USA) was developed to investigate the effects of different geometrical features (such as thickness of strut and coating component) on the mechanical behavior of the stent. The models were created by means

of computer-aided design considering the commercial stent products; SYNERGY stent, TAXUS Express^2 stent and Biomatrix FLEX stent (see Fig. 4.5). Practically, it is very challenging to perform an accurate biomechanical modeling for expanding process of stent delivery system in vivo. The overall response of the system is highly nonlinear due to the large amount of deformations in each component and due to the interactions between adjacent components. For this reason, in this study, only the stent platform, drug-polymer coating, and their interaction were considered to expedite the simulation. To reduce the high computational cost of the stent expansion, 7 rings of each stent platform were taken into account.

	SYNERGY	**TAXUS Express^2**	**Biomatrix FLEX**
Inner Diameter(mm)	2.29	2.08	3.0
Strut Thickness (Radial, mm)	0.08	0.132	0.112
Coating Thickness(μm)	7	22	10
Longitudinal Length(mm)	8.286	9.280	18.52
Number of Links	12	18	18
Number of Rings	7	7	7

Table 4.1 Geometrical specifications of three commercial stent models incorporated in the present thesis [5].

Three different coronary stent designs were considered in this study, and they resemble three commercial intravascular stents. In the following document, they will be referred to as model A (TAXUS Express 2, 2004, Boston Scientific, Intervention Cardiology, MA, USA), model B (SYNERGY, 2013, Boston Scientific, Intervention Cardiology, MA, USA), and model C (Biomatrix FLEX, 2010, Biosensors International,

Singapore), respectively (see Fig. 4.5). The geometrical specifications for these three commercial products are summarized in Table 4.1.

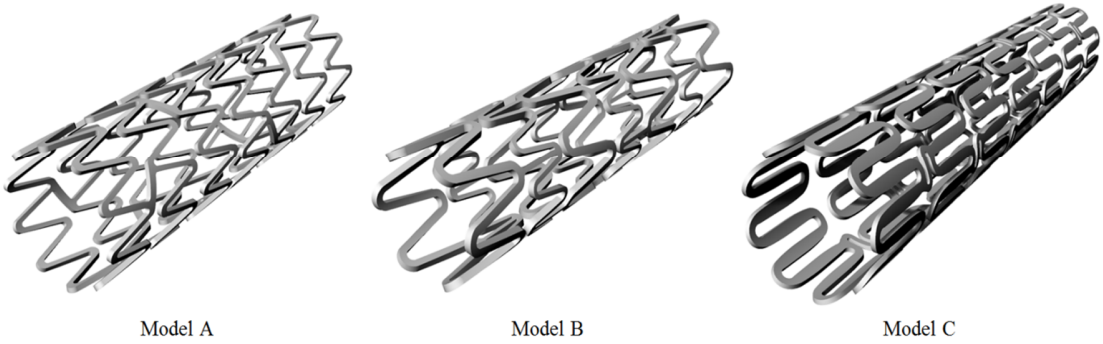

Fig. 4.5 Stent models to display SYNERGY stent (Model A), TAXUS Express2 stent (Model B), and Biomatrix FLEX stent (Model C).

Fig. 4.6 shows the geometrical shapes of the models from our study. The unit model of SYNERGY stent (model A), which is considered as reference model in the current work, contains 7 rings connected by 12 links. The inner diameter in the unexpanded configuration is 2.299mm while the thickness of the stent strut is 0.08mm. The length along longitudinal direction is 8.286 mm and the thickness of coating layer is 7 μm. The unit model of TAXUS Express stent (model B) is composed of 7 rings connected by 18 links. At the initial step, before dilation, the inner diameter was set to 2.08 mm, the strut thickness was 0.132 mm, longitudinal length was 9.280 mm, and the coating thickness was 22 μm. The geometrical dimension of TAXUS stent shows much thicker platform struts and coatings compared to the thicknesses of the others. The modern trend in DES technology is apt to be thinner strut to reduce the probability of occurrence of the side effects such as restenosis or thrombosis. The composition of unit model of Biomatrix FLEX stent has 7 rings and 18 links as well. The initial diameter of

the FLEX is 3.0 mm, and the strut thickness is 0.112 mm. The thickness of coating component is 10 μm which is thinner than that of TAXUS but thicker than that of SYNERGY. The longitudinal length is 18.52 mm.

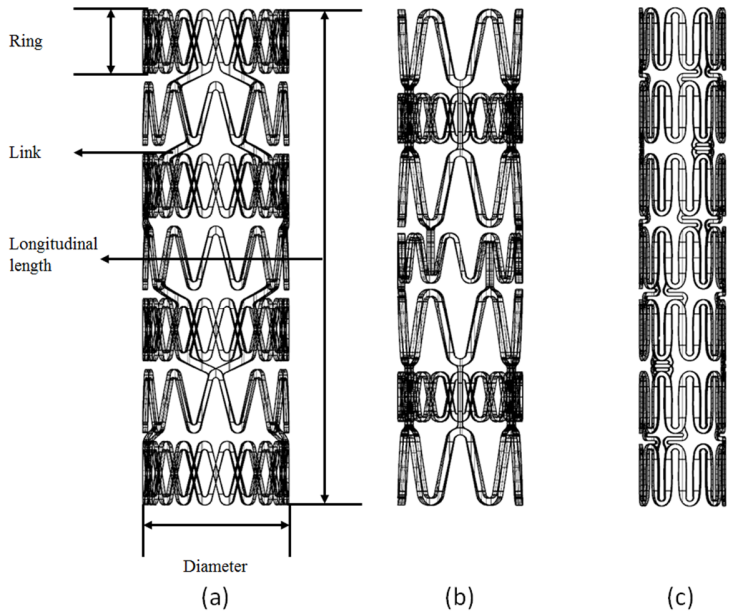

Fig. 4.6 Illustrations to show the geometrical factors of 3 commercial stents models; (a) SYNERGY, (b) Taxus Express2 and (c) Biomatrix FLEX.

6.2 Geometry and mesh generation

During pre-processing, the full 3D FEA models of three different stents were generated using two commercial software, Rhinoceros® 5.0 (Robert Mcneel & Associates, Indianapolis, IN, USA) and Hypermesh 11.0 (Altair Engineering, Inc., USA). Since the difficulties of obtaining the manufactures' specifications on the actual dimensions, the measured dimensions based on digital images were used in this study. These measured dimensions were transferred to create the geometrical models of stent devices using Rhinoceros® 5.0. After the basic structural drawing of stent model has been

generated, the result file is imported to Hypermesh, mesh generating software (see Fig. 4.7). The stent strut model was meshed using the first order 8-node brick element of 3D continuum solid (C3D8R) which supports linear and nonlinear large plastic deformation of model, while the coating component model was meshed using the first order 2D 4-node shell element of S4R which fits analyzing very thin layer. The total numbers of elements for model A, model B, and model C are 946521, 431473, and 905917, respectively. These higher numbers of elements could be applied in view of the rapid development of recent computation technologies. The number of element is very important because it is directly related not only to the computational costs but also to the accuracy of the results. The simulation conditions for the models in this study, especially, have very large nonlinear plastic deformation, which requires to make the mesh as fine as possible to maintain the quality. The computation time for a single job in this study is up to 2 days, using parallelized computing scheme that utilizes 32 CPUs with 128 GB of memory.

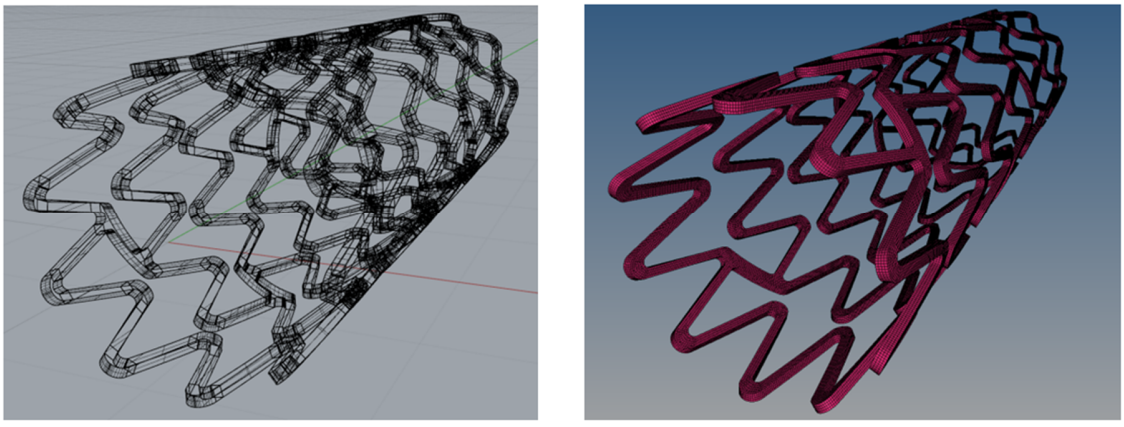

Fig. 4.7 Structural drawing of stent from CAD software (left) and generated full 3D elements mesh (right)

6.3 Material properties

For the model A (SYNERGY stent), Pt-Cr alloy is used for stent platform and poly(lactic-co-glycolic acid) (PLGA) is used for coating polymer material. Pt-Cr alloy is most recently developed material that possesses various advantages such as higher yield strength and radiopacity. In this Pt-Cr alloy, the weight percentage is 33% for Pt, 18% for Cr, 9% for Ni, 2.63% for Mo, 0.001% of C and rest for Fe [4]. The Young's modulus is 203 GPa, the Poisson's ratio is 0.3, and yield strength is 480 MPa [4]. Pt has already been used in a number of cardiovascular and neurovascular implantable devices, where its inert behavior and high radiopacity have been the key drivers in its selection [4]. The tensile properties and density of this Pt-Cr alloy compare favorably with stainless steel metal. This enables stent designs with both thin struts and high radiopacity. The material for coating component of model A, the biodegradable polymer PLGA is used. These days, the PLGA has been one of the strongest candidates for bio-implantable substance due to its advantage on biodegradable and biocompatible property. Although PLGA shows much brittle characteristics compared to styrene-isobutylene-styrene (SIBS), which causes delamination or fragmentation phenomenon, it is more preferred since its bioabsorbable nature. The Young's modulus, Poisson's ratio, and yield strength of PLGA are 1.58 GPa, 0.3, and 29.68, respectively [6].

For the model B (TAXUS stent) from Fig. 4.6, 316L stainless steel and SIBS are applied to the strut and the coating component, respectively. For 316L stainless steel, the Young's modulus is 201 GPa, the Poisson's ratio is 0.3, the yield strength is 330 MPa [7]. For the coating component, SIBS has been widely used for drug carrier for DES system

because of its elastic property. The Young's modulus is 0.002 GPa, the Poisson's ratio is 0.49, and the yield strength is 0.5 MPa [8].

The 316L stainless steel has been also used as material for strut platform of the model C (FLEX stent) in Fig. 4.6. While model B and C have the same material for strut, the model C has biodegradable polymer drug carrier which is called poly(lactic acid) (PLA). The elastic modulus of PLA is 1.30 GPa, the Poisson's ratio is 0.3, and the yield strength is 50.96 MPa, respectively [9]. The physical/mechanical properties of materials that were incorporated in our model are summarized in Table 4.2 and the stress-strain curves for the materials are depicted in Fig. 4.7 and Fig. 4.8.

Material	**Young's Modulus (GPa)**	**Poisson's Ratio**	**Yield Strength (MPa)**
Stainless Steel 316L	201	0.3	330
Pt-Cr Alloy	203	0.3	480
SIBS	0.002	0.49	0.5
PLGA	1.58	0.3	29.68
PLA	1.30	0.3	50.96

Table 4.2 Mechanical properties of materials [4,6-9].

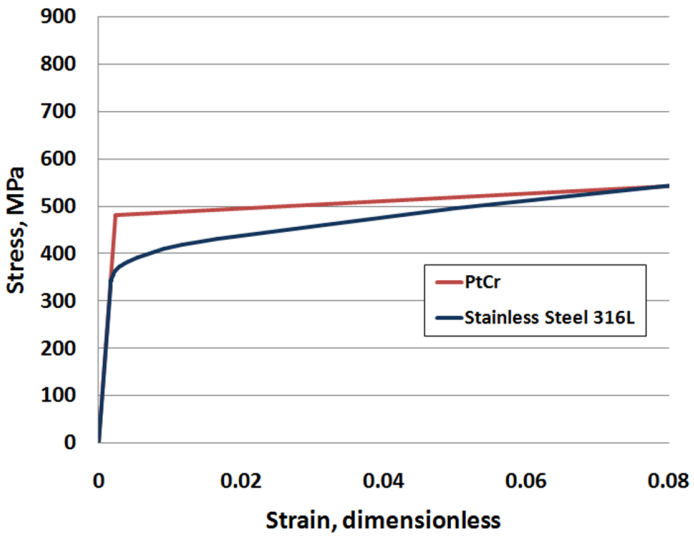

Fig. 4.8 Stress-strain curves for stent platform materials [4,7].

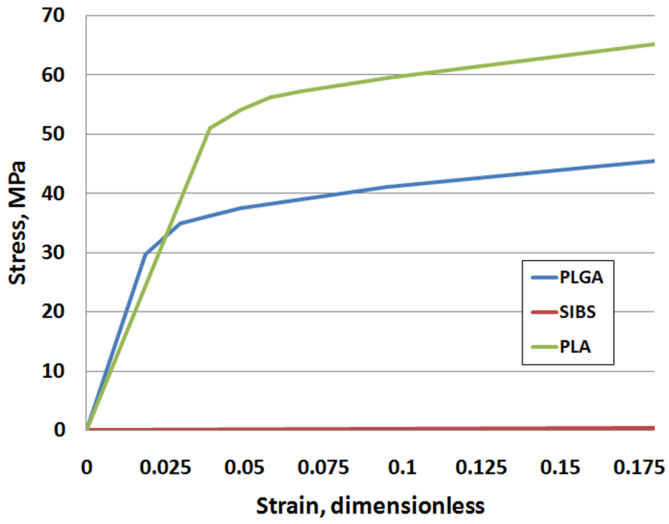

Fig. 4.9 Stress-strain curves for three different polymer coating materials [6,8,9].

The artery and plaque material were defined by a Mooney-Rivlin hyper-elastic constitutive equation. Table 4.3 summarizes the coefficients used for the hyper-elastic constitutive equation to define the material properties of artery and plaque.

	C_{10}[MPa]	C_{01}[MPa]	C_{11}[MPa]	C_{20}[MPa]	C_{30}[MPa]
Artery	0.708	-0.620	0	2.827	0
Plaque	-0.802	0.831	1.157	0	0

Table 4.3 Mechanical properties of artery and plaque [11].

6.4 Simulation conditions

6.4.1 Solver method

A large deformation analysis is performed using ABAQUS commercial code (Hibbit Karlsson & Sorenses, Inc., Pawtucket, RI, USA) based on the FEA. In general, the ABAQUS/Standard program is used in the classical displacement formulation. For a highly nonlinear problem, the matrix equation is solved using a Newton-Raphson's method due to the material plasticity and tie constraint. The method for the convergence criterion is to ensure that both the largest residual in the balance equations and the largest correction to any nodal unknown provided by the current Newton iteration are sufficiently small. In general, for the studied problem the convergence is verified when the residual force is less than a predefined tolerance (in our case, 0.5% of the average force in the structure, averaged over space) and when the largest displacement correction is less than a predefined tolerance (in our case, 10% of the largest incremental displacement).

The numerical computation was performed simulating free expansion of the stent. Instead of applying internal pressure (pressure control method) to the inner surface of stent, predefined radial displacement condition (displacement control method) was applied because the transient behaviors were not analyzed. A surface to surface tie constraint is applied as interaction between stent strut and coating materials so that they

are moving together throughout the simulation. The inelastic constitutive response is described through a von Mises-Hill plasticity model with isotropic hardening employed in the ABAQUS FEA software package [10].

6.4.2 Elements

Since the simulation is based on full 3D modeling, the continuum 3D 8-node reduced integration hexahedral brick element (C3D8R) is used for both stent struts and coating components. Especially for coating components, not only the 3D brick element but also 2D shell element was applied for the comparison purpose. For shell element, 2D 4-node reduced integration shell element was chosen for coating materials.

6.4.3 Loading steps

Determination of an appropriate calculating method, at step module, is one of the most critical parts of conducting FEA. ABAQUS contains several types of solver methods, but they can be subjected into two different cases, i.e., implicit and explicit methods. In our study using ABAQUS/Standard, the implicit static method was used for entire set of calculations. ABAQUS/Explicit method is generally preferred when a model includes dynamic behavior, such as collision, or has a very complicated contact interaction between the parts inside. As mentioned in previous section, implicit static is suitable method for our study, since we do not consider the transient behavior of stent such as dog-boning and/or foreshortening phenomena. In addition, the contact interaction in our model is relatively simple, and the total number of elements is very high. Considering these factors, the implicit method was elected in the current thesis. An

automatic stabilization tool was used for stable convergence, and the default value of its coefficient was set to 0.0002. The maximum number of the increments is 100,000, and the size of each increment step is 0.01 and 0.02 for the minimum and maximum values, respectively.

6.4.4 Loading and boundary conditions

Cartesian coordinate is the default coordinate system in ABAQUS/Standard. However, another coordinate system (Cylindrical system), is required to be added before considering the loading conditions since the displacement should be applied parallel to the radial direction of macroscopic view of stent platform. In the Cylindrical coordinate system, the radial displacement was applied to all the nodes on the inner surface of platform with the value of 0.687 mm for Model A (SYNERGY stent), 0.624 mm for Model B (Taxus Express^2 stent), and 0.9 mm for Model C (Biomatrix FLEX stent), respectively. The amounts of radial displacements were arbitrary selected to achieve 60% of full dilation, because the initial geometries of each stent are different. For the analyses with artery and plaque components, the amount of radial displacement was 0.62975 mm, which was again arbitrary chosen to achieve 55% of full dilation. As the simulations with artery and plaque have same geometry of SYNERGY stent, the amounts of radial displacement are equivalent. The loading conditions are summarized in Table 4.2.

As all simulation models in this study have adopted displacement control, free boundary condition is applied. Since no symmetric boundary condition is applied to the models in our study, the constraints along the longitudinal and tangential direction were not necessary to prevent rigid body motion.

	Model A (SYNERGY)	**Model B (Taxus Express^2)**	**Model C (Biomatrix FLEX)**	**Model A with Artery & Plaque (SYNERGY)**
Displacement Increment, mm	*0.687*	0.624	0.9	0.62975
Dilation, %	60	60	60	55
Coordinate System	*Cylindrical*	*Cylindrical*	*Cylindrical*	*Cylindrical*
Boundary Condition	*Free*	*Free*	*Free*	*Free*

Table 4.4 Loading conditions of each model.

References

1. D. Martin, F. J. Boyle, Computational structural modeling of coronary stent deployment: a review, Comp Method in Biom and Biomedical Eng, (14) (2011) 331-348

2. D. K. Liang, D. Z. Yang, M. Qi, W. Q. Wang, Finite element analysis of the implantation of a balloon-expandable stent in a stenosed artery, Inter Jour of Cardio 104 (2005) 314-318.

3. Mac Donald BJ. Practical stress analysis with finite elements. Glasnevin publishing: Dublin. (2007)

4. B. J. O'Brian, J. S. Stinson, S. R. Larsen, M. J. Eppihimer, W. M. Carroll, A platinum-chromium steel for cardiovascular stents, Biomaterials 31 (2010) 3755-3761.

5. D. J. Allocco, M. V. Jacoski, B. Huibregtse, T. Mickley, K. D. Dawkins, Platinum chromium stent series – The Taxus element, Promus element and Omega stents, Touch Briefings (2011) 134-141

6. H. Liu, T. J. Webster, Mechanical properties of dispersed ceramic nanoparticles in polymer composites for orthopedic applications, International Journal of Nanomedicine, 5 (2010) 299-313.

7. W. Wang, D. Liang, D. Yang, M. Qi, Analysis of the transient expansion behavior and design optimization of coronary stents by finite element method, Journal of Biomechanics 39 (2006) 21-32.

8. C. G. Hopkins, P. E. McHugh, J. P. McGarry, Computational investigation of the delamination of polymer coatings during stent deployment, Annals of Biomedical Eng, 38 (2010) 2263-2273.

9. McCarthy, PLACE Flexible packaging summit 2009 symposium (2009) 657-716.

10. ABAQUS/Standard Analysis User's Manual, Vol I&II (ver. 6.10), (2012). Hibbit, Karlsson & Sorensen, Inc., Pawtucket, Rhode Island.

11. I. Pericevic, C. Lally, D. Toner, D. J. Kelly, The influence of plaque composition on underlying arterial wall stress during stent expansion: The case for lesion-specific stents, Medical Engineering & Physics 31 (2009) 428-433.

Chapter 5. Results and Discussions

In this chapter, the computational results with various parameters will be analyzed and discussed. The parameters that we have explored in the current thesis include element dimensionality, strut thickness, coating thickness, and stent design. The focus of the analysis is primarily on the von-Mises stresses at the maximum location in the components of strut, coating, and arterial wall. In addition, the results about the recoil of stent deployment is addressed and discussed as well. Most computational results are majorly based on the FEA of the model A (SYNERGY stent) system.

1. Results from Computations Using 2D and 3D Coating Elements

Before conducting the parameterization study, the prerequisite step is to compare the results between using 2D and 3D elements for coating component. For the 3D elements, in general, creating a good quality mesh model that has a complicated geometry with high aspect ratio is very challenging. Usually, an element with a high aspect ratio is considered as a low quality element. When an element is constructed with a higher aspect ratio, the shape of the element is distorted, which could cause an inaccurate result. Therefore, it is important to maintain the aspect ratio as close to unity as possible and to generate a number of elements when the shape of a model is like a thin-layer. In the current thesis, the geometrical design of the stent is composed of many curvatures, and in the meantime, the thickness of the coating component is very thin compared with that of the strut (See Fig. 4.4). Hence, creating a number of elements must be accompanied so as to prevent element distortion. For the 2D elements, however,

relatively much less number of nodes are needed even the total number of the elements are as same as that of the 3D element so that the computation cost could be remarkably decreased. Consequently, the result comparison between using 2D and 3D element must be carried out before the parameterization study.

The contour plots of von-Mises stress on the coating component of SYNERGY stent (model A, reference model system) using the 2D shell and the 3D solid element methods are shown in Fig. 5.1. For the loading condition, the displacement control was used, and the amount of the stent expansion in a radial direction was set as 60 % with reference to the initial diameter. The maximum location of the stress, as indicated in Figs. 5.1(a) and (b), does not change for both computations. It is found that the plots based on 2D and 3D coating elements are nearly identical not only for the location but also for the magnitude/distribution of the stress along the coating components.

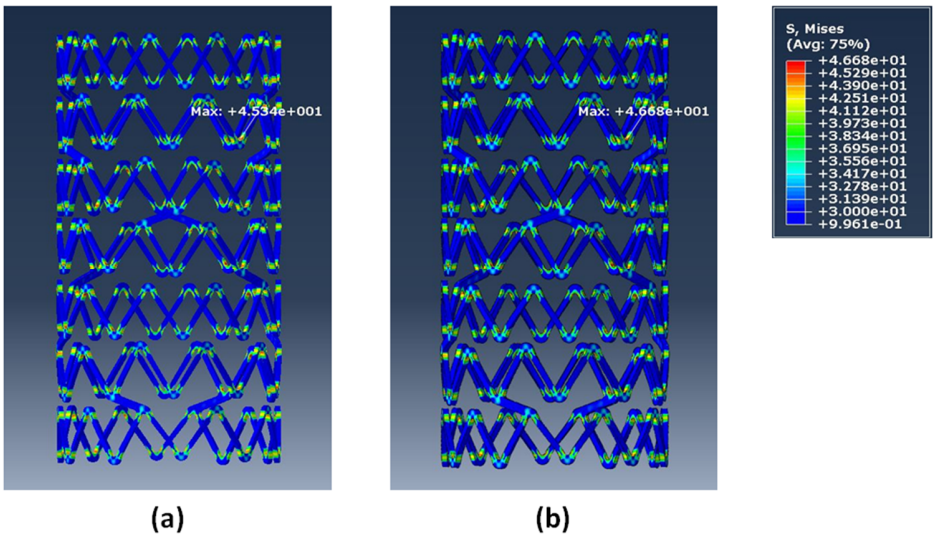

Fig. 5.1 Comparison of stress distribution on the coating of SYNERGY (model A) stent using 2D and 3D elements. (a) 2D shell element and (b) 3D solid element.

In general, to evaluate the 6 stress components with the 3D solid elements, it is necessary to select a proper element that lies on each component in a perpendicular or parallel direction to the axis since the 3D elements follow the global coordinate system whereas the 2D elements have its own local coordinate system. Fig. 5.2 shows the location of the elements used to investigate the stresses shown in Fig. 5.3 and Fig. 5.4. In Fig. 5.3 and Fig. 5.4, we show the profiles of various stress components from computations for model A using 2D and 3D coating elements.

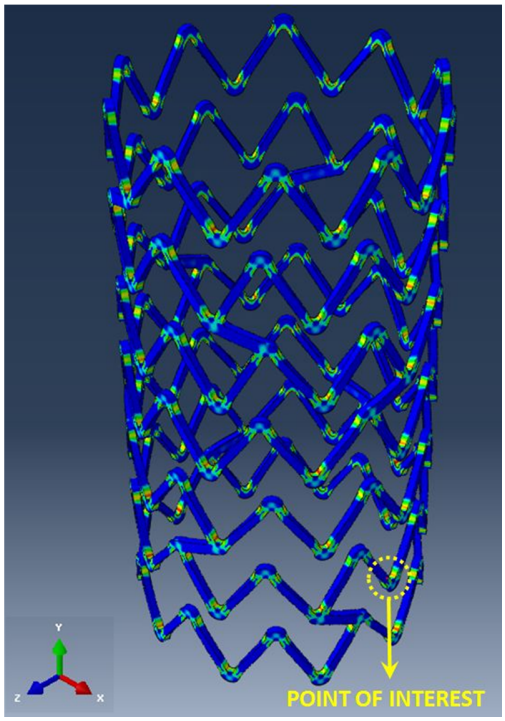

Fig. 5.2 The location of elements used for comparison of 2D and 3D elements.

It should be noted that six stress components (11, 22, 33, 12, 23, and 13 directions, where 1, 2, and 3 represent one of the 3D unit directions) can be analyzed by using the 3D solid elements. On the other hand, the 2D shell elements, which considers plane stress, have only three stress components (11, 22, and 12 directions) since the

stresses with normal direction (3 direction) are neglected. In analyzing our results, it is more convenient to use the cylindrical coordinate system instead of the Cartesian system, i.e., the global coordinate system, defined in ABAQUS/Standard by default. With this Cylindrical coordinate system, the stress components could be readily divided into six different stress components, such as normal/shear stresses in radial, circumferential, and longitudinal directions. Here, we define our system as given in Fig. 5.5. Here, the radial, circumferential, and longitudinal directions were specified with reference to the overall geometry of stent. The yellow arrow indicates the direction of the circumferential normal stress, and the red arrow displays the direction of the radial normal stress.

From Figs. 5.3 and 5.4, it is clearly seen that the stress component of the circumferential normal direction is dominant. The circumferential normal stress curve clearly shows the elastic and plastic region. In the case of the 3D elements, all stress components except the circumferential stress show the value close to zero, which means that their contributions to the magnitude of von-Mises stress have a minor effect. Also, the circumferential normal stress shows its dominance in the 2D elements even though the radial normal stress shows noticeable amount of its magnitude. The maximum value of the circumferential stress was 42.9 MPa for 3D elements and 38.5 MPa for 2D elements.

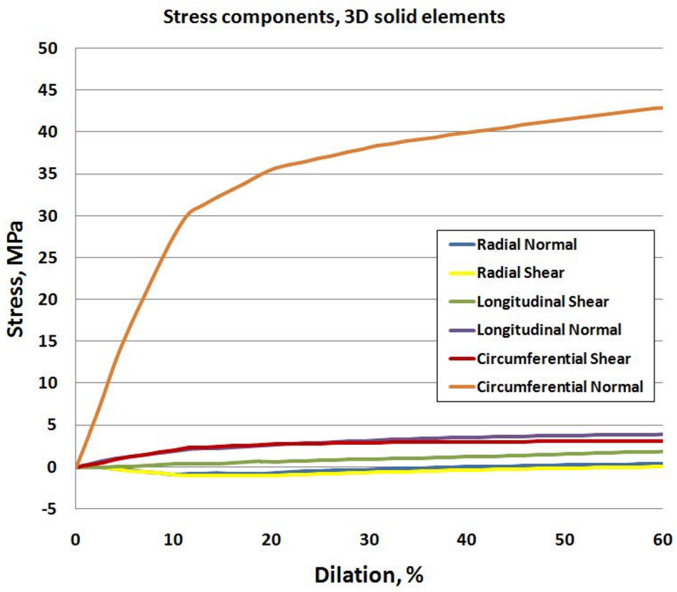

Fig. 5.3 Six stress components in the coating of model A using 3D elements.

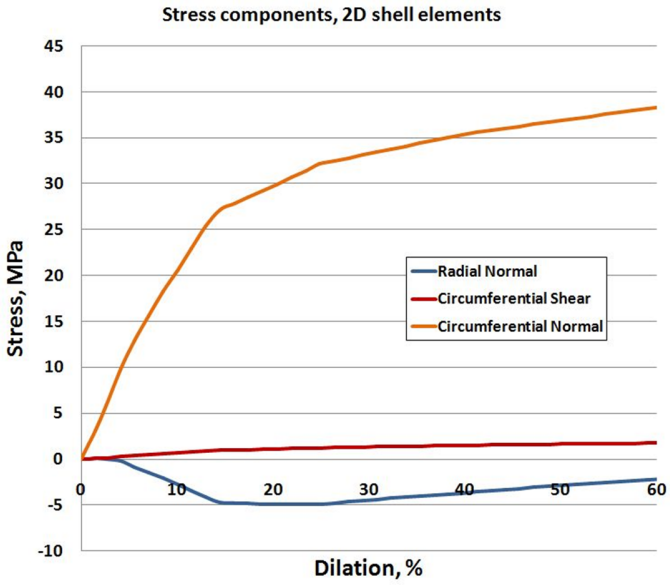

Fig. 5.4 Three stress components in the coating of model A using 2D elements.

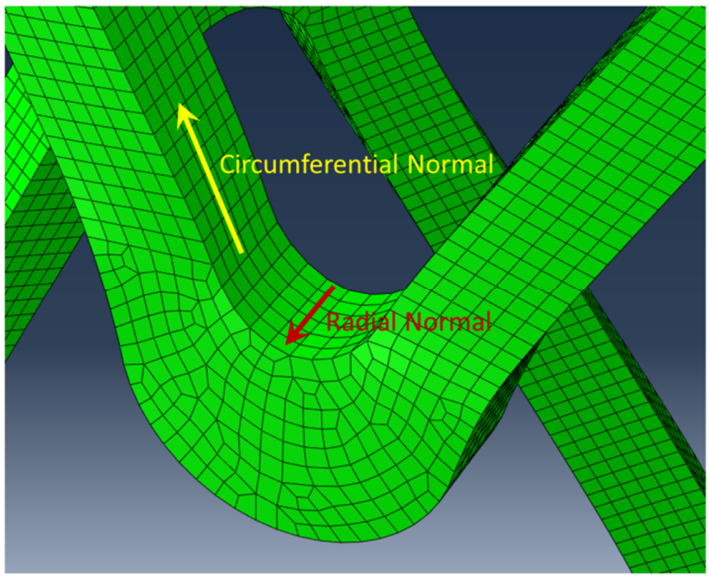

Fig. 5.5 The direction of circumferential and radial normal stresses.

Fig. 5.6 shows the von-Mises stress variation of both cases at the maximum location during expansion up to 60% of full dilation. The difference of two maximum von-Mises stresses from 2D and 3D element systems at the 60% of dilation, which is considered as the complete expansion of the stent, is 0.81%, thus it can be concluded that the von-Mises stress distributions based on the 2D and 3D coating elements are similar. Based on these comparisons, though there are some differences in the individual stress component distributions, it is approximated that all the von-Mises stress predictions in the coating components from the 2D and 3D elements are consistent. Therefore, in analyzing the von-Mises stress distributions, all the rest of the simulations are performed with the coating components with the 2D shell element to reduce the computational costs.

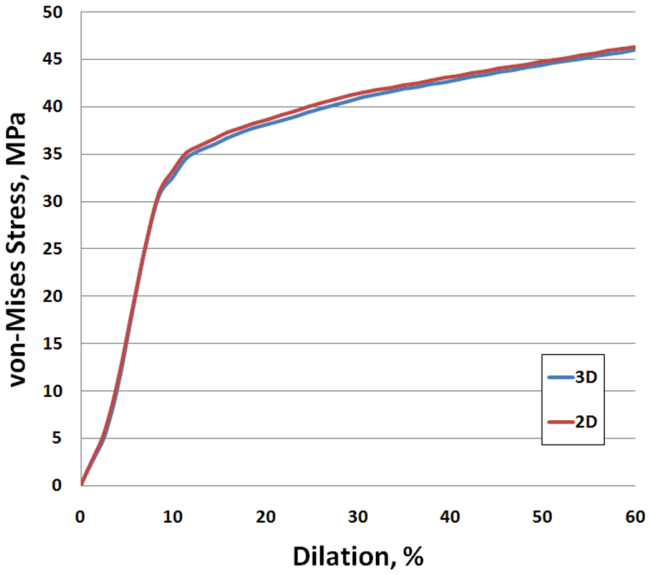

Fig. 5.6 von-Mises stresses at the maximum location as a function of % dilation with 2D and 3D models of model A.

2. Impacts of Stent Strut Thickness

The first set of the simulations evinced the strong influence of the strut thickness on the von-Mises stress distribution along the surface of both the strut and coating components. SYNERGY stent (model A) was used, and the first change of the geometrical parameter was the stent strut thickness, and the values of those are set up as 60 μm, 80 μm, and 100 μm, while the coating thickness is fixed to 7 μm. Fig. 5.7 shows the impact of the strut thickness on the von-Mises stress of the strut itself, and all 3 models are in the same scale with the state of the full expansion with 60% dilation. The locations of local maximum stress zone for these three different conditions are similar, as indicated by the images in the bottom panels of Fig. 5.7. From the results, it is possible to conclude that the red areas that represent relatively high stress concentration increase as the strut thickness becomes thicker. This can be explained by the fact that the strain

increases if the thickness becomes higher. The maximum magnitude of Mises stress is located are on the curves with links. Therefore, it can be considered that these regions are the most vulnerable places to delamination and/or fragmentation of coating.

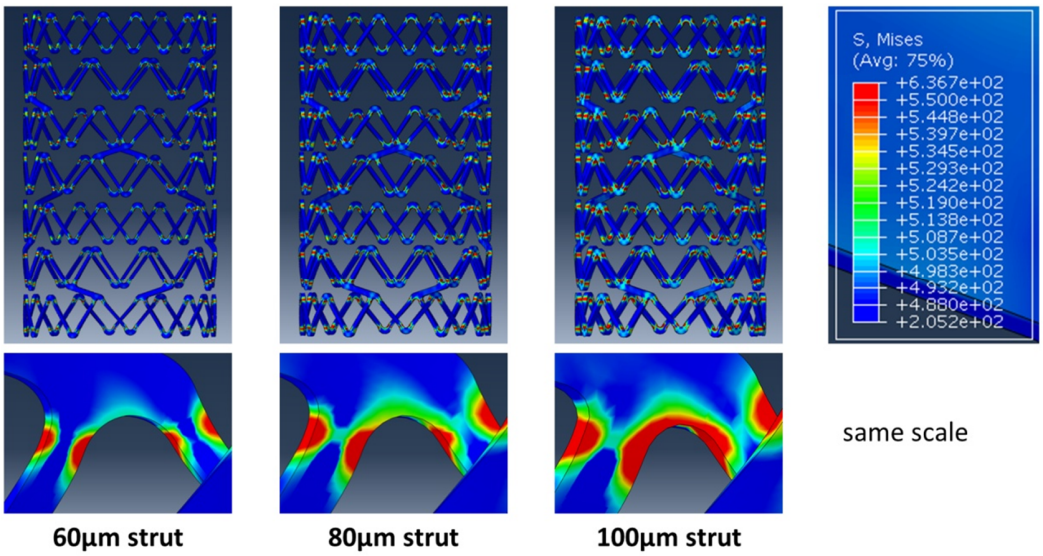

Fig. 5.7 Contour plots of von-Mises stress distributions in the stent platform of model A with different strut thicknesses.

Fig. 5.8 shows the linear relationship between the strut thickness and the maximum stress. The element chosen for analyzing the simulation in Fig. 5.8 is located in the center of the red area from Fig. 5.7. Therefore, it is considered that Fig. 5.8 represents the variations of maximum stresses in the systems with 60, 80, and 100 µm strut thicknesses. At 60% of dilation, the maximum stresses are 586.9 MPa, 607 MPa, and 636.7 MPa for 60 µm, 80 µm, and 100 µm, respectively. From this result, the maximum local von-Mises stress in the stent strut increases by 8.5 % when the strut thickness increases from 60 µm to 100 µm.

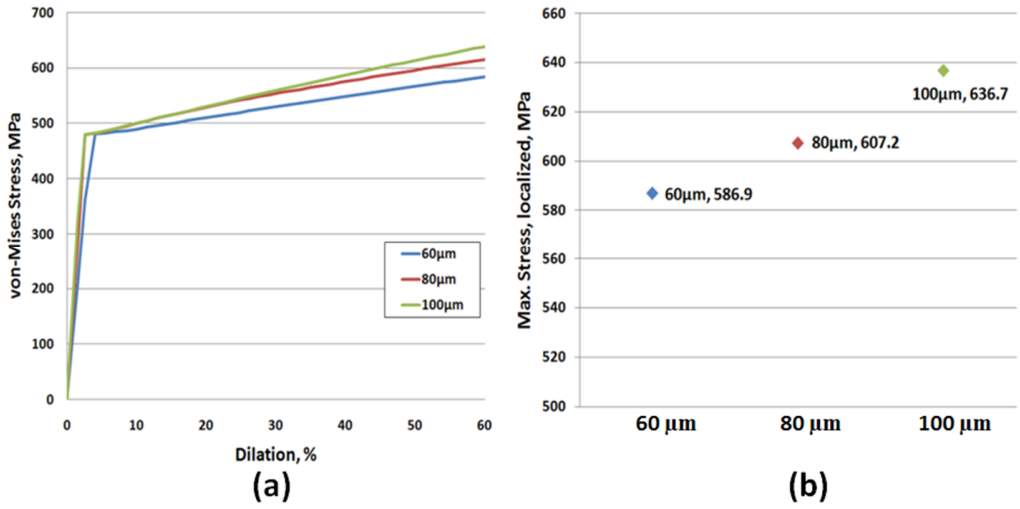

Fig. 5.8 Plots of von-Mises stress distributions on stent strut. (a) von-Mises stress growth with % dilation and (b) Maximum von-Mises stress at the status of full dilation.

In the next figure (Fig. 5.9), we show the contour plots of von-Mises stress distributions on the coating components from the same computations of 60% dilation. These results have an important meaning because they show the stress distributions on the coating component thoroughly, and the shown maximum stress location could be regarded as a vulnerable spot which is prone to be delaminated. The simulation results of the coating components fully expanded are shown in Fig. 5.9 on the same scale to compare the stress differences. In Fig. 5.10, it is easier to identify that the stresses increase as the thickness of the stent strut increases. The location of the maximum stress region is the same as its strut. The magnitude of the maximum stress is 43.98 MPa for 60 µm, 45.34 MPa for 80 µm, and 47.81 MPa for 100µm, respectively. The maximum local von-Mises stress in the coating increases by 8.7 % when the strut thickness increases from 60 µm to 100 µm.

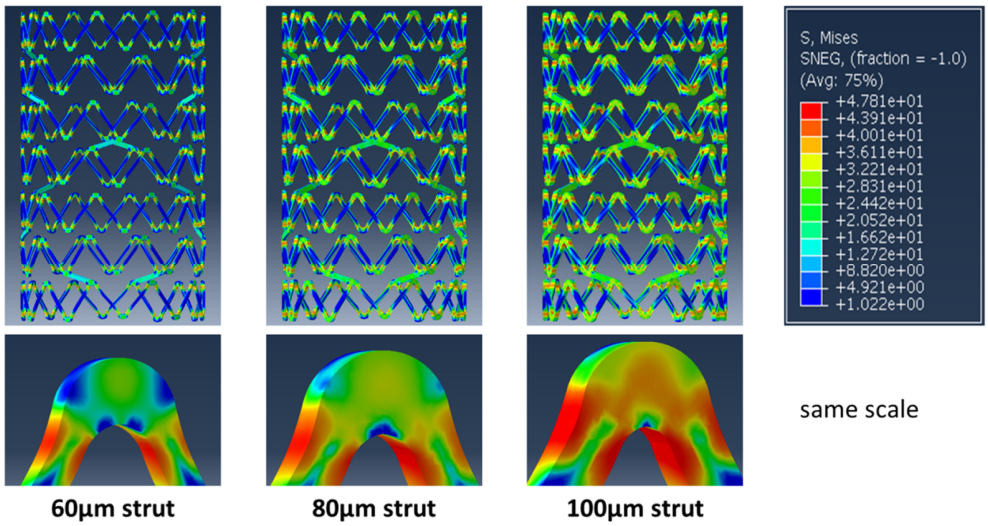

Fig. 5.9 Contour plots of von-Mises stress distributions on the coating component of model A with different strut thicknesses.

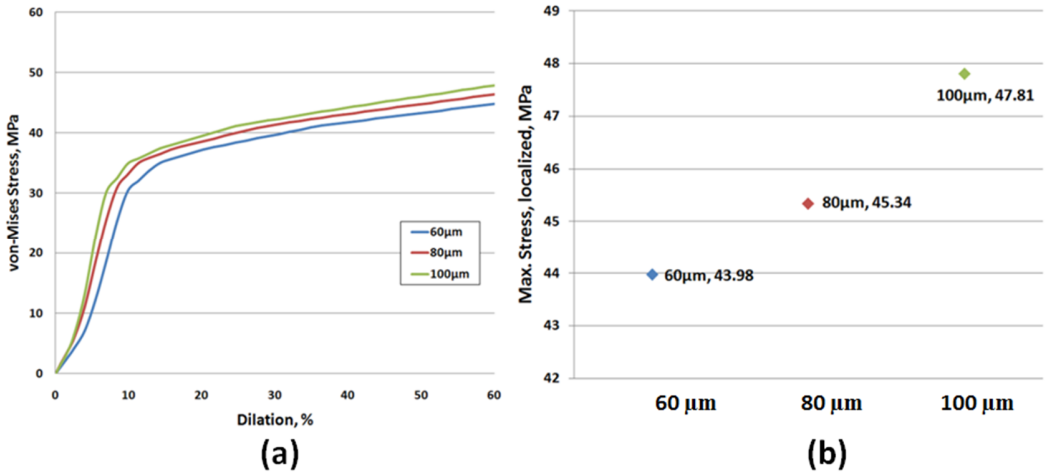

Fig. 5.10 Plots of von-Mises stress distributions on coating component. (a) von-Mises stress growth with % dilation and (b) Maximum von-Mises stress at the status of full dilation.

In Fig. 5.11, the maximum circumferential normal stresses are calculated from 46.5 MPa to 50.16 MPa depending on the strut thicknesses, which means that the stress in that direction is dominant among six stress components. The circumferential normal stress also increases with strut thickness in linear behavior.

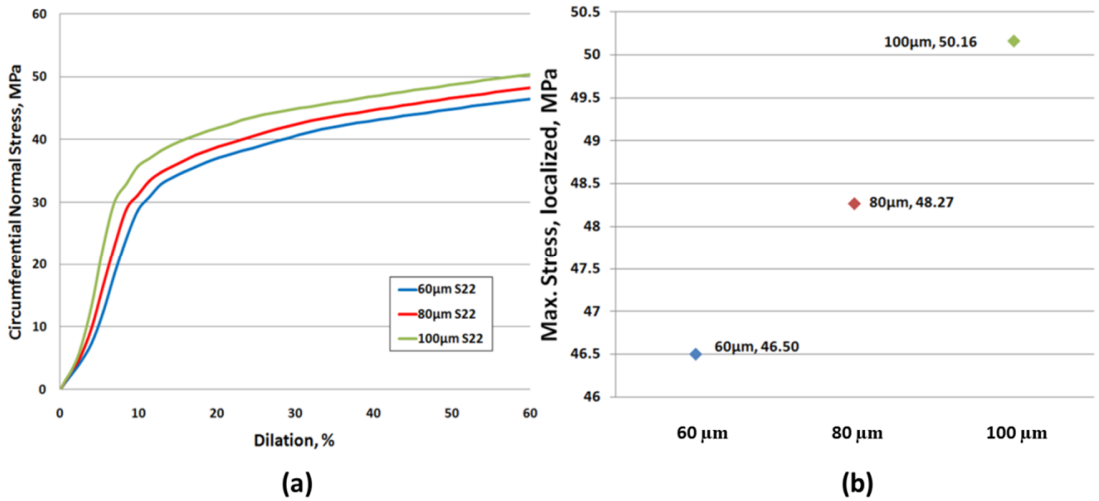

Fig. 5.11 Plots of circumferential normal stress on coating component. (a) Circumferential normal stress growth with % dilation and (b) Maximum circumferential normal stress at the status of full dilation.

Since most of DES are composed of repeated unit cell design, it is would be useful to identify the location of maximum and minimum stress positions along the edge of unit cell. Fig. 5.12 displays the line path (purple lines) along the coating edge of stent strut in the unit cell, and Fig. 5.13 shows the von-Mises stress profiles from the three systems with different thicknesses at the coating edge of strut along the path depicted in Fig. 5.12. In Fig. 5.13, the x-axis represents the distance from the starting point of analysis. To indicate the maximum and minimum point for convenience, the von-Mises stress profile for 80 μm coating thickness was cropped from Fig. 5.13 and re-plotted in Fig. 5.15, since the stress profile will show somewhat repeated patterns depending on the geometry of the unit cell structure of stent. Due to the periodicity, it is considered that the analysis of cropped section shown in Fig. 5.15 can represent the possible variations for the entire stent strut. Fig. 5.14 depicts the image to show the starting/ending path and the maximum/minimum spots for Fig. 5.15. From these results, as shown in Fig. 5.12, it was found that the maximum and minimum points are located at the hinge region of curve and

at the middle of strut between two curves, respectively. The maximum von-Mises stress location was identified as the near the center of hinge (not the center of the hinge) in the inner side of the cell path. In the inner side path, the stress at exact center of hinge is predicted to be much smaller than that in the maximum location. The maximum stress location along the outer side was also near the center of the hinge, not the exact center position.

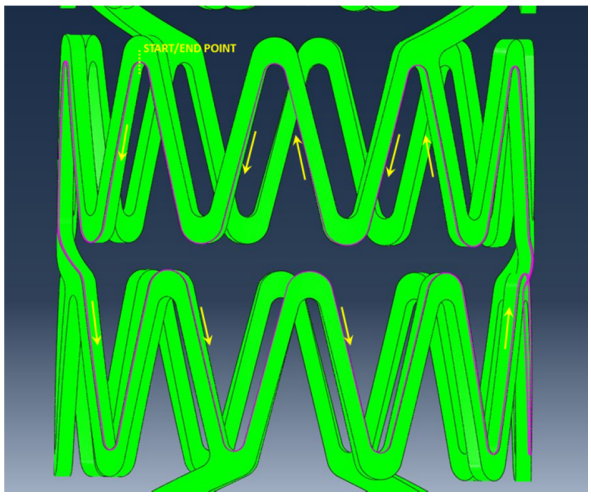

Fig. 5.12 The path on the edge of model A (SYNERGY stent) strut along the unit cell.

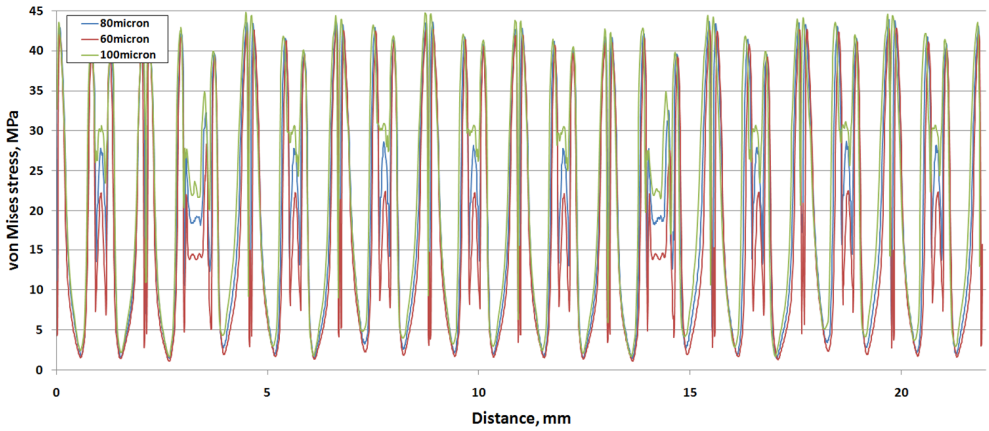

Fig. 5.13 The von-Mises stresses variation on the edge of unit cell as a function of distance and strut thickness.

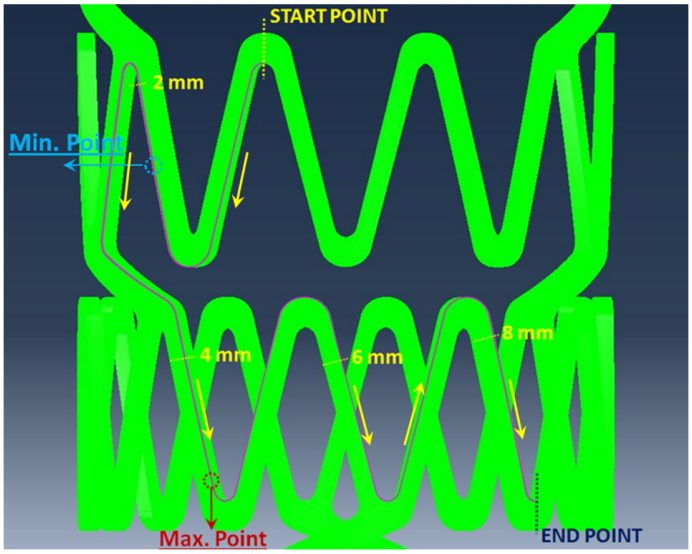

Fig. 5.14 Cropped path of unit cell structure in model A (SYNERGY stent) from Fig. 5.12.

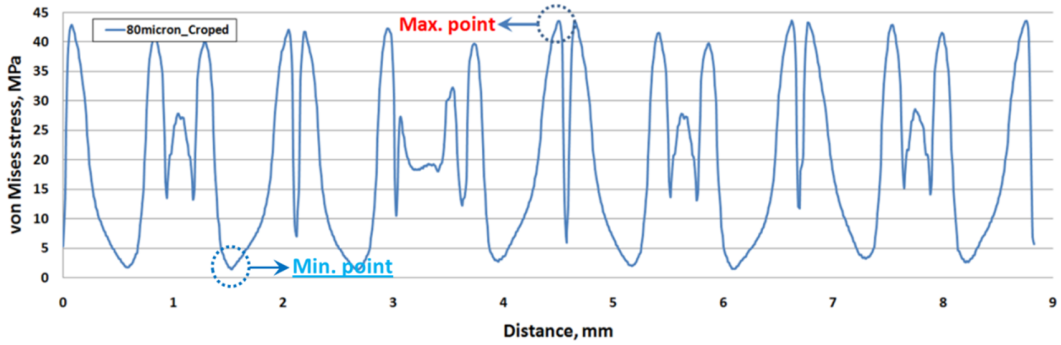

Fig. 5.15 Cropped von-Mises stress curve for 80 µm.

3. Impacts of Coating Thickness

Stresses in the coating component with its thickness variation were also investigated for the second set of the study, where the stents were expanded to achieve the same level of the dilation by 60 % of the initial diameter. We tested three different models with 7µm, 12µm, and 20µm of the coating thicknesses. The strut thickness was set as 80 µm as it is regarded as the reference model.

In investigating the stresses in the coating components, it was found that the increased strain of the outer surface of the coating component by the accretive coating thickness induced higher stress magnitudes. Fig. 5.16 shows the von-Mises stress distributions on the coating components of three models with different coating thicknesses in the same scale. The maximum von-Mises stresses were 46.50 MPa for 7 µm coating, 47.4 MPa for 12 µm, and 48.72 MPa for 20 µm, respectively (see Fig. 5.17). Although the color differences among three models appear relatively smaller compared with those from the simulation with different strut thickness models (see Fig. 5.9), it was calculated that the maximum local von-Mises stress in the coating component increases by 4.7 % when the coating thickness increases from 7 µm to 20 µm.

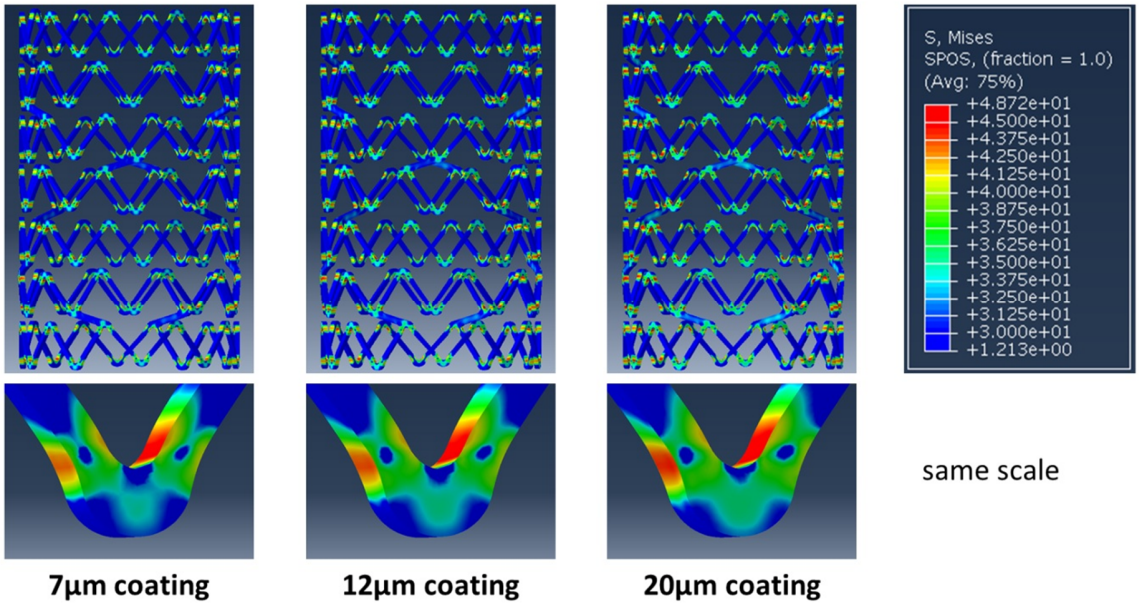

Fig. 5.16 Contour plots of von-Mises stress on coating component as a function of coating thickness.

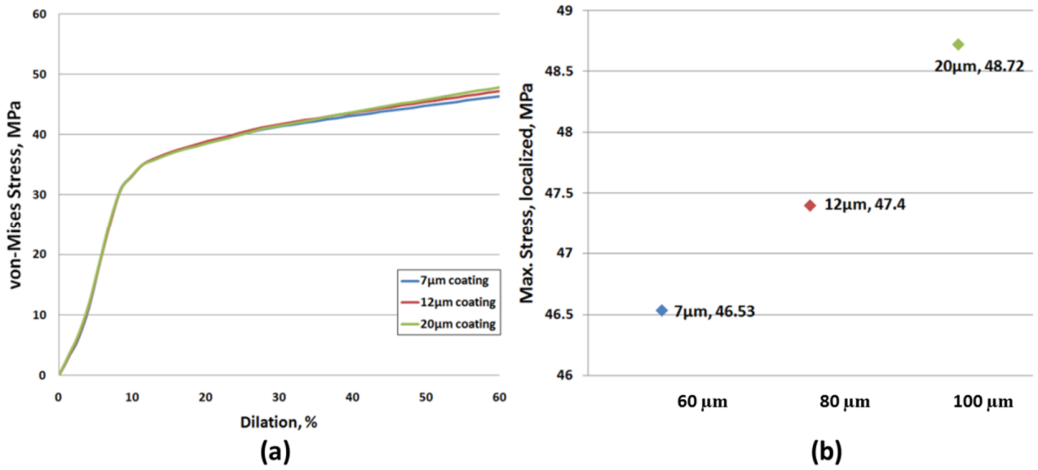

Fig. 5.17 Plots of von-Mises stress on coating component. (a) von-Mises stress growth with % dilation and (b) Maximum von-Mises stress at the status of full dilation.

4. Stresses on the arterial wall & plaque

Up to this point, we have only discussed stress concentration in the DES medical device itself, i.e., stent platform and coating. In this sub-section, we introduce the computations containing the biological environment to address the effects of strut thickness on the stress distributions in the atherosclerotic plaque and arterial wall. Also, results from the recoil phenomena computations are presented.

4.1 Full expansion

To evaluate the effects of strut thickness on the stress concentrations on the inner surface of an arterial wall, the models with three different strut thicknesses are developed. In this set of simulations, the SYNERGY stent system (model A) was also employed. The initial inner diameter of the stent was set as 2.29 mm, and the diameter was 3.55 mm when the stent is fully expanded, which is 55 % dilation with respect to the initial

diameter. As mentioned in the Chapter 4, 55 % of dilation was arbitrary chosen. In this section, the stresses at the full expansion in the artery will be considered.

Fig. 5.18 shows the von-Mises stress distributions in the arterial wall from the three different strut thicknesses when the DES is fully expanded. For direct comparison, the same contour scale was used for individual contour maps in Fig. 5.18. Notable is the fact that a higher stress over 5.929 MPa is shown in the regions directly contacting to the stent. All three stents were expanded by the identical amount as the displacement control method was adopted; each model has the same diameter when it is fully expanded. Therefore, it can be concluded that the difference of the stresses between these models is not derived by the amount of the expansion, but only by the strut thickness. As seen in Fig. 5.18, the magnitude of the stress shows a significant increase from 60 μm to 100 μm of the thickness. The maximum von-Mises stresses from the model A systems with 60 μm, 80 μm, and 100 μm strut thicknesses were 6.145, 6.403, and 6.7 MPa, respectively, as shown in the bar graph of Fig. 5.19.

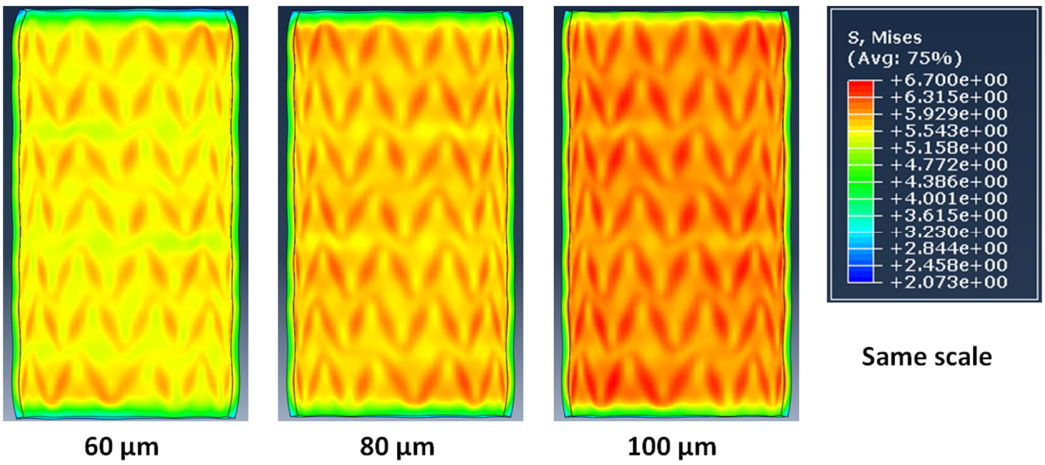

Fig. 5.18 Von Mises stress in arterial wall with different strut thicknesses.

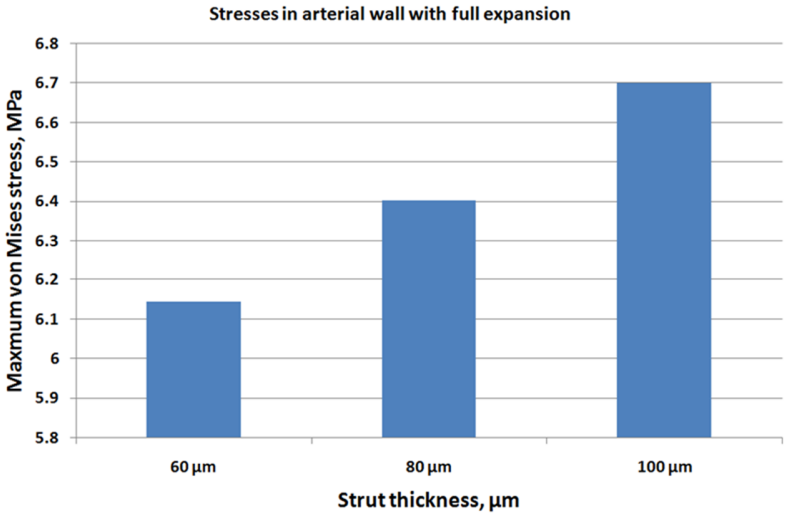

Fig. 5.19 Maximum von Mises stresses on the inner surfaces of arterial walls with different strut thicknesses.

Fig. 5.20 illustrates the von-Mises stress profiles on the inner surface of plaque wall with three different strut thicknesses. The stress distributions on the plaque surface are in particular important because it is known that they are closely related to the fracture of endothelium layer and the ISR occurrence rates. From 5.20, it is seen that the magnitude of von-Mises stress increases with the strut thickness. However, even the overall trend of stress distribution on inner surface of plaque shows similar result from that of artery, the location of maximum von-Mises stress is different. The maximum point of von-Mises stress in the computational system is located at the upper and/or lower edge of plaque. This is because there is higher degree of interactions between stent platform and plaque surface at the end of medical devices. However, since the appropriate area to represent the stress on the plaque is located on the middle part of its inner surface, a selection of a set of elements are required for relevant stress analysis. As given in Fig. 5.21, we have selected three locations to represent the general stress points of model A. With these three locations, the averaged value was used as the value for von-Mises stress

on the inner surface of plaque. The averaged von Mises stresses of the 60 µm, 80 µm, and 100 µm were 2.28, 2.39, and 2.68 MPa, respectively (Fig. 5.22).

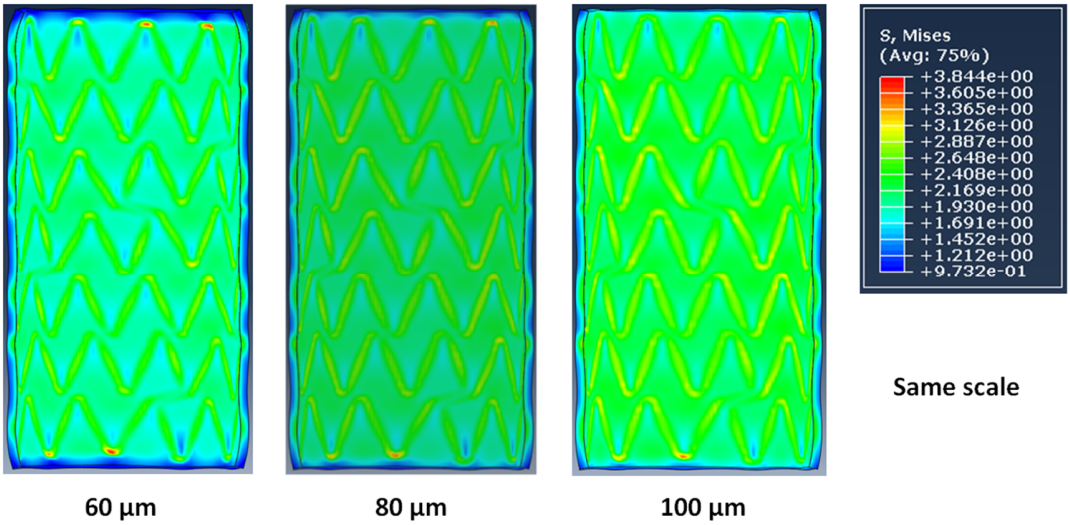

Fig. 5.20 Von-Mises stress in plaque with different strut thicknesses.

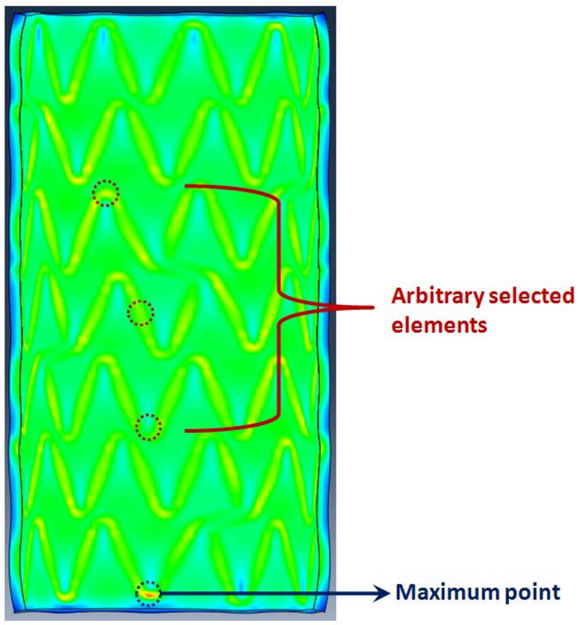

Fig. 5.21 Arbitrary selected elements on inner surface of plaque to represent the averaged von-Mises stress.

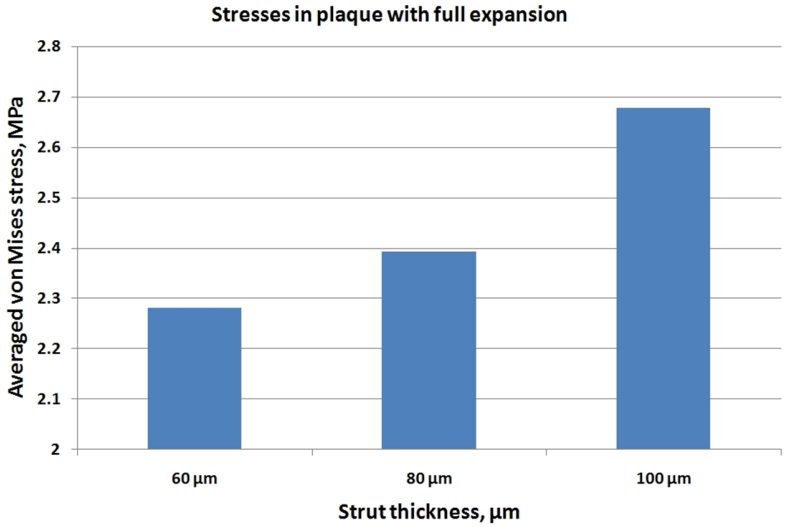

Fig. 5.22 Averaged von-Mises stresses on the inner surfaces of plaque with different strut thicknesses.

4.2 Recoil Rates

When the displacement load exerted on the stent is released to zero (deflation), due to the interactions between artery, plaque and stent, the recoil phenomena are observed. After the removal of the displacement load, the artery and plaque start re-narrowing their lumen because of their hyper-elasticity. For this behavior, the stent will go through recoil whose magnitude of the rate is determined by the thickness and material properties of the stent. In this study, we performed the simulation with three models with different strut thicknesses; 60 µm, 80µm, and 100µm. With these variations, the recoil rate was calculated by,

$$\textbf{Recoil rate} = \frac{D_{\text{inflated}} - D_{\text{deflated}}}{D_{\text{inflated}}} \times 100\% \qquad (5.1)$$

Where $D_{inflated}$ is the inner diameter of the stent when the stent is fully expanded and $D_{deflated}$ is the inner diameter of the stent after the recoil, respectively. Fig. 5.23 shows the percentage recoil rate of three stent models with different thicknesses. The recoil rate for 60 µm is 18.77 %, 80 µm is 14.93 %, and 100 µm is 6.52 %. From these results, we can conclude that the recoil rate of stent strut is highly dependent upon its strut thickness. Since the polymer delamination and ISR problems are most likely to occur after a certain time, the stress analysis after the recoil should be carried out.

Fig. 5.23 The recoil rates of three stents with different thicknesses.

4.3 Stress distributions after recoil

In this section, the von-Mises stresses of each component after recoil will be discussed. As mentioned before, it is very important to observe and analyze the stress distribution after recoil because this status is closely related to the rate of ISR and/or the possibility of polymer coating delamination. In addition, when we modify the thickness of strut, the major difference appears after the deflation. Fig. 5.24 depicts the von-Mises stress distributions on the inner surfaces of arteries with strut thickness variations, and

Fig. 5.25 shows the comparison of maximum von-Mises stresses from the three different models. The maximum Mises stresses were 4.171 MPa for 100 µm, whereas 1.027 MPa for 60µm, which is 75.4% reduction in magnitude.

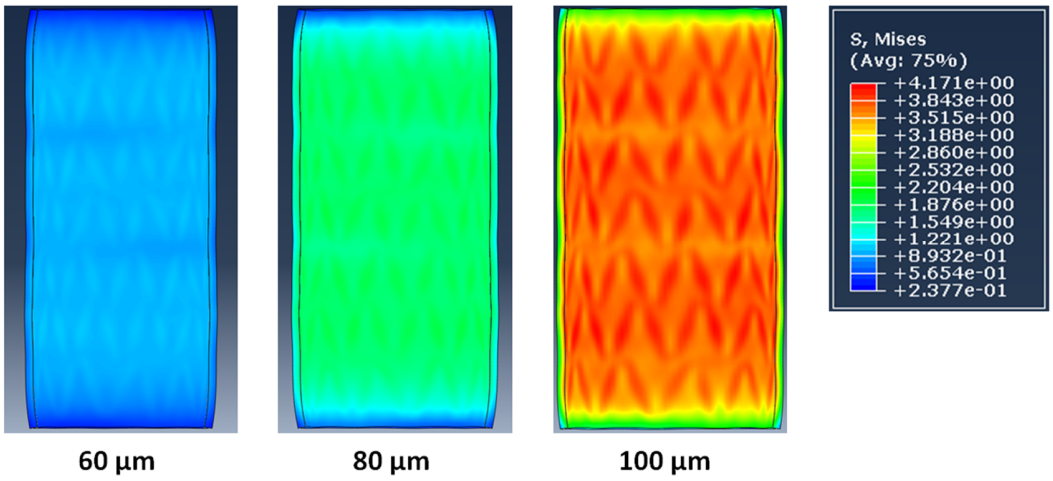

Fig. 5.24 Von-Mises stresses on the inner surfaces of arterial walls after recoil.

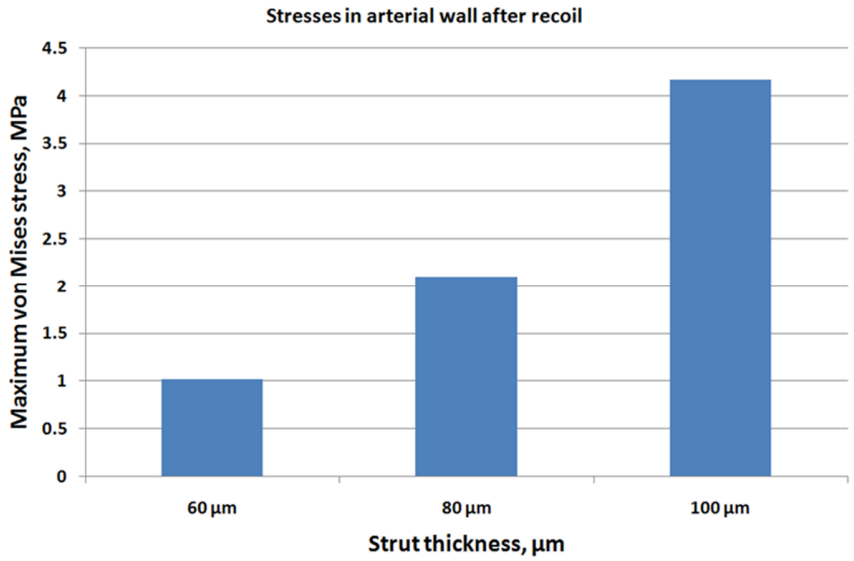

Fig. 5.25 Maximum von-Mises stresses on the inner surface of arterial wall after recoil with different strut thicknesses.

The effect of strut thickness to the von-Mises stress on arterial wall is consistent with other FEA studies. In 2009, H. Zahedmanesh and C. Lally [1] performed FEA computations for stents with different strut thickness parameters. The authors changed the thickness of strut from 50 µm to 140 µm. As seen from Fig. 5.26, the von-Mises stresse distributions on arterial wall are obtained with the states of before and after recoil. The results produced from the authors show a clear difference from the values of our work because the platform materials incorporated in their model is 316L. However, it is apparent that the general trend of increasing stress with strut thickness is observed [1].

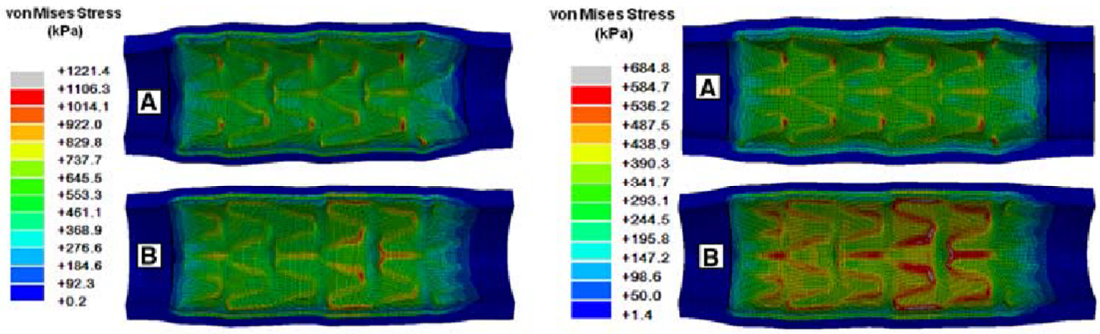

Fig. 5. 26 von-Mises stresses in the arterial wall with thin strut stent (A) and thick strut stent (B) [1].

Fig. 5.27 depicts the von-Mises stress distributions on the inner surfaces of plaques with strut thickness variations. From Fig. 5.27, it is apparent that much higher stress is concentrated when a thicker stent strut is applied. For more quantitative analysis, we show Fig. 5.28 to contain the comparison of averaged von-Mises stresses from the three different models. The averaged Mises stresses were 1.428 MPa for 100 µm, whereas 0.307 MPa for 60µm, which is 78.4% reduction in magnitude as the strut

thickness decreases. Hence, it is thought that the thickness of DES strut is a critical parameter to influence the risk of ISR.

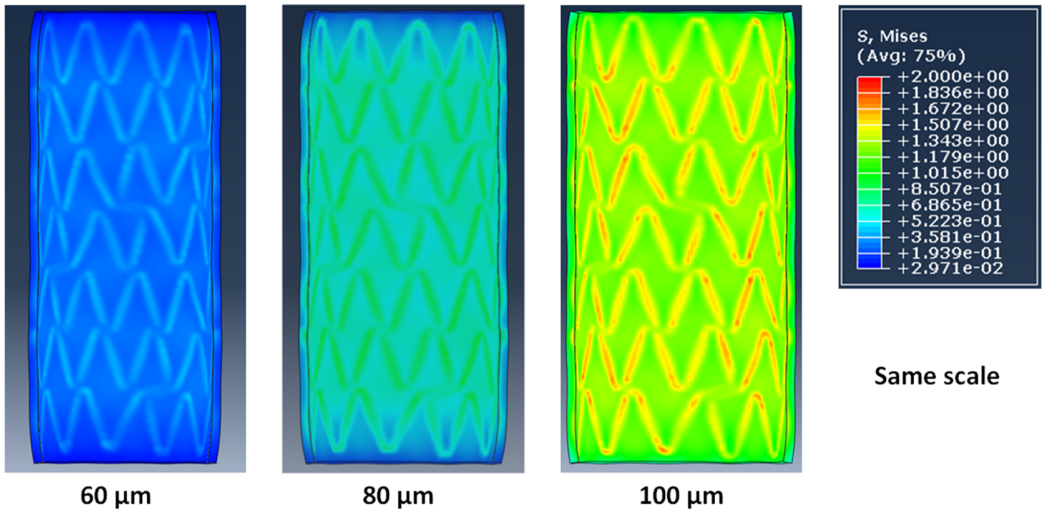

Fig. 5.27 Contour map of von-Mises stresses on the inner surface of plaque after recoil from model A systems with different strut thicknesses.

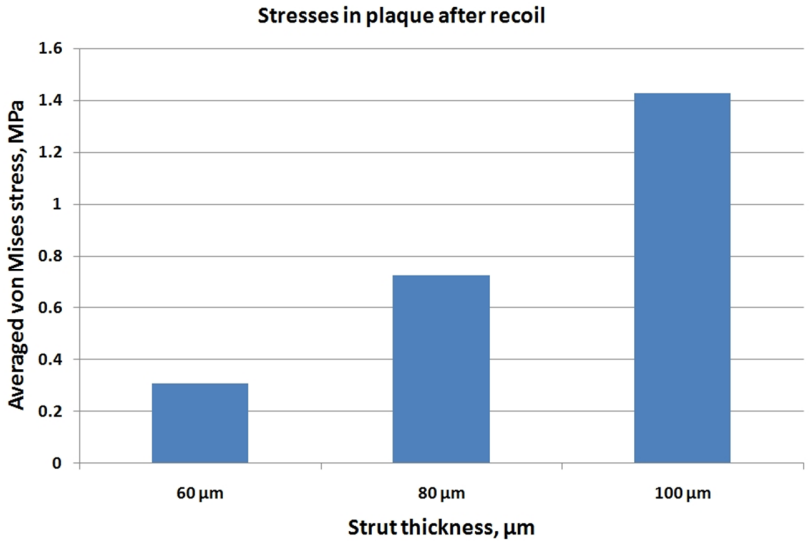

Fig. 5.28 Averaged von-Mises stresses on the inner surface of plaque after recoil from model A with different strut thicknesses.

Fig. 5.29 shows the von-Mises stress distributions in the polymer coating for each model after recoil. Similar to the previous results of free expansion, the computation shows that the magnitude of Mises stress increases with the strut thickness of stent

platform at the identical location from previous results. Fig. 5.30 illustrates the comparison of maximum Mises stresses with the variation of strut thickness. The maximum Mises stresses were 31.91 MPa for 60µm, 33.61MPa for 80µm, and 37.53 MPa for 100µm, respectively. As the strut thickness increases from 60 µm to 100 µm, the maximum Mises stress increases by 14.9 %.

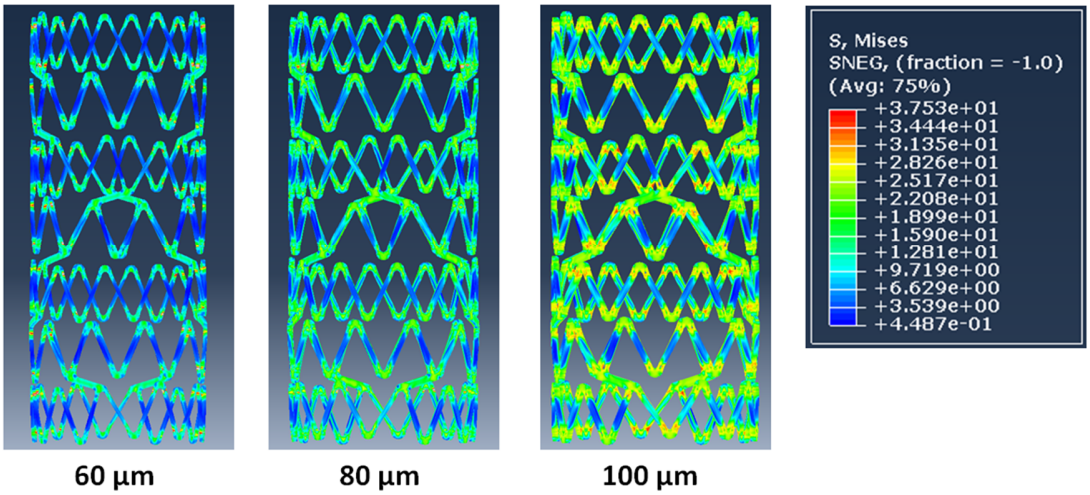

Fig. 5.29 Von-Mises stresses on the polymer coatings after recoil.

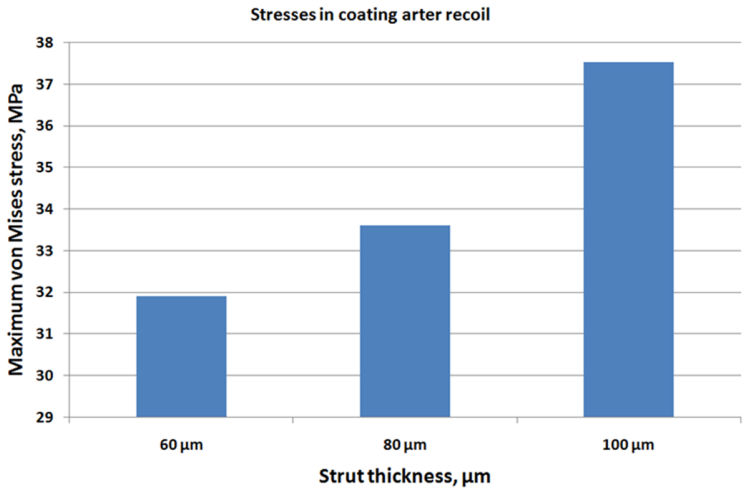

Fig. 5.30 Maximum von-Mises stresses on the polymer coatings after recoil with different strut thicknesses.

Fig. 5.31 shows the von-Mises stress difference between before and after recoil on the coating components of model A DES. As expected, in all cases, maximum Mises stress is considerably decreased after recoil. The percent changes of maximum von-Mises stresses on coating in the systems before and after the recoil were 25.1% for 60 μm, 24.8% for 80 μm and 19.8% for 100 μm, respectively, which shows that, in general, higher stress reduction is expected in the system with thin strut after recoil.

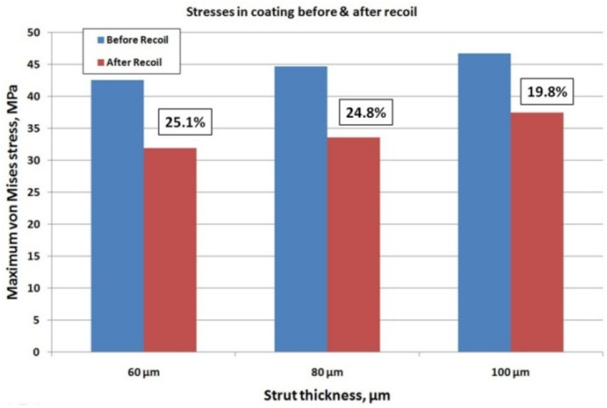

Fig. 5.31 Comparison of maximum von-Mises stresses on coating (% change) before and after the recoil

Until now, all the result of Mises stress on the components have increased with the thickening the stent strut thickness. However, the last part of result that is evaluating the von-Mises stresses on the strut after recoil shows different results. In Fig. 5.32 and Fig. 5.33, the contour maps of von-Mises stress distributions and the maximum stresses in the stent strut after recoil are respectively shown for the model A systems with different strut thicknesses. As we can see from Fig. 5.32 and Fig. 5.33, the general trend is different from previous results; the Mises stresses on the strut of 80μm are higher than 100μm strut. The maximum von-Mises stresses were 623.8 MPa for 60μm, 663.5MPa for 80 μm, and 645.6 MPa for 100μm, respectively. As we discussed in previous section, the plastic behavior and/or the stresses are highly related to the recoil ratio. When 80 μm and

100 µm stents are compared, 100 µm stent shows much less recoil ratio than that of 80µm. Once the fully expanded stent starts to recoil, the stress on the strut begins to be alleviated. However, after a certain point, the stress starts regaining its stress because of its plastic property. Therefore, it can be explained that the von-Mises stresses on the strut with 80µm shows higher magnitude than that of 100µm. Interestingly, the case of 60µm does not follow this rule. According to the previous finding, the magnitude of von-Mises stress should be the highest among the three models, however, the maximum von-Mises stresses for 60µm was 623.8 MPa which is the lowest. Adopting the finding from previous section, the magnitude of maximum stress is a function of strut thickness itself. Therefore, this result could be explained by that the thickness contribution to its von-Mises stress is major while the effect of recoil is minor.

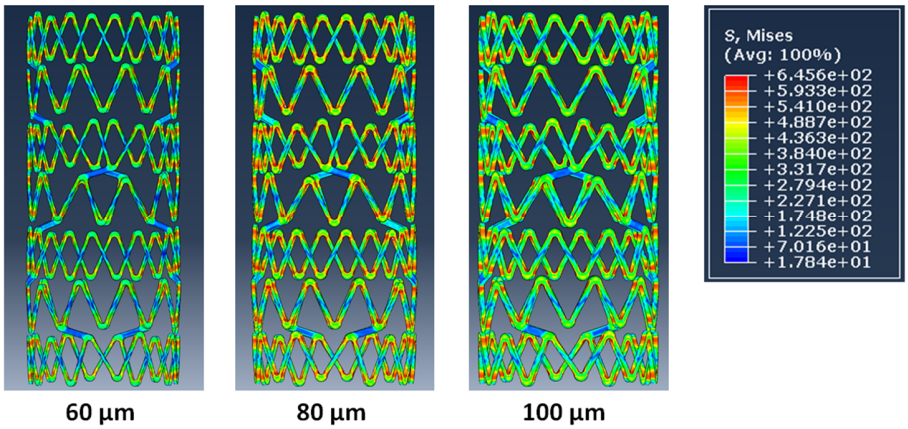

Fig. 5.32 Contour map of von-Mises stress distributions on the stent struts after recoil.

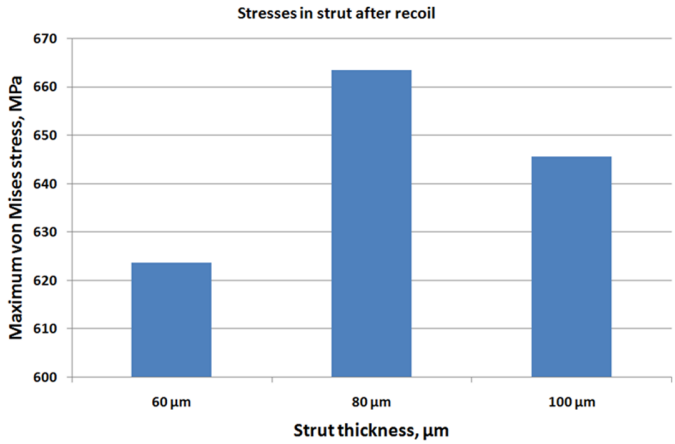

Fig. 5.33 Maximum von Mises stresses on the polymer after recoil with different strut thicknesses.

Fig. 5.34 shows the relative changes of maximum von-Mises stresses on the stent platform of three systems with different strut thicknesses between before and after recoil. 60 µm model shows highest difference of 14.75% whereas 100 µm model shows only 2.2%. It is noteworthy that Mises stress becomes greater after recoil which is opposite to that of results for coatings. This phenomenon could be explained by that the residual stress is greater than the magnitude of induced Mises stress by full expansion due to high stiffness characteristic of Pt-Cr alloy materials. The percent change of maximum von-Mises stresses between before and after the recoil is 14.75% for 60 µm, 13.9% for 80 µm, and 2.2% for 100 µm, respectively.

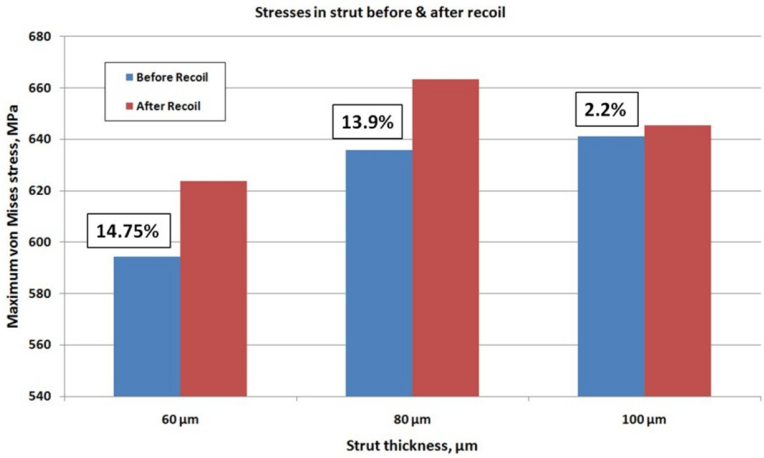

Fig. 5.34 Comparison of maximum von-Mises stresses on stent platform (% change) before and after the recoil

The von-Mises stress distribution and the location of maximum point in stent strut are observed in similar figuration with other FEA studies. In 2006, Donnelly et al. [2], have carried out the research about the stress on stent strut. They adopted commercial BMS (Abbott Opencell stent) to predict the von-Mises stress distribution on stent strut (see Fig. 5.35). It is thought this work is one of the few reports to contain the stress distributions in the stent strut. According to their results, the maximum Mises stresses were observed as 580.5 MPa and 540.7 MPa when the stent is fully expanded and elastically recoiled, respectively. The maximum Mises stress on strut after recoil is decreased since the recoil is occurred within its elastic regime, and the existence with contributions of artery and plaque wall was neglected. Even though the direct comparison of this result to our work is not feasible due to the dissimilar simulation conditions (i.e., material properties, loading conditions), the authors also showed that the location of maximum point is the near-link area [2].

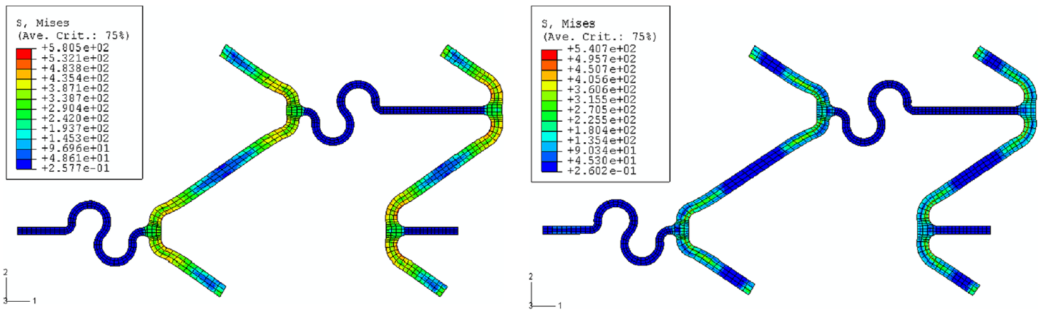

Fig. 5.35 von-Mises stress distribution on Abbott Opencell stent (BMS) [2].

Again, it is important to keep track on the locations of maximum and minimum Mises stress after recoil. As shown in Fig. 5.36, the regions for the maximum and minimum stresses still roughly belong to the near-hinge curve area of inside path and middle of strut between curves, respectively, even though the exact locations have been somewhat altered. Therefore, it is again expected that there is a higher chance of drug-polymer coating fracture in this near-hinge area even after the recoil. In Fig. 5.37, the von-Mises stress variations are plotted as a function of distance from the pre-defined starting point of unit cell structure. The indicators for max/min points shown in Figs. 5.36 and 5.37 are corresponded to each other.

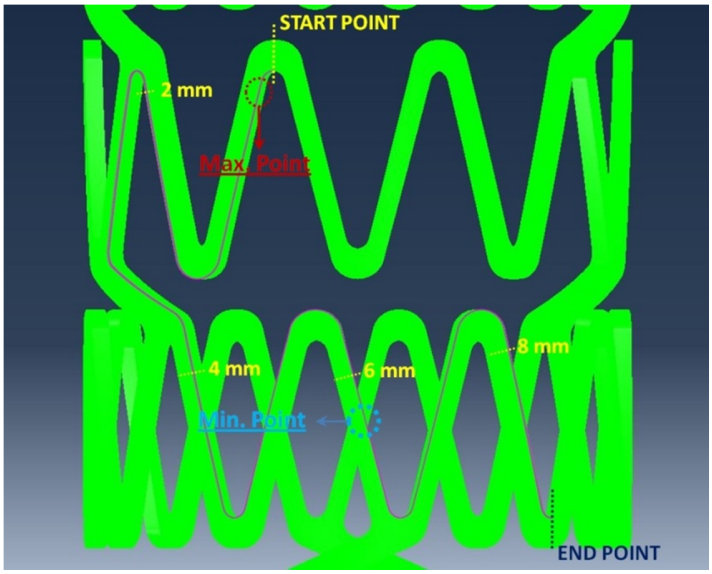

Fig. 5.36 The location of maximum and minimum von-Mises stresses on the coating after recoil.

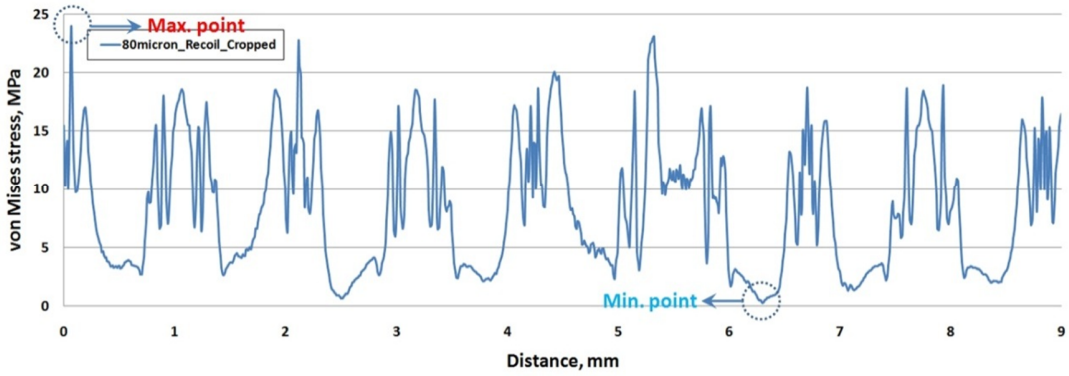

Fig. 5.37 The curve of von-Mises stress on the coating along the cropped path after recoil.

5. Stents Comparison: Model A, B, and C

5.1 Stress distributions in the stent platform

Next, we performed FEA simulations to compare the mechanical behaviors of three different models, A, B, and C (SYNERGY, TAXUS Express, and FLEX, respectively), as introduced in Chapter 4. Fig. 5.38 illustrates the predicted von-Mises stresses on stent strut platforms of these three different commercial stents after 60 % of dilation from the initial diameters. Unlike the previous results (based only on the model

A, SYNERGY stents), unfortunately, they do not share the same scale of legends so that the direct comparison is impossible. Each of their simulation conditions is not identical as the geometrical parameters and applied material properties are different for these three DES products. 316L stainless steel was used for the model B (TAXUS Express^2) stent and model C (Biomatrix FLEX) stent strut material, whereas Pt-Cr alloy was used for the model A (SYNETGY) stent. The SYNERGY stent has PLGA biodegradable coating component, TAXUS Express^2 has SIBS, and Biomatrix FLEX stent contains PLA polymer as drug carrier. As seen in Fig. 5.38, Model B and model C are showing highest Mises stresses on the curves whereas model A shows maximum stress location on both end sides of curves. Although the direct comparison is not readily available, the contour plots shown below implies that it is feasible to predict the regions of high concentrated stress where the delamination would be most likely to occur.

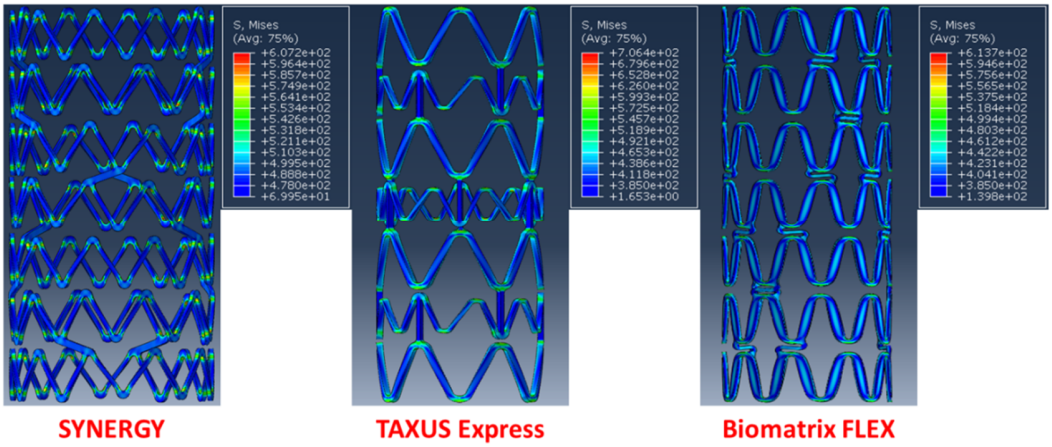

Fig. 5.38 Contour plots of von-Mises stress distributions on stent strut in three different commercial stent products.

Fig. 5.39 shows (a) the von-Mises stress profiles on the stent strut during deployment and (b) the maximum Mises stress values for each model. As can be seen from this figures, the two stents (model A and model C), the newer commercial products, show considerably less von-Mises stress concentrations compared to the model B which is 1st generation of DES. At the early stage of deployment, Model A shows much higher stress than other models, but the stress of Model C continuously increases and becomes greater than Model A after the yield point (see Fig. 5.39(a)) due to the material property of 316L stainless steels. Although the materials used for each models are different, the general tendency of newer generation stents show much less than that of earlier generation stent. The result shows that the Model A exhibits the lowest maximum stress of 607.2 MPa, whereas the Model B shows the highest maximum stress of 706.4 MPa (see Fig 5.39(b)).

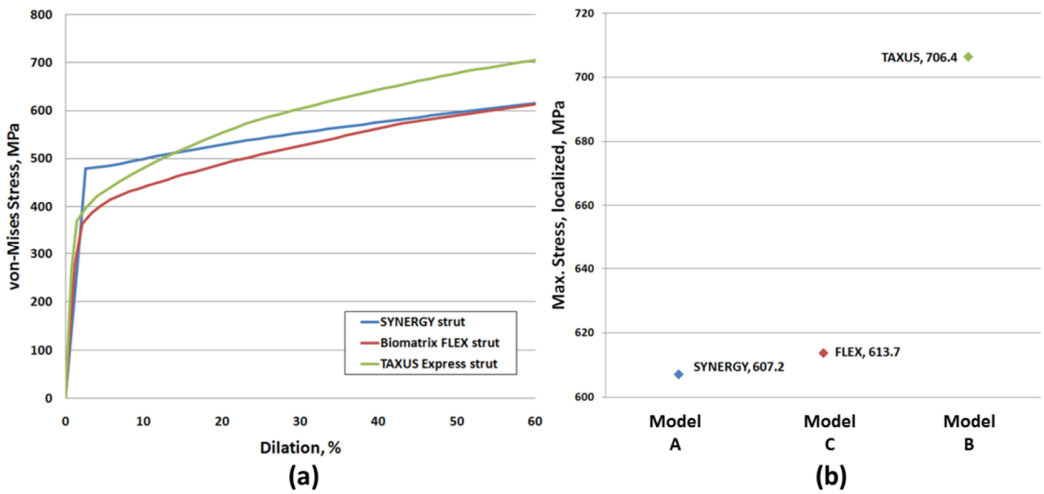

Fig. 5.39 Plots of (a) von-Mises stress profiles on the stent strut as a function of % dilation and (b) the maximum Mises stress from three different types of DES products.

5.2 Stress distributions in the coating

The last set of computation in this work includes evaluating the von-Mises stresses on the coating components in the three commercial DES. Fig. 5.40 illustrates the contour plots of von-Mises stress distributions on coatings for each model. The magnitude difference of maximum stress is glaringly obvious in coating comparison, as shown in Fig. 5.40; the Model B shows very low and locally concentrated Mises stress compared with other models.

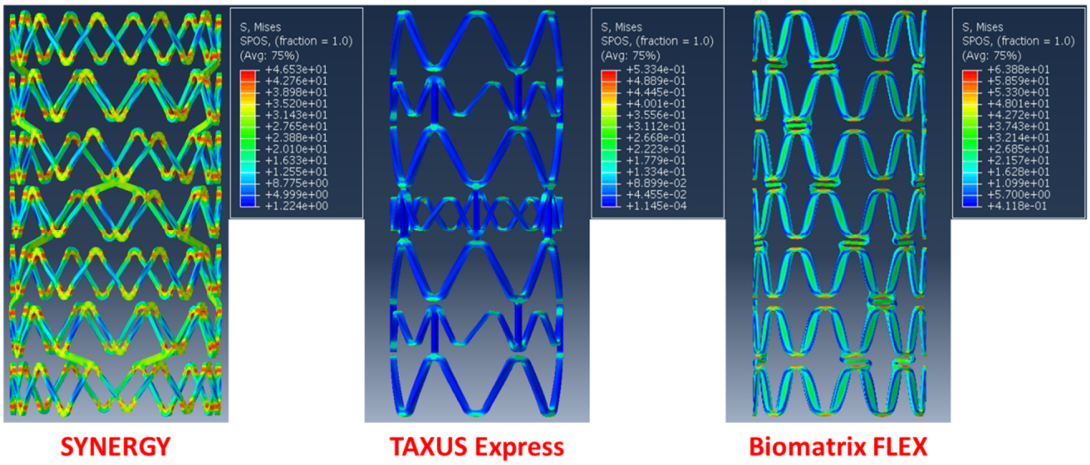

Fig. 5.40 Contour plots of von-Mises stress distributions on coating components in three different commercial stent products.

Fig. 5.41 illustrates the maximum von-Mises stresses on the coating components of the three model systems. Since the SIBS, the drug carrier polymer for model B, has almost elastomer material properties such as very low modulus and yield strength, the maximum Mises stress is 0.5334 MPa which is almost negligible. The highest maximum stress is 63.88 MPa which is monitored in model B, whereas model A shows 46.53 MPa.

To predict and investigate the coating delamination of coating, another approach could be utilized as well as observation of von-Mises stress. As mentioned in previous

section, Hopkins et al. [3], performed the FEA simulations to reveal the coating delamination phenomena. The authors adopted cohesive zone model as the governing equation for describing this behavior. From their result, the critical bonding strength that can initiate the delamination of coating (SIBS coating) is calculated as 0.009 MPa, whereas our study predicts 0.5334 MPa for the coating fracture and/or fragmentation. The stent system is comprised of stainless steels with three different types of drug-polymer coatings. The majority factor to differentiate these two studies would be the different degrees of dilation. The study from Hopkins measures the bonding strength at the status of initiation of delamination whereas this thesis observes the maximum stress at the status of fully expanded status. In the present state, prediction of coating delamination at specific point of dilation is unfeasible since the observed stress on the coating component in this study is based on von-Mises stress. Therefore, again, it is not currently possible to directly compare these two sets of results because the computational systems and the analysis approaches are clearly different. Currently, the prediction of coating delamination related to the shear stress analysis will be implemented in the future work as will be mentioned in the next chapter.

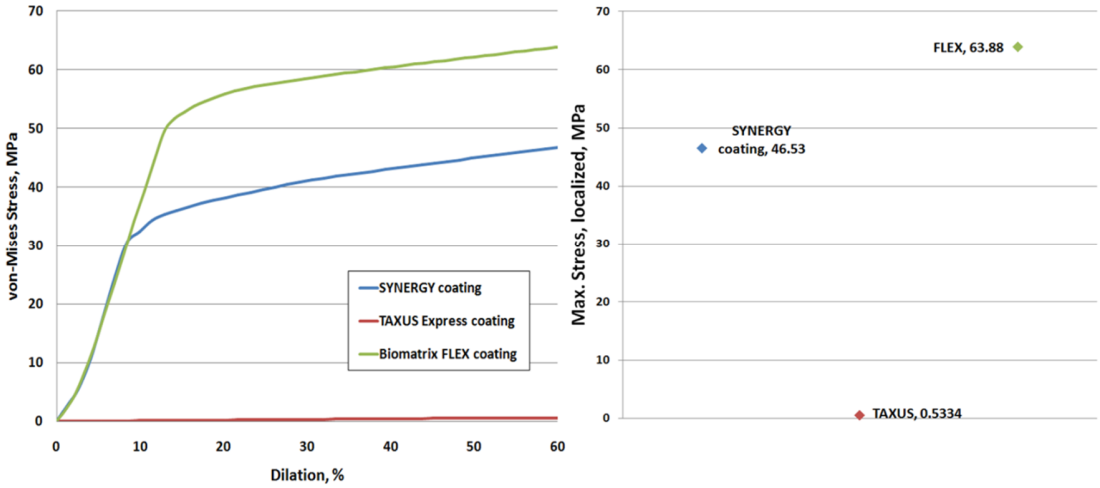

Fig. 5.41 Plots of (a) von-Mises stress profiles on the coating as a function of % dilation and (b) the maximum Mises stress from three different types of DES products.

To identify the locations of maximum and minimum stress locations for models B and C, same method using the unit cell analysis has been adopted. Figs. 5.42 to 5.45 show the locations of maximum and minimum von-Mises stress concentrations for model B and C, respectively. For both of the model B and C systems (TAXUS Express and FLEX products, respectively), it was found that the maximum stress points are located at the center position of hinge area, which is clearly different from the case of model A (near-hinge area). In addition, the maximum stress location in model B was identified in the position of the outer path of smaller ring (the stent platform of model B is composed of two sizes of ring structures, i.e., small and large rings), while the maximum stress was observed in the position of inner path of the unit cell structure.

Fig. 5.42 The location of maximum von-Mises stress on the coating component of model B.

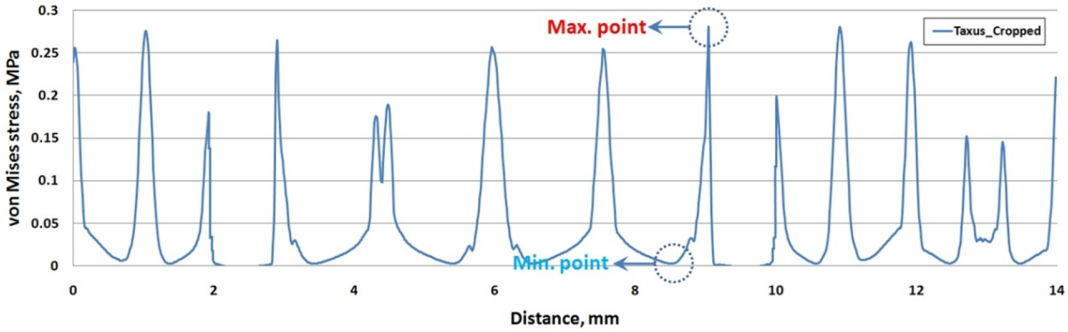

Fig. 5.43 The curve of von-Mises stress on the coating component of model B along the cropped path of the unit cell structure analysis.

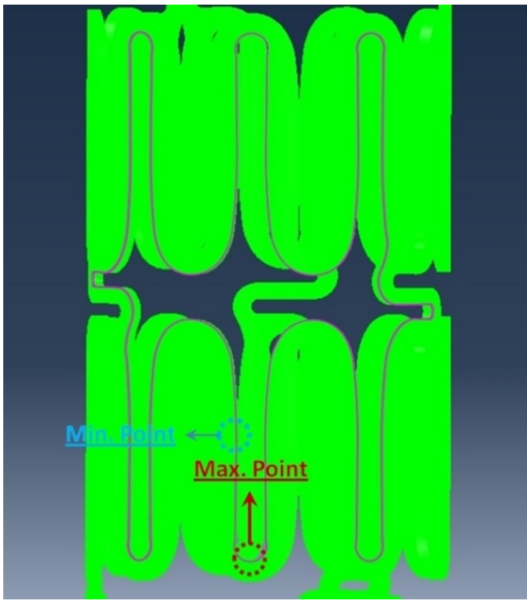

Fig. 5.44 The location of maximum von-Mises stress on the coating component of model C.

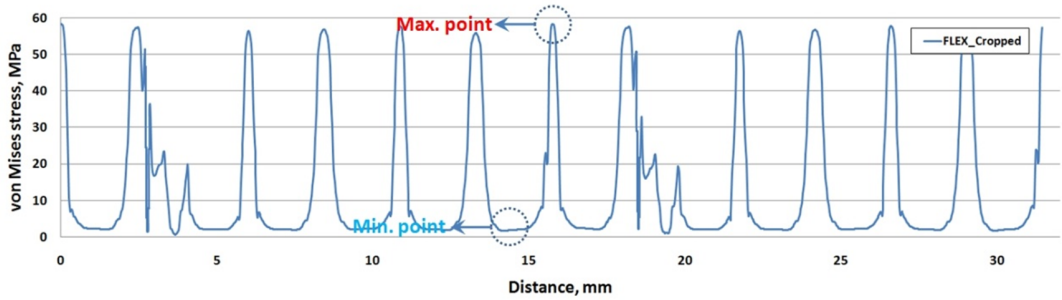

Fig. 5.45 The curve of von-Mises stress on the coating component of model C along the cropped path of the unit cell structure analysis.

As a final remark, it is considered that the validation of the generated computational results is necessary. However, experimental measurements for the mechanical behaviors from these small DES medical devices are not trivial tasks. For now, the simulation results of maximum stress locations show qualitatively consistent prediction to the experimental coating fracture phenomenon as shown in Chapter 1. The FEA model developed through the current study is thought to be readily applied to

predict the mechanical responses of DES systems including thin coating components. Further, it is anticipated that this work can be used as a basis to guide the optimized DES designs including the geometry and material factors. In the future, it is planned to extend the present research to incorporate much advanced computational analysis techniques and theories.

References

1. H. Zahedmanesh, C. Lally, Determination of the influence of stent strut thickness using the finite element method: implications for vascular injury and in-stent restenosis, Med Biol Eng Comput 47 (2009) 385-393.

2. E. W. Donnelly, M. S. Bruzzi, T. Connolley, P. E. McHugh, Finite element comparison of performance related characteristics of balloon expandable stents, Comp Met in Biom and Biomed Eng 10 (2007) 103-110.

3. C. G. Hopkins, P. E. McHugh, J. P. McGarry, Computational investigation of the delamination of polymer coatings during stent deployment, annals of Bio Eng 38 (2010) 2263-2273.

Chapter 6. Summary

Advanced computational numerical methods have emerged as essential tools for the assessment and optimization of the performance of biomedical devices such as coronary stent products. In the present thesis, we employed the finite element analysis (FEA) computation technique to predict the mechanical behavior of drug-eluting stents (DES) medical devices that are interfaced with drug-polymer coatings. To date, FEA has been widely utilized in a large number of studies of DES products to investigate the mechanical properties and their biomechanical impact on the diseased coronary artery during deployment. Over the past decade, rapid improvement of computational power has led to a considerable improvement in the level of complexity and sophistication involved in these studies. Today, elaborate models of commercially available stents, tri-folded catheter balloons, and stenotic arteries are regarded as the norm, despite the idealized or simplified material properties are often used to describe the behavior of complicated biological tissues. However, the contemporary research trend also includes the development of sophisticated hyper-elastic constitutive material models that can replace the previous simplified approximations.

In this study, unlike the previous investigations focusing on bare metal stents (BMS), we have considered the comprehensive DES system that incorporates the drug-polymer coating in the FEA model. FEA model has been developed to reliably predict the stress distributions in the various components of DES system. The developed FEA model allows to evaluate and compare the impacts of material/geometrical parameters. Our

models also include the examination of the stress distributions in the biological environment, i.e., atherosclerotic plaque and arterial wall.

Validation work has been initially carried out to verify that 2D and 3D coating elements produce consistent results. Then, using 2D coating elements, the influences of strut thicknesses and coating thicknesses on the von-Mises stress concentrations in the coating were examined. From the results, it has been observed that the strut thickness and coating thickness of stent are one of the dominant factors to determine its mechanical performance. DES system with thicker strut exhibited much higher von-Mises stress accumulation than thinner strut. And, it was also predicted that the stress on coating component increases as the coating thickness increases. Incorporation of the arterial wall and atherosclerotic plaque components in the computational system enables to investigate the stresses on the inner surface of arterial wall that can be utilized to understand the rate of in-stent restenosis (ISR). In our study, it has been found that the strut thickness plays a very important role in determining the degree of recoil phenomenon. Through a series of FEA computations, we showed that the recoil rate increases and the stress on the arterial wall decreases by adopting thinner struts in noticeable amounts. In addition, the regions with maximum and minimum von-Mises stress were identified, and the circumferential normal stress is turned out to be the major contributor to the stress concentrations out of the 2D three stress components.

Finally, it is considered that the development of a more complicated model would be necessary to quantitatively examine the fracture mechanisms of DES coatings with various geometry/material designs. Toward this, developing models containing multi-layered 3D elements for coating components is required to evaluate the shear stress

components in the coating/stent platform interface areas. Further, an advanced fracture theory such as cohesive zone model can be included in the computational analysis. However, all of these efforts will require a comprehensive 3D analysis that significantly limits the size of the computational domain even with the modern computational techniques and resources. Development of such advanced model remains as a future work with considerable challenges.

1. Limitations

- Evaluating shear stresses was unable to be performed since using 2D elements.
- Material properties for drug-polymer component are assumed to be pure polymer and homogeneous.
- Consideration of transient behavior of stent deployment was neglected.

2. Findings

- FEA model to predict the stress distributions in the various components including drug-polymer coating in DES medical devices has been developed.
- 2D and 3D coating elements showed almost identical results in von-Mises stress.
- Maximum local von-Mises stress in the stent strut increases by 8.5 % when the strut thickness increases from 60 μm to 100 μm.
- Maximum local von-Mises stress in the coating component increases by 4.7 % when the coating thickness increases from 7 μm to 20 μm.

- Normal stress along the stent circumferential direction shows the highest distribution.
- Incorporation of the arterial wall and atherosclerotic plaque compounds in the computational system enables to investigate the stresses on the inner surface of arterial wall that can be utilized to understand the rate of ISR.
- The recoil rate increases and the stress on the arterial wall decreases by adopting thinner struts in noticeable amounts.
- The regions with maximum and minimum von-Mises stresses in coating components for each model were identified.
- Adhesion strength between the coating and the strut platform must be greater than
    - 50~55 MPa for the SYNERGY system
    - 0.6~1.0 MPa for the TAXUS Express^2 system
    - 65~70 MPa for the Biomatrix FLEX system

  considered in the current work to avoid the coating delamination upon implantation.

3. Future works

- Developing models containing multi-layered 3D elements for coating component is required to investigate shear stresses.
- Refinement of model will require including more accurate material properties (i.e., existence of drug phases).

- Pressure control with explicit method needs to be adopted to evaluate transient behavior of stent in future work.
- Propose optimum DES with advanced materials and geometric design.